ASD-TDR-62-26

ESTABLISHMENT OF THE APPROACH TO, AND DEVELOPMENT OF, INTERIM DESIGN CRITERIA FOR SONIC FATIGUE

TECHNICAL DOCUMENTARY REPORT NO. ASD-TDR-62-26

June 1962

Flight Dynamics Laboratory
Aeronautical Systems Division
Air Force Systems Command
Wright-Patterson Air Force Base, Ohio

Project No. 1370, Task No. 137001

(Prepared under Contract No. AF 33(616)-7694
by the North American Aviation, Inc., Los Angeles, California;
G. E. Fitch, T. R. Dutko, L. M. Brennan,
A. G. Tipton, P. M. Belcher, P. Wang, and P. A. Clawson, authors.)

NOTICES

When Government drawings, specifications, or other data are used for any purpose other than in connection with a definitely related Government procurement operation, the United States Government thereby incurs no responsibility nor any obligation whatsoever; and the fact that the Government may have formulated, furnished, or in any way supplied the said drawings, specifications, or other data, is not to be regarded by implication or otherwise as in any manner licensing the holder or any other person or corporation, or conveying any rights or permission to manufacture, use, or sell any patented invention that may in any way be related thereto.

Qualified requesters may obtain copies of this report from the Armed Services Technical Information Agency, (ASTIA), Arlington Hall Station, Arlington 12, Virginia.

This report has been released to the Office of Technical Services, U.S. Department of Commerce, Washington 25, D.C., in stock quantities for sale to the general public.

Copies of this report should not be returned to the Aeronautical Systems Division unless return is required by security considerations, contractual obligations, or notice on a specific document.

FOREWORD

The research work in this report was performed by North American Aviation, Inc., Los Angeles Division, International Airport, Los Angeles 19, California, for the Flight Dynamics Laboratory, Directorate of Aeromechanics, Deputy Commander/Technology, Aeronautical Systems Division, Wright-Patterson Air Force Base, under AF Contract Nr AF33(616)-7694. This research is part of a continuing effort to obtain design criteria to advance the state-of-the-art in the area of resonant fatigue of aircraft structures which is part of the Air Force Systems Command's Applied Research Program 750A, the Mechanics of Flight. The Project Nr is 1370, "Dynamic Problems in Flight Vehicles" and the Task Nr is 137001 "Resonant Fatigue of Structures". Mr. M. J. Cote of the Flight Dynamics Laboratory was the Project Engineer. The research was conducted from 15 January 1961 to 15 January 1962.

The work was conducted in the Engineering Department of North American Aviation, Inc. (Los Angeles Division) with Mr. G. E. Fitch as Contractor Project Engineer. Participating effort, both in the accomplishment of this contract and in the writing of this report, was contributed by the following persons: Messrs. T. R. Dutko (Structures), L. M. Brennan and E. Hanson (Mission Analysis), P. M. Belcher and A. G. Tipton (Structural Dynamics and Acoustic Environment), and P. A. Clawson and P. Wang (Test Techniques).

ABSTRACT

A literature survey provided the background from which an approach was selected for development of design criteria for sonic fatigue. The approach selected was accelerated, discrete frequency life-testing, the results of which are interpreted using a sine-random equivalence analysis. This approach offers the best compromise between economy, accuracy, and lead time to cover structural design problems for advanced design, design development, and prooftesting of completed vehicle structure. Methods were extracted from the literature with which to predict the acoustic environment and determine the duration of various environments from mission analysis. Fatigue data and an examination of cumulative damage are presented in support of the sine-random equivalence technique. This method takes advantage of the extensive fatigue S-N data available in the industry. Examples of the application of the analytical-empirical techniques are presented.

This report has been reviewed and is approved.

William C. Nielsen

WILLIAM C. NIELSEN
Colonel, USAF
Chief, Flight Dynamics Laboratory

2-16M, 300, 8-31-62

TABLE OF CONTENTS

LIST OF ILLUSTRATIONS

LIST OF TABLES

LIST OF SYMBOLS

Symbol			Units
A	=	Area	sq in.
a	=	Panel dimension	in.
b	=	Panel dimension	in.
C	=	Velocity of sound	ft/sec
c	=	Damping coefficient	
c_c	=	Critical damping coefficient	
D	=	Flexural rigidity	lb/in.
D	=	Fatigue damage	
D	=	Jet diameter	in.
D_c	=	Critical fatigue damage	
E	=	Modulus of elasticity	psi
ϵ	=	Strain	in./in.
F_S	=	Shear stress	psi
F_{tu}	=	Ultimate tensile strength	psi
f	=	Frequency	cycles/sec
f_o	=	Resonance (natural) frequency	cycles/sec
g	=	Acceleration of gravity	ft/sec^2
h	=	Panel thickness	in.
K	=	Coefficient	
K_t	=	Stress concentration	
M	=	Mach number	
m	=	Mass flow	lb/sec
N	=	Number of load cycles to failure	
N_S	=	Number of load cycles to failure at a standard load condition	
n	=	Applied number of load cycles	
n	=	Velocity exponent sound pressure	
n_i	=	Load cycles at condition i	
n_{sr}	=	Remaining cycles of life at a standard load condition after previous application of n_i cycles	
$P_{(x)}$	=	Probability	
P_a	=	Ambient pressure	psi
p	=	Pressure	db or psi
R	=	Cycle load ratio	
rms	=	Root mean square	
s	=	Instantaneous stress	psi
S	=	Stress	psi
S_e	=	Endurance limit stress	psi
s_{max}	=	Maximum applied stress	psi
$\overline{s^2}$	=	Mean square stress	(psi)^2

Symbol			Units
$\sqrt{\bar{s}^2}$	=	Root mean square stress	psi
S_{PD}	=	Peak damage stress level	psi
SPL	=	Sound pressure level	db or psi
T_{AF}, T_{BF}, T_{CF}	=	Total flight time per mission A, B, or C, including takeoff and landing operations	minutes
T_{AO}, T_{BO}, T_{CO}	=	Total time for all operations listed in mission A, B, or C outline, including ground operations as flight per mission flow	minutes
T_a	=	Ambient temperature	°R
t	=	Thrust	lb
t_{ai}, t_{bi}, t_{ci}	=	Time in minutes on each mission (A, B, or C) flown, during which operation number i is conducted at designated power setting	
V	=	Effective exhaust velocity	ft/sec
w	=	Weight flow	lb/sec
X	=	Longitudinal engine coordinate	
Δ X	=	Downstream shift for supersonic exit Mach numbers	in.
Y	=	Radial coordinate	

Subscripts

e	=	Condition at jet exhaust exit plane
F	=	Flight conditions
H	=	Discrete frequency loading
l	=	Numbered operation in designated mission outline
o	=	Standard
R	=	Random
S	=	Sinusoidal
S	=	Static ground condition
T	=	Total

Greek Symbols

α	=	Stress-load ratio
β	=	Panel aspect ratio
γ	=	Multimode correction factor
δ	=	Damping ratio = c/c_c
λ	=	Nonlinearity factor

Greek Symbols			Units
μ	=	Poisson's ratio	
ρ	=	Density	slugs/f_t^3
ρ_o	=	Standard air density	slugs/f_t^3
$\Delta\phi$	=	Shift in the angle of maximum SPL	degrees
ω	=	Frequency	radians per sec

GLOSSARY OF TERMS

Acoustic, acoustical - of or pertaining to sound, the former specifically to physical properties of the sound.

Boundary layer - region of retarded fluid flow resulting from viscosity adjacent to a surface.

Convection velocity - time rate of downstream motion of a local pressure disturbance in a flow.

Correlation - a statistical measure of the coherence or similarity between the instantaneous magnitudes of two or possibly the same (autocorrelation), time series (cross-correlation).

Correlation function - correlation defined as a function of time delay between the two (or same) functions; this function is usually normalized to a number between -1 and +1 by the product of the rms values of the two time functions.

Cumulative damage - theory that fatigue damage initiates with the first load cycling and accumulates linearly or nonlinearly until failure occurs.

Damping - a mechanism of energy dissipation.

Decay rate - time rate at which a quantity decreases.

Decibel (db) - logarithmic ratio of acoustic pressure to a reference pressure ($20 \log_{10}$ pressure/reference pressure); or logarithmic ratio of acoustic power to a reference power ($10 \log_{10}$ power/reference power).

Edge fixity - the degree of rotational restraint along the edges of a structural panel.

Environment - the properties of the acoustic pressure field (e.g., frequency spectrum at a point and/or spatial properties of the pressure in the neighborhood of a point).

Fatigue - the failure of materials under repeated or alternating stresses too small to cause rupture when applied statically.

Frequency - time rate of recurrence of a phenomenon.

Gaussian distribution - probability distribution function used to describe the distribution of instantaneous stress magnitudes in random vibration.

Goodman diagram - a means of presenting fatigue loading parameters (mean stress, alternating stress, load ratio, minimum and maximum stress) on one plot.

Harmonics - pressure disturbances at frequencies which are integer multiples of the fundamental.

Mean alt - average altitude at which a particular operation is to be flown, assuming standard atmospheric conditions.

Mean a/s - average true airspeed at which a particular operation is to be flown, assuming standard atmospheric conditions.

Mission flight time - total time from start of takeoff roll to end of landing roll.

Mission outline - a tabulated series of operations which describe one type of mission flown by the designated type of air vehicle design, and containing an assignment of engine maintenance run time in support of the mission.

Mission total operation time - total time for all operations including flight time and engine ground run time associated with each particular mission.

Mode - the spatial configuration of a structure in resonance.

Noise - interchangeable with sound.

Octave band - a frequency range whose upper limiting frequency is twice the lower.

Operation - one segment of a mission outline which is assumed to be representable by a single set of acoustic environmental conditions for each engine power setting.

Operation hr/1000 flt hr - the number of hours spent at each tabulated condition of operation and power setting during the period wherein the air vehicle accumulates 1000 flight hours.

Power setting - the throttle-selected power output of the engines.

Power spectral density - the density of power in unit bandwidths.

Pseudo noise - interchangeable with turbulence pressure fluctuations.

Pure tone - a pressure disturbance which is periodic and which has no harmonics.

Radiation (of pressure) - the mode of propagation of pressure disturbance occurring in the phenomenon, sound.

Random S-N curve - an S-N curve which describes fatigue behavior of material subjected to stresses whose instantaneous magnitudes form a random time series.

Random time series (as of sound or stress) - a time series which has no periodicity.

Rayleigh probability density function - the density function used to describe the density of stress peaks occurring in structures responding randomly in a single mode.

Resonance - a condition of vibration of structure wherein the inertial and restoring forces are equal and dissipative forces control the motion.

Separated flow - fluid flow which is detached from a solid boundary.

Service life - a specified time period, usually in hours, that a component or vehicle must survive without failure.

Sinusoidal - pertaining to motions, etc, which are simply harmonic.

Siren - a device for producing high-intensity sound which is primarily periodic.

S-N curve - a plot of stress against number of cycles to failure; it is usually plotted S versus N on semilog plotting paper.

Sound - a pressure disturbance which propagates in an acoustic medium.

Sound pressure level - 20 times the logarithm to the base 10 of the ratio of the sound pressure to a reference pressure.

Octave - a pressure level which accounts for all energy in an octave band.

Overall - a pressure level which accounts for all energy in the total frequency range.

Stress -

Alternating stress amplitude - one-half the range of stress.

Mean stress - the algebraic mean of the maximum and minimum stress in one cycle.

Minimum stress - the lowest algebraic value of the stress in the stress cycle.

Peak or maximum stress - the highest algebraic value of the stress in the stress cycle.

Range of stress - the algebraic difference between maximum and minimum stress in one cycle.

Vibration - an oscillation of a structural element.

INTRODUCTION

Essential to the establishment of criteria for the design of structure for acoustical fatigue are techniques for the specification of the forcing pressure fields, and means of evaluating the fatigue-producing responses of the structures loaded by these pressures. It has been the objective of a study, the results of which are presented in this report, to make available to the airframe designer such techniques.

The evaluation of response offered depends primarily on empirical data, either particular to the problem at hand or to existing results from earlier studies. This is essential, since analytical dynamic stress evaluation for structure in general, in sufficient detail to describe stresses of the highly local character important to fatigue, is not now possible. The methods presented are by no means unique. They do have the advantage of relative simplicity; the empirical method of structural evaluation uses equipment (the high-intensity siren) which is widely available in the industry; they reflect existing successful practice; and future improvements in the treatment of any of the elements will be incorporable.

The primary orientation of the report is toward the presentation of the method. It is addressed to the reader in need of solutions to the problems it considers. In the main, references to the literature are made to support or to examine deficiencies in the elements of its construction. Detailed consideration of these elements is given in leading to the essential contribution of the report, which is an effort to bridge the technological and linguistic gulf between the dynamicist and the designer by presenting, in complete detail, examples of application of the method to realistic design problems.

In order to implement its emphasis on producing a detailed, usable method, the study has slighted generality to some extent. The emphasis in propulsion systems is, for example, with jet and rocket engines; this is because the vast majority of design problems lie with vehicles thus powered. So too with response, where the target has been the response to pressure fields having amplitudes random-in-time. Where available, references to the means of estimating the pressure characteristics of sources other than jets have been given. Means of treating structure required to sustain acoustic load for very short periods of time, less than 10^4 cycles of stress reversal, do not yield to the "statistics of multiple, low-magnitude stresses" approach presented here, but involve the probability of encountering one cycle exceeding ultimate stress during the required life. This question is not treated; when it is encountered, the problem can usually be solved by a slightly conservative treatment.

Nor are all matters within the restricted province of this report solved. For example, the quantitative adjustments required for treatment of coupled modes is a relatively unimportant consideration which occurs infrequently. However the entire matter of the spatial properties of the pressure fields and

the responding structures is an example which is critical to the essential nature of the problem. Each of these examples can be expected to yield only slowly, and probably incompletely, to a great deal of investigation. In detail questions of minor importance, typified by the first of these examples, the designer can make slight detail changes or, alternatively, adopt a conservative adjustment to his analyses. In the latter, the spatial correlation, a good deal more imaginative analysis may be required. When, as will often happen, conservatism is the only acceptable recourse, the dictates of flight safety and the potential difficulty and cost of maintenance must determine his decision. But the designer faced such questions before acoustical fatigue became a significant design consideration.

Section I

ACOUSTIC ENVIRONMENT

1.0 NOISE SOURCES

The acoustic environment of air vehicles arises from propulsion systems and turbulent boundary layers. The magnitude of the sound pressure level generated by a propulsion system is maximum during static ground operation with maximum propulsion system power, and decreases as flight speed and altitude are attained. The boundary layer noise increases with increasing flight speed and attains a maximum value at the maximum dynamic pressure experienced during flight. Rarely are structures found which cannot endure 145 db, over-all, of propulsion system sound pressure level. Experience with vehicles up to Mach 3.0 indicates that the excitation of attached boundary layers is not damaging to normal structure. A time history of the boundary layer and propulsion system noise for a typical air vehicle is shown in figure 1. The sound pressure levels could be obtained by measurements on the actual vehicle, but the vehicle is not available when knowledge of the acoustic environment is needed to establish a design which will withstand the imposed acoustic loading. Scaled models which simulate the noise producing mechanism of the vehicle could also be used for supplementary data. Sound pressure levels can also be estimated, utilizing existing information in the literature; this is the method presented in this report.

1.1 PROPULSION SYSTEM NOISE

Propulsion system noise is a function of the power produced by the system. Large jet and rocket engines generate intense sound fields in the vicinity of the exhaust. This sound field is comprised of broad-band random pressure fluctuations that are normally expressed as rms values. Because of the random nature of these pressure fluctuations, a number of peaks occur that exceed the rms value by a factor of 3 or 4. The sound spectra generated by propulsion systems that employ propellers contain at discrete frequencies that are related to the period of rotation of the propeller. Calculations of the sound pressures generated by propellers have been presented in Reference 1 in such a manner that engineering estimates may be obtained by a few simple calculations employing the appropriate graphs and charts. Additional theoretical and empirical information on propellers, pulse jets, and reciprocating engines can be obtained from References 2, 3, and 4. The equations and design charts available in the literature for propellers, pulse jets, and reciprocating engines will not be included in this report because of the limited use foreseen for these propulsion systems on future aircraft. The jet engine, however, will be treated in detail with sufficient information included to assist designers in obtaining engineering estimates of the sound pressure levels of high-performance jet engines.

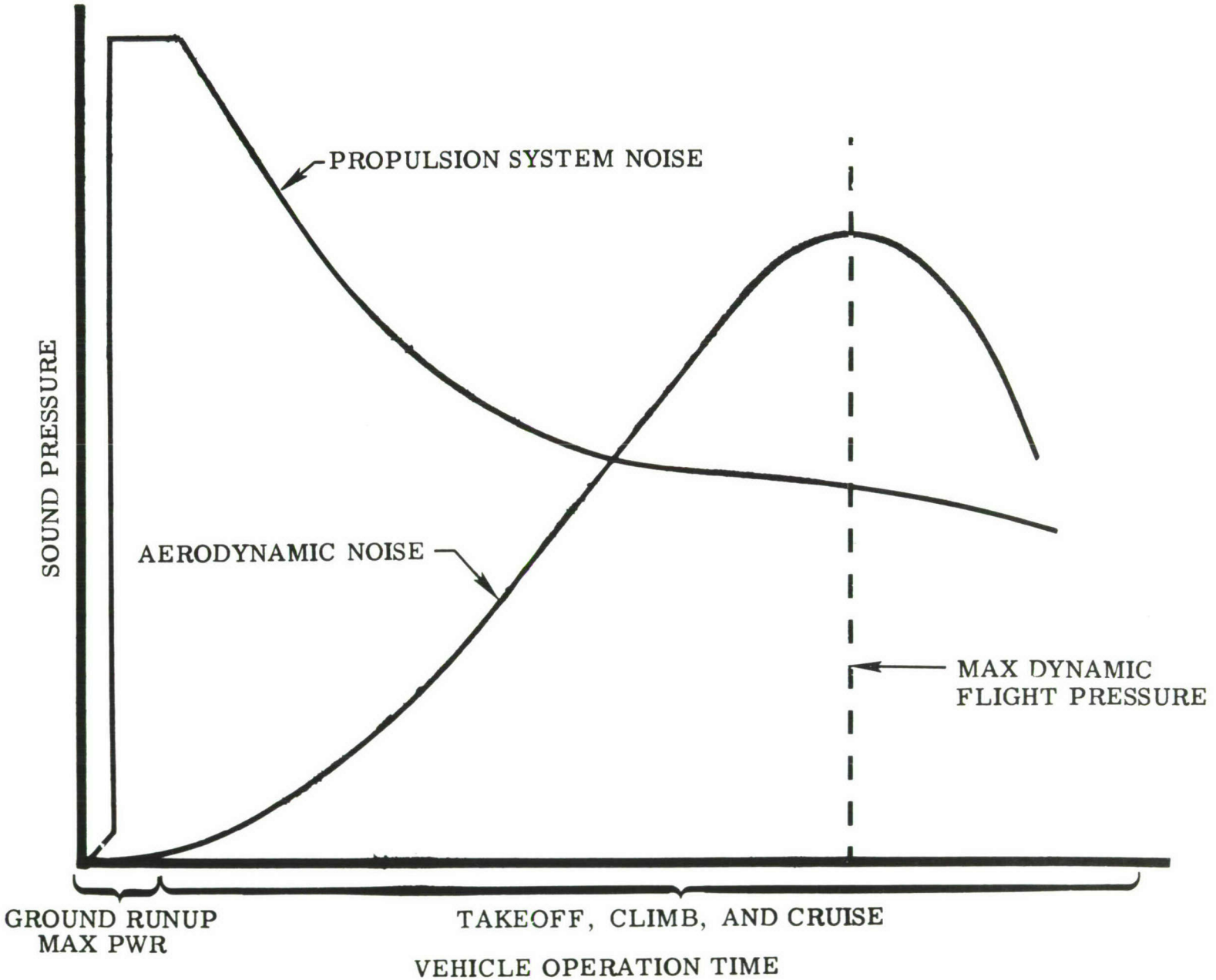

Figure 1. Typical Time History of Vertical Noise Source Sound Pressures

A sample problem will be solved (in Section VI) for an air vehicle with two 30,000-pound thrust afterburning supersonic jet engines to illustrate the methods presented in this report.

1.2 JET AND ROCKET ENGINE NOISE

Jet and rocket engine noise is generated by turbulent mixing of the high-velocity exhaust gas with the ambient atmosphere. This turbulent mixing region extends a considerable distance downstream from the engine exhaust nozzle, resulting in an axially extended sound source. The sound pressures radiated from regions in the jet exhaust close to the nozzle exit are predominantly of high-frequency content, while those radiated from regions in the exhaust a distance downstream are predominantly of low-frequency content. A theoretical treatment of sound pressure radiated by this turbulence appears in Reference 5. The restrictions imposed in the theory, however, limit applicability to far field fluctuations radiated from subsonic jets. The most intense acoustic pressures are rediated in the near field, attenuating to much lower levels in the far field; and prediction of these near field pressures will be emphasized. A theoretical method is not available in the literature which will yield values of the magnitude of the acoustic pressures radiated from the engine exhaust; therefore, engineering estimates of these fluctuating pressure are based on empirical data. Jet engines operating at maximum power are normally choked; the procedures presented in this report will, therefore, assume sonic or supersonic exhaust gas flow at the nozzle exit.

Because of the nature of the mixing process of the exhaust gas with the ambient atmosphere, the exhaust velocity decays at a lesser rate toward the center of flow than near the outer boundaries, resulting in a cone of constant velocity equal to the exit velocity and extending a distance downstream from the nozzle exit. The end of this cone for jets having sonic (Mach 1) exhaust velocities is defined as the sonic point, downstream of which the flow is entirely subsonic. Supersonic exhaust velocities also decay to a point of sonic velocity. The position of this point downstream of the supersonic nozzle exit has been determined empirically in Reference 6.

Downstream of the sonic point, supersonic and sonic engines exhibit similar noise-producing characteristics. The maximum sound pressures in the sound field of a supersonic jet are generated in the vicinity of the sonic point, as shown in References 7 and 8. For stabilized supersonic flow, it appears that the pressure radiated from the supersonic portion is not large with respect to the pressure generated by the subsonic region. The most significant difference between the noise fields of sonic and relatively shock-free supersonic flow is a downstream shift of the apparent noise sources, which is a function of the exit Mach number.

ESTIMATION OF SOUND PRESSURE LEVELS

A procedure appears in Reference 1 for estimating the near-field sound pressure levels of a sonic jet in the 10,000-pound thrust class. This procedure has been revised when extrapolation to supersonic jets of 20,000 pounds to 30,000 pounds thrust rating is necessary. The over-all sound pressure level contours shown in figure 2 represent the sound fields of a sonic jet with an exhaust velocity of 1850 feet per second and can be used as a reference condition for calculation of the sound pressures for other more or less powerful engines, provided the appropriate scaling parameters are applied. Far-field acoustic pressures are theoretically proportional to the exhaust velocity raised to the eighth power, but as the distance to the jet exhaust decreases the sound pressure becomes proportional to a lesser velocity exponent than the eighth. Figure 2, reproduced from Reference 1, has been revised to show the effect of the variable near-field velocity. exponent. An increase in exhaust velocity results in a rotation away from the jet axis, as is shown in figure 3 for exhaust velocities up to 4000 feet per second. Sound pressure frequency spectra are obtained from figure 4, which has been reproduced from Reference 1, and extended in such a way that frequency spectra upstream of the nozzle exit may be obtained. The procedure which utilizes these revised figures of Reference 1 is summarized as follows:

1. Calculate the effective exhaust velocity of the engine

$$V_e = \frac{tg}{w} \tag{1}$$

2. Calculate and add the change in sound pressure level to each reference contour, utilizing the effective velocity and the velocity exponent "n" for each contour.

$$SPL = 10\ n \log \frac{V_e}{1850} \tag{2}$$

3. Multiply the dimensionless parameters x/D and y/D in figure 2 by the exhaust exit diameter to adjust sound pressure level contours to the air vehicle's dimensions.

4. Shift the contours in Item 3 downstream a distance Δx when extrapolating to supersonic exhaust velocities.

$$\Delta x = 6.5\ D_e\ (M_e - 1)^2 \tag{3}$$

5. Rotate the contours in Item 4 through the angle $\Delta\phi$ which is determined from figure 3 about the point on the jet axis Δx downstream.

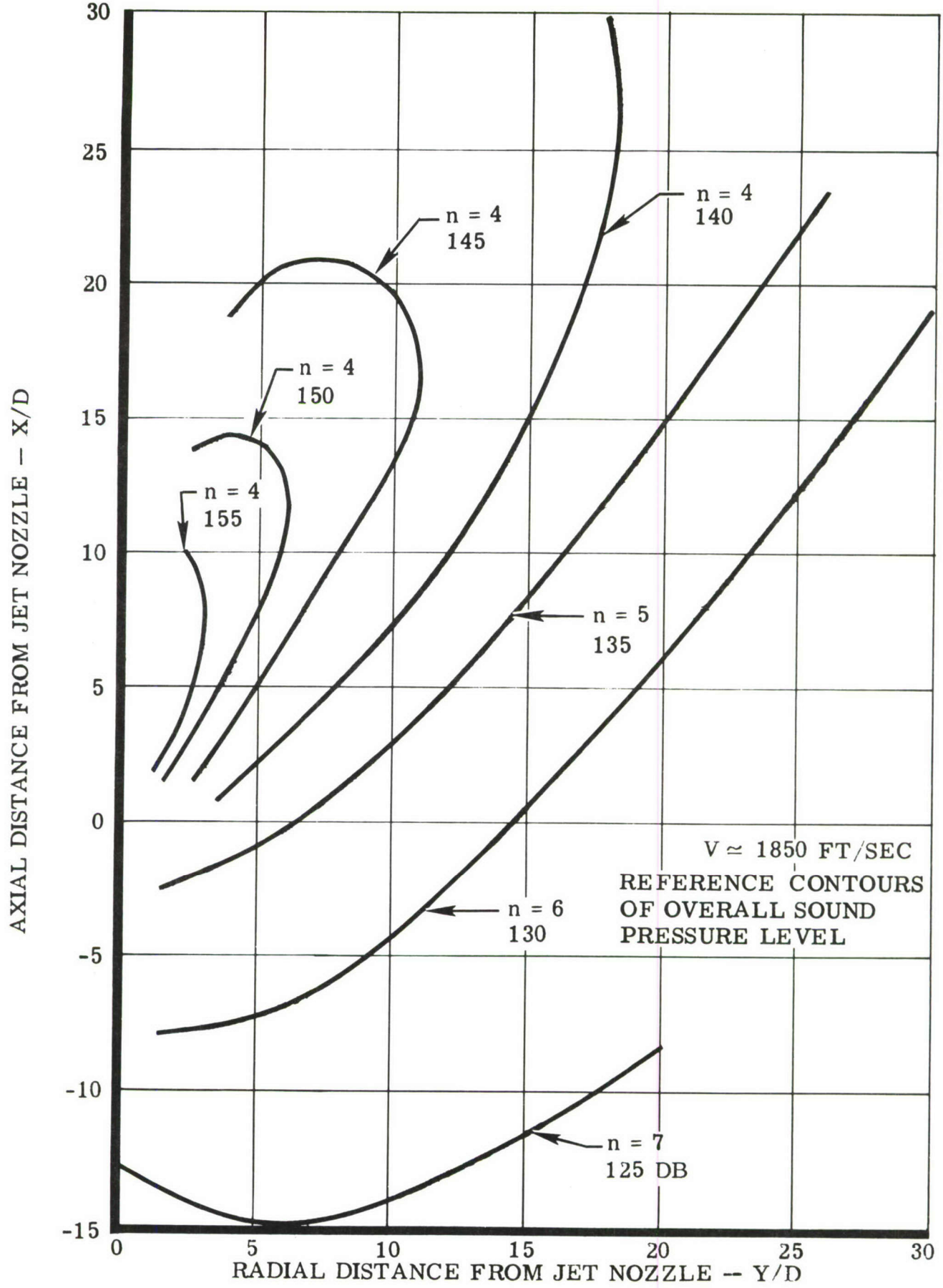

Figure 2 . Near Sound Field of a Turbojet

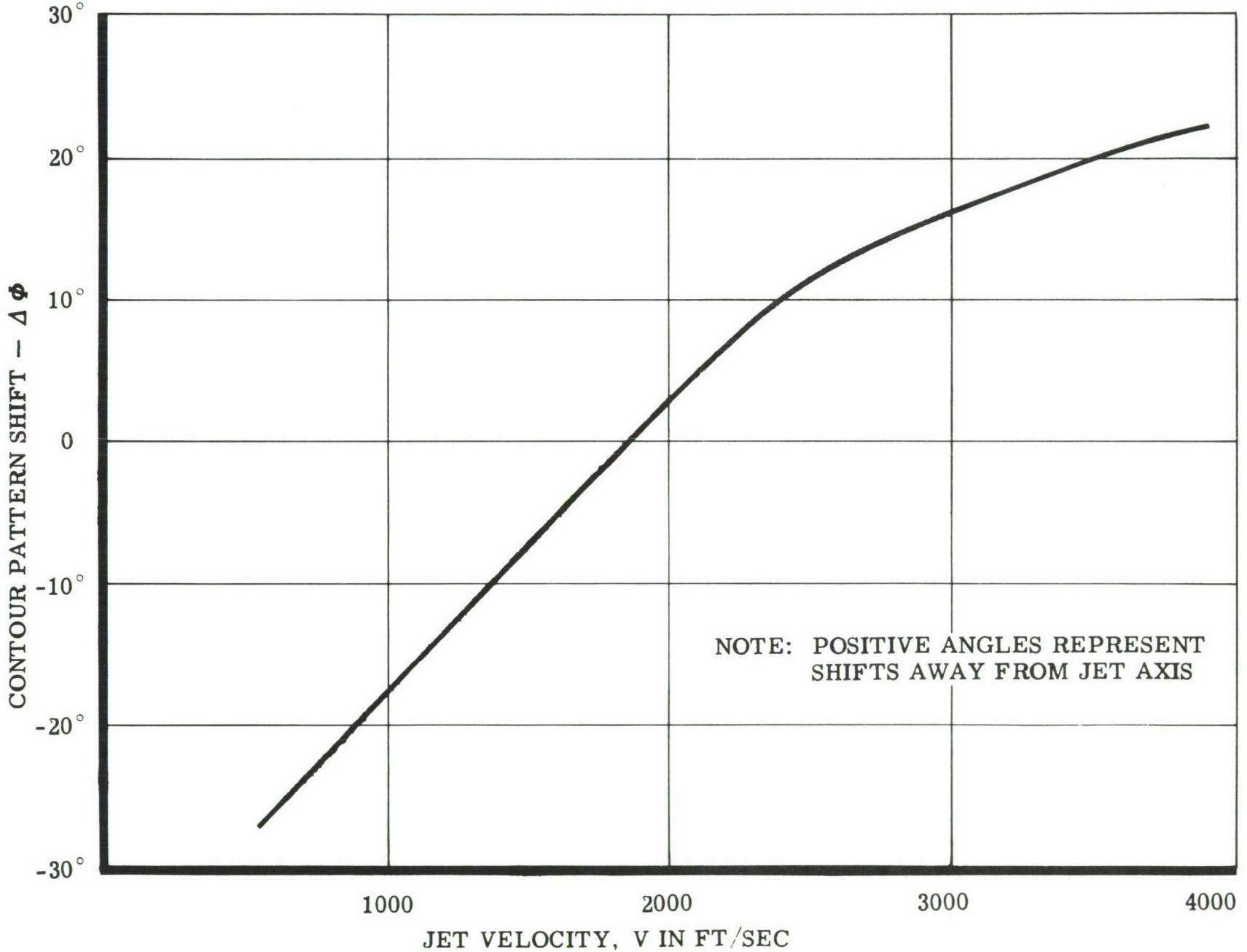

Figure 3 . Velocity Dependence of Over-all SPL Contour Pattern

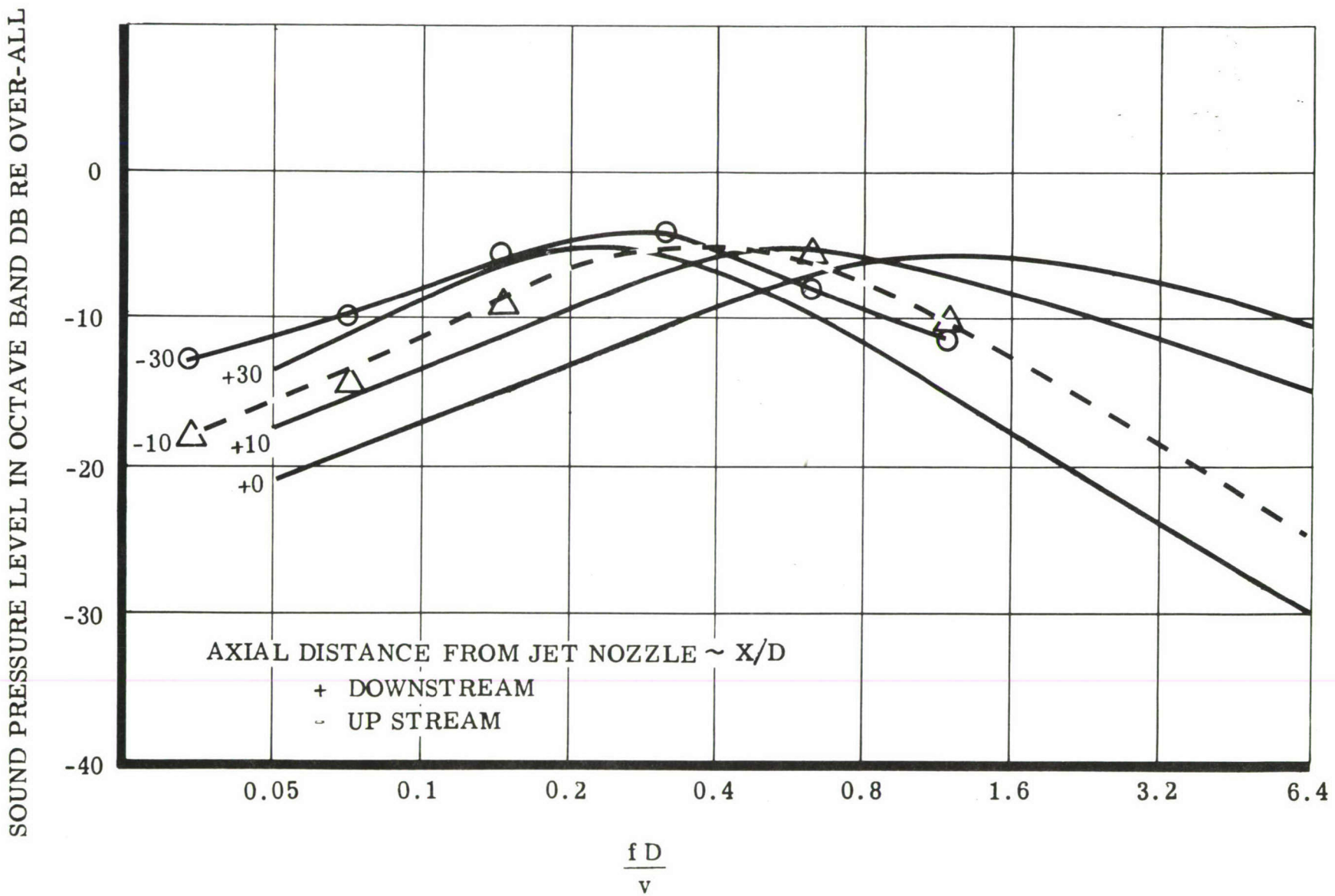

Figure 4 . Spectrum of Jet Noise Near Field

6. Calculate the frequency spectra for any position in the near sound field, from figure 4, from knowledge of the over-all free-field sound pressure level in Item 5 and the jet velocity and diameter.

The sound pressure levels in Item 6 are free-field values for one engine operating above a reflecting ground plane. The presence of air vehicle surfaces in the noise field increases the pressure over the free-field values. References 9 and 10 show an increase of 3 db over free-field values. The effect of multiengine configurations, however, is quite complex and very little data are presently available on the subject. Unpublished empirical data show that conservative predictions result when the sound pressure for each engine is added in accounting for the effect of multiengine configurations.

EFFECT OF AMBIENT CONDITIONS

Substantial changes in ambient conditions also affect the predicted sound pressure levels during ground runup. At extremely low ambient temperatures, engine thrust usually increases resulting in increased exhaust velocity and slightly higher sound pressures. This increased sound pressure level can be calculated by employing the appropriate exhaust velocities in the following relationship. The near field velocity exponent n is obtained from figure 2.

$$\Delta \text{SPL} = 10n \log \frac{V_{\text{cold day}}}{V_{\text{standard day}}} \tag{4}$$

As the vehicle attains forward velocity and altitude, the near field over-all sound pressure levels decrease by an amount calculated from the following equation. This equation is applicable for regions both close to the engine centerline and forward of the exhaust nozzle. Conservative values would result from neglecting the Mach number term and could also be applied to regions downstream of the nozzle exit.

$$\Delta \text{SPL} = -10 \log \left(\frac{V_e}{V_e - V_F}\right)^n \left(\frac{1}{1 - M_F}\right)^2 \left(\frac{P_{as}}{P_{aF}}\right) \left(\frac{T_{aF}}{T_{as}}\right)^{1/2} \tag{5}$$

A slight frequency spectrum shift to lower frequencies would result if the relative velocity ($V_e - V_F$) is used in fugure 4; this could be included as a refinement in the analysis.

1.3 AERODYNAMIC NOISE

The random pressure fluctuations in high-speed turbulent flow adjacent to air vehicle boundaries is a source of structural excitation. Turbulent

boundary layer noise is the predominant cause of aerodynamic noise experienced during flight for streamlined aerodynamic configuration without protrusions or cavities. The effect of cavities and protrusions together with oscillating shock waves during supersonic flight can greatly increase the magnitude of the fluctuating pressure in a turbulent boundary layer. A summary of the data now available because of these irregular conditions is contained in Reference 11, revealing in some cases a 20 db increase in fluctuating pressure over the normal turbulent boundary layer value due to cavities, jet exhaust impingement, separated flow, and oscillating shock waves. It is not possible at this time to establish realistic design guides for these irregular conditions. Fatigue failures have been experienced because of these conditions, and if they are unavoidably designed into an operating vehicle, the regions affected should be closely scrutinized during design and prototype flight tests.

Prediction of turbulent boundary layer pressure fluctuations can be readily obtained, utilizing empirical data from Reference 13. These data are based on actual microphone measurements of subsonic aircraft. The over-all noise level of the turbulent boundary layer is related to the free-stream dynamic pressure; for subsonic speeds, the ratio of the over-all rms value of the fluctuating boundary layer pressure to the free stream dynamic pressure is a constant. The numerical value of this constant, evaluated from independent experimental data, varies slightly, but a constant ratio of 0.006 is taken as a representative value. Unpublished data reveal that for supersonic speeds, the ratio of boundary layer fluctuating pressure to the free-stream dynamic pressure is less than the subsonic value of 0.006. Utilizing this value would yield conservative estimates for supersonic cases. The frequency spectra for subsonic boundary layer pressures have been expressed as a function of nondimensional parameters involving Mach number, boundary layer thickness, and flight speed in Reference 13 for a number of test conditions including in-flight measurements. Reference 11 considers a wider range of empirical data and introduces a viscosity ratio in the dimensionless parameters. The dimensionless parameters of both References 11 and 13 are employed in order to condense all of the respective empirical data into a narrow range of values which can be represented approximately by a single curve. Engineering estimates of the frequency spectra of aerodynamic boundary layer noise can be obtained directly from these references for subsonic flight speeds. Published information concerning pressure spectra for supersonic speeds is not available, and extrapolation to supersonic speeds must be viewed with caution.

CORRELATION

The correlation functions which describe the consistency of the pressure fluctuations over structural surfaces are necessary to describe completely the effective forcing fluctuating pressures. Comparing the spatial correlation

of jet engine noise in Reference 14 and boundary layer noise in Reference 12 reveals that boundary layer noise is poorly correlated compared with engine noise, therefore causing less structural response for the same fluctuating pressure level. A discussion of the difficulties involved in using correlation information in design work appears in Section VI.

1.4 VALIDITY AND APPLICATION OF SOUND PRESSURE PREDICTION

Due to the complexity of the acoustic environment, a certain amount of error is unavoidably generated when predictions are made. A degree of realistic conservatism, however, is inherent in the prediction technique in order to account for nonconservative errors arising from reflections due to air vehicle structure in the sound field and deviations of the jet exhaust turbulent structure from that of the reference condition.

Predictions accurate enough for purposes of initial structure design can be obtained even though exact predictions are impossible to achieve due to reflections and shielding effects of the air vehicle structure and the complex nature of sound generation of the turbulent jet exhaust. The turbulent structure of the jet exhaust is related to the radiated sound field and any deviation from the reference condition, which is the exhaust flow of a jet engine of 10,000-pound thrust with an effective exhaust velocity of 1850 feet per second and its related sound field, is a source of error. Extrapolating from the Mach 1 exit reference condition to supersonic exhaust velocities is valid when relatively shock-free exhaust flow exists which occurs when the static pressure in the exhaust gas at the nozzle exit is close to ambient. Optimum propulsion system performance is obtained when the above condition is achieved and as a result designers normally strive toward that end.

When the turbulent shearing region in the jet exhaust is altered by the introduction of a high percentage of secondary air, as in aft fan engines, an uncertainty appears as to the validity of a prediction technique based on little or no secondary air flow. The prediction technique does show, however, the expected trend that a fan engine utilizing a high percentage of secondary air generates less noise than a jet using little or no secondary air flow when compared on an equal thrust basis. This is due to the increased mass flow and corresponding decrease in average effective exhaust velocity necessary to produce the same thrust as a relatively high-velocity, low-mass flow of a jet with no secondary air flow.

Section II

SERVICE USAGE AND MISSION PROFILES

2.0 SERVICE LIFE REQUIREMENTS

This section presents a method for defining the expected lifetime cumulative acoustic environment for various air vehicle design types. A series of mission outlines is given for each of the air vehicle types considered. These mission outlines will guide the designer in computing summary tables of total utilization hours in each significant condition of engine power setting, altitude, and airspeed, including engine ground runs. A method is given for the further breakdown of engine ground-run times by expected variations in ambient air temperature conditions. The parameters selected are those used in the prediction of significant sound pressures in the acoustic environment of the vehicle. The cumulated times provide the durations of the various pressures and types of acoustic environment. The durations with appropriate safety factors, if any, provide the necessary life criteria for sonic fatigue. An example problem is computed for a hypothetical design air vehicle in Section VI.

2.1 SERVICE USAGE AND OPERATIONAL DATA

For the purpose of this portion of the study, airborne vehicles were classified into nine types: intercept fighter; tactical fighter; strategic attack; tactical attack; cargo transport; helicopter; surface-launched missiles; air-launched missiles; and drones. Since the most serious problems arising from acoustic stress fatigue are intimately connected with the advent of modern high-power jet engines and high-speed flight, principal attention was devoted to the first five of these types. Although some applications of high power and speed have been and will be made in the latter four types of airborne vehicles, it is considered that their utilization lives can best be predicted using the general techniques developed here, but slanted to the peculiarities of individual design performance rather than in a generalized treatment as applied to the first five types of vehicles.

At the end of Phase I of this study, it had become evident that a major source of acoustic excitation in air vehicles of the near future would be from high-powered engine runups while the air vehicle is on the ground. This portion of the air vehicle utilization life prediction was, then, accorded priority attention in Phase II. It was found that no USAF records of aircraft utilization were adequately detailed to provide any useful historical data to aid in these predictions. A source was found, however, in the data being recorded under Air Force Contracts AF33(616)-3356 and AF33(616)-7066 by the staff at Battelle Memorial Institute. By placing automatic time-history recorders in selected

operational aircraft of the Strategic Air Command, they are determining engine ground run power settings in operational use over periods of about one year. Although their investigation is still in progress, much of their summarized data was provided for background information for this study. The engine ground run times, included in the Phase I mission profiles were adjusted to bring them in line with these pertinent operational data. The revised engine ground run utilizations, as derived from the modified mission outlines, are summarized in Table 1.

A further factor which emerged during the investigation was the effect of ambient temperature conditions on engine performance and acoustic power levels generated during high-power engine ground runs. On a cold day takeoff, the generated sound power can be as much as twice that for a standard day takeoff even with the throttle settings restricted within normal engine operating limits. Warm day takeoffs, with many air vehicle designs, call for the use of thrust augmentation devices such as water-alcohol injection or JATO which, again, may raise or alter the acoustic environment expected for standard day takeoffs. A lifetime acoustic environment, then, computed for assumed standard conditions, might be unduly conservative; the determination of whether the air vehicles based in a cold climate or those based in a hot climate are subjected to a more severe acoustic environment depends on individual design factors. The solution is to compute, for each design, the expected lifetime fatigue for an air vehicle based in each extreme climate and then selecting the more severe situation as the design environment for sonic fatigue.

Figure 5 shows the range of average monthly temperatures for representative sites within the U.S. throughout the year. The average temperatures of Yuma and Fairbanks are considered extreme, and therefore, enclose the average temperature curves of the 15 Air Force base locations in the U.S. which were checked as well as the curves for 12 cities in Europe, North Africa, and Asia. The more extreme temperature maxima and minima are also of interest. The long-term temperature maximum for Yuma and the long-term minimum for Fairbanks are also shown in figure 5 . The length of time that the temperatures stay at these extremes is small. For example, although the 34-year low extreme for Fairbanks is -66°F, temperatures of less than -60°F have been recorded for a total of only 2 hours during the last 14 years, and temperatures of less than -40°F occur only about 4 percent of the time during January.

Table 2 presents the percent of time of occurrence of given temperature intervals at two bases, based on the temperatures occurring at Yuma and Fairbanks, respectively. A hot climate base and a cold climate base are shown, rather than an average base or a numerical average of the two sets of temperatures, in order to retain a representation of the extreme temperatures. An average base, say in the midcontinent of the U.S., would not exhibit either the high or the low extreme temperatures, and an average of the temperatures of of the two given bases would not be typical of any actual base. It is possible

ENGINE GROUND RUN SUMMARY

HOURS PER 1000 FLIGHT HOURS

Air Vehicle Classification	Power Setting				
	IDLE	80-90%	MILITARY	MAX (Static)	Takeoff
Intercept Fighter	267.33	27.71	6.63	5.91	7.26
			12.54	13.17	
Tactical Fighter	250.72	24.76	5.86	5.21	6.52
			11.07	12.73	
Strategic Attack	98.85	11.35	2.05	1.89	1.58
			3.94	3.47	
Tactical Attack	214.33	30.01	4.71	4.29	4.29
			9.00	8.58	
Cargo Transport	190.05	22.00	3.97	3.67	4.89
			7.64	8.56	
Helicopter	242.00	75.60	10.00	8.89	6.67
			18.89	15.56	

314.84

267.33
27.71
6.63
5.91
7.26
314.84 ground time per 1000 flight hrs.

6.52 TO
11.07 Grnd.

5
300

Table 1 . ENGINE GROUND RUN SUMMARY

YEAR ROUND AVERAGE TEMPERATURES
AT
REPRESENTATIVE BASE SITES

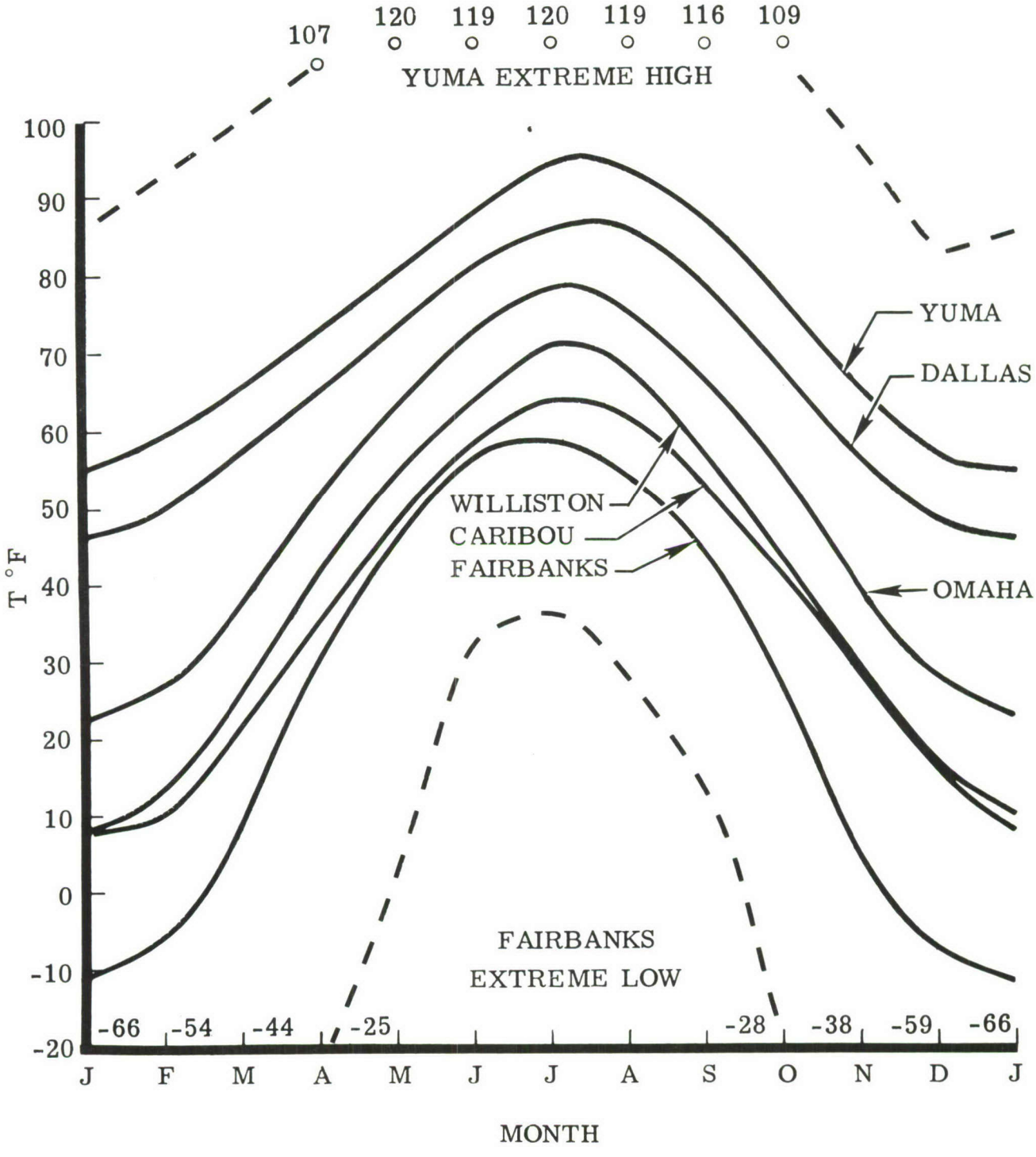

Figure 5 . Average Temperatures

ENGINE GROUND RUN AMBIENT CONDITIONS

Temp Span (°F)*	Percentage of Total Time	
	Hot Climate Base (Yuma, Ariz.)	Cold Climate Base (Fairbanks, Alaska)
105 - 120	3.5%	
85 - 104	22.0%	0.3%
65 - 84	26.0%	6.0%
45 - 64	39.0%	18.0%
25 - 44	9.0%	22.0%
5 - 24	0.5%	24.0%
-15 - +4		20.0%
-35 - -16		8.0%
-55 - -36		1.5%
-65 - -56		0.2%

*In applying these data to environment computations, the mean temperature of each of these spans should be used, as was done in Table 25.

Table 2 . Engine Ground Run Ambient Conditions

that one synthetic temperature distribution would serve for a design criterion, but it is felt that a more realistic approach would be to use the two extreme distributions side-by-side.

The temperatures given are based on full 24-hour records. It is felt probable that the city temperatures recorded should be adjusted upward from 10°F to 20°F to better reflect engine operating conditions, because engine runups are likely to be conducted predominantly on sun-heated aprons and runways. This adjustment was not attempted in this study, for the two extreme climates selected, because of a lack of available data.

Because flight operations (selection of cruise altitude, speed, etc) are normally adjusted to suit the immediate conditions of temperature-pressure, it would be much more difficult to take account of climatological variations in this portion of the lifetime utilization of an air vehicle. It is not considered worthwhile to attempt a refinement to account for this for acoustic environment computations, so a standard atmosphere is assumed for in-flight portions of the mission outlines.

2.2 MISSION OUTLINES

Mission outlines for the various types of air vehicles under consideration are given in Tables 3 through 19. Three missions each are given for the first four types. Two missions are considered adequate to describe the utilization of cargo transports, the fifth type, and a single mission each is given for helicopters, surface- and air-launched missiles, and drones.

As discussed in paragraph 2.1, it is felt that lifetime utilizations of the last four types are determined by individual design performance and that generalized definitions are neither warranted nor feasible within the scope of this study. Therefore, the mission outlines for the helicopters and unmanned air vehicles are brief and leave more to the designer's discretion in establishing expected lifetime utilization.

The mission outlines in Tables 3 through 19 are fairly definitive, giving total mission times, as well as all engine ground run times, and a sequence of flight operations. The principal items left for the designer to supply are the details of design speed and altitude performance. These missions are representative of the utilization each type of air vehicle will experience and, if filled in by the designer, will provide a usable summary of the life utilization of the air vehicle. They are intended, however, as a guide rather than as an arbitrary definition of usage for every design. In the example presented in Section VI, it was found desirable to make minor alterations in one of the profiles, and it is expected that similar variations may be used for the individual designs to which this method is applied.

The designer should select the set of mission outlines most appropriate to his design; insert climb, combat, and descent times; altitudes and speeds which are compatible with the air vehicle performance; and balance out the remainder of the time for each mission with cruise conditions. The method of computation of cumulative hours of each mission with cruise conditions. The method of computation of cumulative hours of each operation per 1000 flying hours is indicated on the mission outlines. Finally, the conditions of similar acoustic environment from each of the three completed missions may be summed and the climate distributions applied to ground operations as described in paragraph 2.1. The result is a summary of times at each significant set of acoustic environment conditions, related to 1000 hours of flight life. The total design flight-life may be from 2,000 to 30,000 flight hours and is a matter for contractual specification for each design. For an intercept fighter with a design life of 3000 hours, all the times given in Table 1 should be multiplied by 3 to reflect the total operational lifetime.

INTERCEPT FIGHTER - MISSION A

HIGH-ALTITUDE INTERCEPT
WEAPONS LOAD ON 55 PERCENT OF THESE MISSIONS
WEAPON RELEASE CYCLES ON 30 PERCENT OF THESE MISSIONS

Oper No. (i)	Operation Description	Power Setting (Note 1.)	Operation Min/Mission (t_{ai})	Mean Alt	Mean A/S	Operation Hr/1000 Flt Hr (Note 2.)
1.	Engine Start	IDLE	1.00	S. L.	0	8.47
2.	Taxi out + Taxi in and Park	IDLE	7.00	S. L.	0	59.2
		80-90%	1.50	S. L.	0	12.7
3.	Power Check	MIL	.0.05	S. L.	0	0.42
4.	Pre T. O. Interval	IDLE	2.00	S. L.	0	16.94
5.	Take off	MAX	.0.50	S. L.		4.23
6.	Accelerate	MIL				
7.	Climb to Best Cruise Alt and A/S	MIL				
8.	Cruise - Climb	CRUISE				
9.	Acceleration and Climb to Combat Alt and A/S	MAX				
10.	Combat	MAX				
11.	Descend to Best Cruise Alt and A/S	IDLE				
12.	Cruise - Climb	CRUISE				
13.	Descend for Landing	IDLE				
14.	Landing	IDLE				
15.	Maintenance	IDLE	8.40	S. L.	0	71.10
		80-90%	0.40	S. L.	0	3.48
		MIL	0.40	S. L.	0	3.48
		MAX	.0.40	S. L.	0	3.48
Mission A Flight Time ($T_{AF} = \sum_{5}^{14} t_{ai}$)			65.00			550
Mission A Total Oper Time ($T_{AO} = \sum_{1}^{15} t_{ai}$)			86.65			734

NOTES: 1. Max settings within all operating limits
2. Operation hours per 1000 flight hours = (t_{ai}/T_{AF}) 550 hr = $8.47(t_{ai})$

Table 3 . INTERCEPT FIGHTER - MISSION A

INTERCEPT FIGHTER - MISSION B

MEDIUM-ALTITUDE INTERCEPT
WEAPONS LOAD ON 50 PERCENT OF THESE MISSIONS
WEAPON RELEASE CYCLES ON 30 PERCENT OF THESE MISSIONS

Oper No. (i)	Operation Description	Power Setting (Note 1.)	Operation Min/Mission (t_{bi})	Mean Alt	Mean A/S	Operation Hr/1000 Flt Hr (Note 2.)
1.	Engine Start	IDLE	1.00	S. L.	0	3.85
2.	Taxi out + Taxi in and Park	IDLE	7.00	S. L.	0	26.90
		80-90%	1.50	S. L.	0	5.77
3.	Power Check	MIL	0.05	S. L.	0	0.19
4.	Pre T. O. Interval	IDLE	2.00	S. L.	0	7.69
5.	Take off	MAX	0.50	S. L.		1.92
6.	Accelerate	MAX				
7.	Climb to Best Cruise Alt and A/S	MAX				
8.	Cruise - Climb	CRUISE				
9.	Accelerate to Combat A/S	MAX				
10.	High-Speed Turns	MAX				
11.	Decelerate to Best Cruise	IDLE				
12.	Cruise - Climb	CRUISE				
13.	Descend for Landing	IDLE				
14.	Landing	IDLE				
15.	Maintenance	IDLE	8.40	S. L.	0	32.30
		80-90%	0.40	S. L.	0	1.54
		MIL	0.40	S. L.	0	1.54
		MAX	0.40	S. L.	0	1.54
Mission B Flight Time ($T_{BF} = \sum_{5}^{14} t_{bi}$)			65			250
Mission B Total Oper Time ($T_{BO} = \sum_{1}^{15} t_{bi}$)			86.65			333.5

NOTES: 1. Max settings within all operating limits.
2. Operation hours per 1000 flight hours = (t_{bi}/T_{BF}) 250 hr = 3.845 (t_{bi})

Table 4. INTERCEPT FIGHTER - MISSION B

INTERCEPT FIGHTER - MISSION C

TRANSITION

Oper No. (i)	Operation Description	Power Setting (Note 1.)	Operation Min/Mission	Mean Alt	Mean A/S	Operation Hr/1000 Flt Hr (Note 2.)
1.	Engine Start	IDLE	1.00	S. L.	0	2.22
2.	Taxi out + Taxi in and Park	IDLE	7.00	S. L.	0	15.55
		80-90%	1.50	S. L.	0	3.33
3.	Power Check	MIL	0.05	S. L.	0	0.11
4.	Pre T. O. Interval	IDLE	2.00	S. L.	0	4.44
5.	Take off	MAX	0.50	S. L.		1.11
6.	Accelerate	MIL				
7.	Climb to Best Cruise Alt and A/S	MIL				
8.	Cruise - Climb	CRUISE				
9.	Descend for Landing	IDLE				
10.	Landing	IDLE				
11.	Maintenance	IDLE	8.40	S. L.	0	18.67
		80-90%	0.40	S. L.	0	0.89
		MIL	0.40	S. L.	0	0.89
		MAX	0.40	S. L.	0	0.89
Mission C Flight Time ($T_{CF} = \Sigma_5^{10} t_{ci}$)			90			200
Mission C Total Oper Time ($T_{CO} = \Sigma_1^{11} t_{ci}$)			111.65			248

NOTES: 1. Max Settings Within All Operating Limits.
2. Operation Hours per 1000 flight hours = (t_{ci}/T_{CF}) 200 hr = 2.22 (t_{ci})

Table 5 . INTERCEPT FIGHTER - MISSION C

TACTICAL FIGHTER - MISSION A

LOW-LEVEL BOMBING
WEAPONS LOAD ON 30 PERCENT OF THESE MISSIONS
WEAPON RELEASE CYCLES ON 25 PERCENT OF THESE MISSIONS

Oper No. (i)	Operation Description	Power Setting (Note 1.)	Operation Min/Mission (t_{ai})	Mean Alt	Mean A/S	Operation Hr/1000 Flt Hr (Note 2.)
1.	Engine Start	IDLE	1.00	S. L.	0	4.62
2.	Taxi out + Taxi in and Park	IDLE	7.00	S. L.	0	32.34
		80-90%	1.50	S. L.	0	6.93
3.	Power Check	MIL	0.05	S. L.	0	0.23
4.	Pre T. O. Interval	IDLE	3.00	S. L.	0	13.86
5.	Take off	MAX	0.50	S. L.		2.31
6.	Accelerate to Climb Speed	MIL				
7.	Climb to Best Cruise Altitude	MIL				
8.	Cruise	CRUISE				
9.	Descend to Target Area	85%				
10.	Combat	MAX				
11.	Climb to Best Cruise Altitude	MIL				
12.	Cruise	CRUISE				
13.	Descend to Sea Level to Land	IDLE				
14.	Landing	IDLE				
15.	Maintenance	IDLE	8.40	S. L.	0	38.81
		80-90%	0.40	S. L.	0	1.84
		MIL	0.40	S. L.	0	1.84
		MAX	0.40	S. L.	0	1.84
Mission A Flight Time ($T_{AF} = \sum_{5}^{14} t_{ai}$)			65			300
Mission A Total Oper Time ($T_{AO} = \sum_{1}^{15} t_{ai}$)			87.65			405

NOTES: 1. Max power settings within all operating limits
2. Operation hours per 1000 flight hours = (t_{ai}/T_{AF}) 300 hr = 4.62 (t_{ai})

Table 6. TACTICAL FIGHTER - MISSION A

TACTICAL FIGHTER - MISSION B

TRANSITION
WEAPONS LOAD ON 30 PERCENT OF THESE MISSIONS
WEAPON RELEASE CYCLES ON 25 PERCENT OF THESE MISSIONS

Oper No. (i)	Operation Description	Power Setting (Note 1.)	Operation Min/Mission (t_{bi})	Mean Alt	Mean A/S	Operation Hr/1000 Flt Hr (Note 2.)
1.	Engine Start	IDLE	1.00	S. L.	0	5.55
2.	Taxi out + Taxi in and Park	IDLE	7.00	S. L.	0	38.85
		80-90%	1.50	S. L.	0	8.25
3.	Power Check	MIL	0.05	S. L.	0	0.28
4.	Pre T. O. Interval	IDLE	3.00	S. L.	0	16.65
5.	Take off	MAX	0.50	S. L.		2.78
6.	Accelerate to Climb Speed	MAX				
7.	Climb to Best Cruise Altitude	MAX				
8.	Cruise Climb	CRUISE				
9.	Accelerate to Combat	MAX				
10.	High-Speed Turns	MAX				
11.	Descend to Land	IDLE				
12.	Landing	IDLE				
13.	Maintenance	IDLE	8.40	S. L.	0	40.62
		80-90%	0.40	S. L.	0	2.22
		MIL	0.40	S. L.	0	2.22
		MAX	0.40	S. L.	0	2.22
Mission B Flight Time ($T_{BF} = \sum_{5}^{12} t_{bi}$)			90			500
Mission B Total Oper Time ($T_{BO} = \sum_{1}^{13} t_{bi}$)			112.65			625

NOTES: 1. Max power settings within all operating limits
2. Operation hours per 1000 flight hours = (t_{bi}/T_{BF}) 500 hr = 5.55 (t_{bi})

Table 7. TACTICAL FIGHTER - MISSION B

TACTICAL FIGHTER - MISSION C

CLOSE SUPPORT
WEAPONS LOAD ON 30 PERCENT OF THESE MISSIONS
WEAPON RELEASE CYCLES ON 25 PERCENT OF THESE MISSIONS

Oper No. (i)	Operation Description	Power Setting (Note 1.)	Operation Min/Mission (t_{ai})	Mean Alt	Mean A/S	Operation Hr/1000 Flt Hr (Note 2.)
1.	Engine Start	IDLE	1.00	S. L.	0	2.86
2.	Taxi out + Taxi in and Park	IDLE	7.00	S. L.	0	20.00
		80-90%	1.50	S. L.	0	4.29
3.	Power Check	MIL	0.05	S. L.	0	0.14
4.	Pre T. O. Interval	IDLE	3.00	S. L.	0	8.58
5.	Take off	MAX	0.50	S. L.		1.43
6.	Accelerate to Climb Speed	MIL				
7.	Accelerate and Climb to Low Combat	MAX				
8.	Combat	MAX				
9.	Climb to Best Cruise Altitude	MIL				
10.	Cruise	CRUISE				
11.	Descend to Low Combat	85%				
12.	Combat	MAX				
13.	Descend to Land	IDLE				
14.	Landing	IDLE				
15.	Maintenance	IDLE	8.40	S. L.	0	24.00
		80-90%	0.40	S. L.	0	1.14
		MIL	0.40	S. L.	0	1.14
		MAX	0.40	S. L.	0	1.14
Mission C Flight Time ($T_{CF} = \sum_{5}^{14} t_{ci}$)			70			200
Mission C Total Oper Time ($T_{CO} = \sum_{1}^{15} t_{ci}$)			92.65			265

NOTES: 1. Max power settings within all operating limits
2. Operation hours per 1000 flight hours = (t_{ci}/T_{CF}) 200 hr = 2.86 (t_{ci})

Table 8 . TACTICAL FIGHTER - MISSION C

STRATEGIC ATTACK - MISSION A

HIGH-ALTITUDE BOMBING
WEAPON RELEASE CYCLES ON 75 PERCENT OF THESE MISSIONS

Oper No. (i)	Operation Description	Power Setting (Note 1.)	Operation Min/Mission (t_{ai})	Mean Alt	Mean A/S	Operation Hr/1000 Flt Hr (Note 2.)
1.	Engine Start	IDLE	1.5	S. L.	0	2.29
2.	Taxi out + Taxi in and	IDLE	14.0	S. L.	0	21.40
	Park	80-90%	3.0	S. L.	0	4.58
3.	Power Check	MIL	0.05	S. L.	0	0.0764
4.	Pre T. O. Interval	IDLE	3.0	S. L.	0	4.58
5.	Take off	MAX	0.5	S. L.		0.764
6.	Accelerate	MIL				
7.	Climb to Best Cruise Alt and A/S	MIL				
8.	Cruise - Climb	CRUISE				
9.	Accelerate and Climb to Operating Alt	MAX				
10.	High-Speed Cruise	MAX				
11.	Descend to Best Cruise Alt and A/S	IDLE				
12.	Cruise - Climb	CRUISE				
13.	Descend for Landing	IDLE				
14.	Landing	IDLE				
15.	Maintenance	IDLE	12.6	S. L.	0	19.23
		80-90%	0.6	S. L.	0	0.916
		MIL	0.6	S. L.	0	0.916
		MAX	0.6	S. L.	0	0.916
Mission A Flight Time ($T_{AF} = \sum_{5}^{14} t_{ai}$)			360			550
Mission A Total Oper Time ($T_{AO} = \sum_{i=1}^{15} t_{ai}$)			397.85			608

NOTES: 1. Max power settings within all operating limits
2. Operation hours per 1000 flight hours =

$$\left(\frac{t_{ai}}{T_{AF}}\right) 550 \text{ hr} = 1.528\ (t_{ai})$$

Table 9 . STRATEGIC ATTACK - MISSION A

STRATEGIC ATTACK - MISSION B

TRANSITION

Oper No. (i)	Operation Description	Power Setting (Note 1.)	Operation Min/Mission (t_{bi})	Mean Alt	Mean A/S	Operation Hr/1000 Flt Hr (Note 2.)
1.	Engine Start	IDLE	1.5	S. L.	0	1.50
2.	Taxi out + Taxi in and Park	IDLE	14.0	S. L.	0	14.00
		80-90%	3.0	S. L.	0	3.00
3.	Power Check	MIL	0.05	S. L.	0	0.05
4.	Pre T. O. Interval	IDLE	3.0	S. L.	0	3.00
5.	Take off	MAX	0.05	S. L.		0.50
6.	Accelerate	MAX				
7.	Climb to Intermediate Alt	MAX				
8.	Accelerate to High Speed	MAX				
9.	High-Speed Climb	MAX				
10.	Max Speed Cruise - Climb	MAX				
11.	Descend to Best Cruise Altitude and A/S	IDLE				
12.	Cruise - Climb	CRUISE				
13.	Descend for Landing	IDLE				
14.	Landing	IDLE				
15.	Maintenance	IDLE	12.6	S. L.	0	12.60
		80-90%	0.6	S. L.	0	0.60
		MIL	0.6	S. L.	0	0.60
		MAX	0.6	S. L.	0	0.60
Mission B Flight Time ($T_{BF} = \sum_{5}^{14} t_{bi}$)			300			300
Mission B Total Oper Time ($T_{BO} = \sum_{1}^{15} t_{bi}$)			337.85			337.85

NOTES: 1. Max settings within all operating limits.
2. Operation hours per 1000 flight hours = $\left(\frac{t_{bi}}{T_{BF}}\right)$ 300 hr = (t_{bi})

Table 10 . STRATEGIC ATTACK - MISSION B

STRATEGIC ATTACK - MISSION C

LOW STRIKE
WEAPON RELEASE CYCLES ON 75 PERCENT OF THESE MISSIONS

Oper No. (i)	Operation Description	Power Setting (Note 1.)	Operation Min/Mission (t_{ci})	Mean Alt	Mean A/S	Operation Hr/1000 Flt Hr (Note 2.)
1.	Engine Start	IDLE	1.5	S. L.	0	0.938
2.	Taxi out + Taxi in and Park	IDLE	14.0	S. L.	0	8.75
		80-90%	3.0	S. L.	0	1.875
3.	Power Check	MIL	0.05	S. L.	0	0.0313
4.	Pre T. O. Interval	IDLE	3.0	S. L.	0	1.875
5.	Take off	MAX	0.5	S. L.	0	0.3125
6.	Accelerate	MIL				
7.	Climb to Best Cruise Alt and A/S	MIL				
8.	Cruise - Climb	CRUISE				
9.	Descend to Combat Alt	85%				
10.	Low-Alt Combat	MAX				
11.	Climb to Best Cruise Alt and A/S	MIL				
12.	Cruise - Climb	CRUISE				
13.	Descend for Landing	IDLE				
14.	Landing	IDLE				
15.	Maintenance	IDLE	12.6	S. L.	0	8.50
		80-90%	0.6	S. L.	0	0.375
		MIL	0.6	S. L.	0	0.375
		MAX	0.6	S. L.	0	0.375
Mission C Flight Time ($T_{CF} = \sum_{5}^{14} t_{ci}$)			240			150
Mission C Total Oper Time ($T_{CO} = \sum_{1}^{15} t_{ci}$)			277.85			173.6

NOTES: 1. Max settings within all operating limits.
2. Operation hours per 100 flight hours = $(t_{ci}/T_{CF})150$ hr = 0.625 (t_{ci})

Table 11 . STRATEGIC ATTACK - MISSION C

TACTICAL ATTACK - MISSION A

LOW STRIKE
WEAPON RELEASE CYCLES ON 50 PERCENT OF THESE MISSIONS

Oper No. (i)	Operation Description	Power Setting (Note 1.)	Operation Min/Mission (t_{ai})	Mean Alt	Mean A/S	Operation Hr/1000 Flt Hr (Note 2.)
1.	Engine Start	IDLE	1.50	S.L.	0	6.67
2.	Taxi out + Taxi in and Park	IDLE	10.00	S.L.	0	44.50
		80-90%	3.00	S.L.	0	13.33
3.	Power Check	MIL	0.05	S.L.	0	0.23
4.	Pre T.O. Interval	IDLE	3.00	S.L.	0	13.33
5.	Take off	MAX	0.50	S.L.		2.28
6.	Accelerate to Climb Speed	MIL				
7	Climb to Best Cruise Altitude	MIL				
8.	Cruise	CRUISE				
9.	Descend to Target Altitude	85%				
10.	Combat	MAX				
11.	Climb to Best Cruise Altitude	MIL				
12.	Cruise	CRUISE				
13.	Descend for Landing	IDLE				
14.	Landing	IDLE				
15.	Maintenance	IDLE	10.50	S.L.	0	46.80
		80-90%	0.50	S.L.	0	2.28
		MIL	0.50	S.L.	0	2.28
		MAX	0.50	S.L.	0	2.28
Mission A Flight Time ($T_{AF} = \sum_{5}^{14} t_{ai}$)			90			400
Mission A Total Oper Time ($T_{AO} = \sum_{1}^{15} t_{ai}$)			120.05			536

NOTES: 1. Max power settings within all operating limits
2. Operation hours per 1000 flight hours = (t_{ai}/T_{AF}) 400 hours = 4.45 (t_{ai})

Table 12 . TACTICAL ATTACK - MISSION A

TACTICAL ATTACK - MISSION B

HIGH-ALTITUDE BOMBING
WEAPON RELEASE CYCLES ON 50 PERCENT OF THESE MISSIONS

Oper No. (i)	Operation Description	Power Setting (Note 1.)	Operation Min/Mission (t_{bi})	Mean Alt	Mean A/S	Operation Hr/1000 Flt Hr (Note 2.)
1.	Engine Start	IDLE	1.50	S. L.	0	4.62
2.	Taxi out + Taxi in and Park	IDLE	10.00	S. L.	0	30.80
		80-90%	3.00	S. L.	0	9.24
3.	Power Check	MIL	0.05	S. L.	0	0.15
4.	Pre T. O. Interval	IDLE	3.00	S. L.	0	9.24
5.	Take off	MAX	0.50	S. L.		1.54
6.	Accelerate to Climb Speed	MIL				
7.	Climb to Cruise	MIL				
8.	Cruise - Climb	CRUISE				
9.	Climb to High Cruise Altitude	MIL				
10.	Cruise - Climb	CRUISE				
11.	Combat	MAX				
12.	Descend to Sea Level	IDLE				
13.	Landing	IDLE				
14.	Maintenance	IDLE	10.50	S. L.	0	32.40
		80-90%	0.50	S. L.	0	1.54
		MIL	0.50	S. L.	0	1.54
		MAX	0.50	S. L.	0	1.54
Mission B Flight Time ($T_{BF} = \sum_{5}^{13} t_{bi}$)			130			400
Mission B Total Oper Time ($T_{BO} = \sum_{1}^{14} t_{bi}$)			160.05			494

NOTES: 1. Max power settings within all operating limits
2. Operation hours per 1000 flight hours = (t_{bi}/T_{BF}) 400 hr = 3.08 (t_{bi})

Table 13 . TACTICAL ATTACK - MISSION B

TACTICAL ATTACK - MISSION C

HIGH-ALTITUDE BOMBING
WEAPON RELEASE CYCLES ON 50 PERCENT OF THESE MISSIONS

Oper No. (i)	Operation Description	Power Setting (Note 1.)	Operation Min/Mission (t_{ci})	Mean Alt	Mean A/S	Operation Hr/1000 Flt Hr (Note 2.)
1.	Engine Start	IDLE	1.50	S.L.	0	1.58
2.	Taxi out + Taxi in and Park	IDLE	10.00	S.L.	0	10.5
		80-90%	3.00	S.L.	0	3.15
3.	Power Check	MIL	0.05	S.L.	0	0.05
4.	Pre T.O. Interval	IDLE	3.00	S.L.	0	3.15
5.	Take off	MAX	0.50	S.L.		0.53
6.	Accelerate to Climb Speed	MIL				
7.	Climb to Best Cruise Altitude	MIL				
8.	Cruise - Climb	CRUISE				
9.	Descend for Landing	IDLE				
10.	Landing	IDLE				
11.	Maintenance	IDLE	10.50	S.L.	0	11.03
		80-90%	0.50	S.L.	0	0.53
		MIL	0.50	S.L.	0	0.53
		MAX	0.50	S.L.	0	0.53
Mission C Flight Time ($T_{CF} = \sum_{5}^{10} t_{ci}$)			190			200
Mission C Total Oper Time ($T_{CO} = \sum_{1}^{11} t_{ci}$)			220.05			232

NOTES: 1. Max power settings within all operating limits
2. Operation hours per 1000 flight hours = (t_{ci}/T_{CF}) 200 hr = 1.05 (t_{ci})

Table 14. TACTICAL ATTACK - MISSION C

CARGO TRANSPORT - MISSION A

SHORT LIFT
NORMAL OPERATIONAL CONFIGURATION

Oper No. (i)	Operation Description	Power Setting (Note 1.)	Operation Min/Mission (t_{ai})	Mean Alt	Mean A/S	Operation Hr/1000 Flt Hr (Note 2.)
1.	Engine Start	IDLE	1.5	S. L.	0	7.50
2.	Taxi out + Taxi in and Park	IDLE	14.0	S. L.	0	70.0
		80-90%	3.0	S. L.	0	15.00
3.	Power Check	MIL	0.05	S. L.	0	0.25
4.	Pre T. O. Interval	IDLE	3.0	S. L.	0	15.00
5.	Take off	MAX	0.8	S. L.		4.00
6.	Accelerate to Climb Speed	MIL				
7.	Climb to Best Cruise Altitude					
8.	Cruise	CRUISE				
9.	Descend for Landing	IDLE				
10.	Landing	IDLE				
11.	Maintenance	IDLE	12.60	S. L.	0	63.00
		80-90%	0.60	S. L.	0	3.00
		MIL	0.60	S. L.	0	3.00
		MAX	0.60	S. L.	0	3.00
Mission A Flight Time ($T_{AF} = \sum_{5}^{10} t_{ai}$)			120			600
Mission A Total Oper Time ($T_{AO} = \sum_{1}^{11} t_{ai}$)			156.75			782

NOTES: 1. Max power settings within all operating limits
2. Operation hours per 1000 flight hours = (t_{ai}/T_{AF}) 600 hr = 5.00 (t_{ai})

Table 15 . CARGO TRANSPORT - MISSION A

CARGO TRANSPORT - MISSION B

LONG RANGE LIFT
NORMAL OPERATIONAL CONFIGURATION

Oper No. (i)	Operation Description	Power Setting (Note 1.)	Operation Min/Mission (t_{bi})	Mean Alt	Mean A/S	Operation Hr/1000 Flt Hr (Note 2.)
1.	Engine Start	IDLE	1.50	S.L.	0	1.67
2.	Taxi out + Taxi in and	IDLE	14.00	S.L.	0	15.53
	Park	80-90%	3.00	S.L.	0	3.33
3.	Power Check	MIL	0.05	S.L.	0	0.06
4.	Pre T.O. Interval	IDLE	3.00	S.L.	0	3.33
5.	Take off	MAX	0.80	S.L.	0	0.89
6.	Accelerate to Climb Speed	MIL				
7.	Climb to Cruise	MIL				
8.	Cruise - Climb	CRUISE				
9.	Climb to Best Cruise Altitude	MIL				
10.	Cruise	CRUISE				
11.	Descend for Landing	IDLE				
12.	Landing	IDLE				
13.	Maintenance	IDLE	12.60	S.L.	0	13.99
		80-90%	0.60	S.L.	0	0.67
		MIL	0.60	S.L.	0	0.67
		MAX	0.60	S.L.	0	0.67
Mission B Flight Time ($T_{BF} = \sum_{5}^{12} t_{bi}$)			360			400
Mission B Total Oper Time ($T_{BO} = \sum_{1}^{13} t_{bi}$)			396.75			440

NOTES: 1. Max power settings within all operating limits
2. Operation hours per 1000 flight hours = (t_{bi}/T_{BF}) 400 hr = 1.11 (t_{bi})

Table 16 . CARGO TRANSPORT - MISSION B

HELICOPTER MISSION

AIRLIFT
NORMAL OPERATIONAL CONFIGURATION

Oper No. (i)	Operation Description	Power Setting (Note 1.)	Operation Min/Mission (t_{ai})	Mean Alt	Mean A/S	Operation Hr/1000 Flt Hr (Note 2.)
1.	Engine Start	IDLE	1.00	S. L.	0	22.20
2.	Taxi out + Taxi in and Park	IDLE	1.50	S. L.	0	33.30
		80-90%	3.00	S. L.	0	66.60
3.	Power Check	MIL	0.05	S. L.	0	1.11
4.	Lift Off and Climb	MAX	0.30	S. L.		6.66
5.	Cruise	CRUISE				
6.	Hover	MIL				
7.	Climb	MAX				
8.	Cruise	CRUISE				
9.	Descent	85-90%				
10.	Touchdown	MIL				
11.	Maintenance	IDLE	8.40	S. L.	0	186.50
		80-90%	0.40	S. L.	0	8.88
		100%	0.40	S. L.	0	8.88
Mission A Flight Time ($T_{AF} = \sum_{4}^{10} t_{ai}$)			45			1000
Mission A Total Oper Time ($T_{AO} = \sum_{1}^{11} t_{ai}$)			59.55			1325

NOTES: 1. Max power settings within all operating limits
2. Operation hours per 1000 flight hours = (t_{ai}/T_{AF}) 1000 hr = 22.2 (t_{ai})

Table 17 . HELICOPTER MISSION

DRONE - MISSION A

TARGET TRAINING

Oper No. (i)	Operation Description	Power Setting (Note 1.)	Operation Min/Mission (t_{ai})	Mean Alt	Mean A/S	Operation Hr/1000 Flt Hr (Note 2.)
1.	Engine Start					
2.	Taxi out + Taxi in and Park					
3.	Power Check					
4.	Pre T.O. Interval					
5.	Take off					
6.	Accelerate to Climb Speed					
7.	Climb to Cruise					
8.	Cruise					
9.	Maneuver at Operating Altitude					
10.	Descend to Land					
11.	Landing					
12.	Maintenance					
Mission A Flight Time ($T_{AF} = \sum_{5}^{11} t_{ai}$)						1000
Mission A Total Oper Time ($T_{AO} = \sum_{1}^{12} t_{ai}$)						

NOTE: 1. Max power settings within all operating limits
2. Operation hours per 1000 flight hours = (t_{ai}/T_{AF}) 1000 hr = (t_{ai})

Table 18. DRONE - MISSION A

SURFACE-LAUNCHED MISSILE MISSION

Oper No. (1)	Operation Description	Power Setting	Operation Time (Minutes)	Mean Alt	Mean A/S
1.	Engine Maintenance Ground Runs				
2.	Prelaunch Run Up				
3.	Launch and Boost				
4.	Climb				
5.	Cruise				
6.	Target Run				

AIR-LAUNCHED MISSILE MISSION

Oper No. (i)	Operation Description	Power Setting	Operation Time (Minutes)	Mean Alt	Mean A/S
1.	Engine Maintenance Test Stand Runs				
2.	Captive Flights	(Note 1.)			
3.	Launch				
4.	Target Run				

NOTE: 1. Use mission outlines for parent aircraft to determine these portions of the environment.

Table 19 . SURFACE- AND AIR-LAUNCHED MISSILE MISSIONS

Section III

STRESS RESPONSE

3.0 STRESS RESPONSE

It is the purpose of this section to provide enough development of the dynamics of vibrating plates to support the discrete frequency life test method and the sine-random equivalence technique. Most of the method presented is the technique of Belcher, Van Dyck, and Eshleman, Reference 15.

Since the elements in airframe structure most susceptible to acoustically induced excitation are the external cover panels and the attached substructure, spars, ribs, or frames, the stress response of plates is the appropriate starting point. This is justified even when fatigue failures occur in the substructure, as is often the case, because the fatigue stressing of the substructure is usually induced by the high amplitude vibration of the skin panels.

3.1 STRESS RESPONSE TO ACOUSTIC LOADS AT RESONANCE

Acoustic pressures exert a load on exposed structure with instantaneous amplitudes which may vary randomly in time. The exhaust noise from a jet engine is such random source; it has a Gaussian distribution of instantaneous pressure variations, except that pure tone components may be detectable at more or less uniform intensities. The engine intake noise of jet engines has similar characteristics, with more pronounced line spectral quantities.

The analysis of structure subjected to random pressures is based on the approach of Miles, Reference 16 , who treated a linear oscillator having a single degree of freedom. Powell, Reference 17, has extended the methods to include several modes of vibration and spacial correlation. Powell's approach, however, requires more knowledge of the structure than is usually available. An extension of Miles work, in the direction of practicality, was made by Belcher, Van Dyck, and Eshlemen, Reference 15. Their stress ratio (random-to-sinusoidal) development is shown here and is taken directly from Reference 15 .

"At resonance, the mean-square stress response, $\overline{s_r^2}$, of a linear single-degree-of-freedom system having response frequency f_o, damping δ (fraction of critical damping), and stress response to unit static load s_o, to a random force of spectral density p_r (rms sound pressure squared in a one cycle-per-second bandwidth) is

$$\overline{s_r^2} = \frac{\pi}{4\delta} f_o s_o^2 p_r^2 \qquad (6)$$

"Similarly, for sinusoidal excitation

$$s_s^2 = \left(\frac{1}{2\delta}\right)^2 s_o^2 p_s^2 \tag{7}$$

where p_s is the rms sinusoidal excitation pressure. Elimination of s_o yields

$$\frac{s_r^2}{s_s^2} = f_o \pi \delta \frac{p_r^2}{p_s^2} \cdot \quad \text{(end of quote)} \tag{8}$$

Convenient and extremely useful results can be obtained from the aforementioned relationship. For equal mean square stress response,

$s_r^2 = s_s^2$

$$\frac{p_s^2}{p_r^2} = \pi f_o \delta \tag{9}$$

The logarithmic pressure ratio, sound pressure level, is defined as

$$SPL = 20 \log \frac{\text{pressure in dynes/cm}^2}{0.0002} \text{ db} \tag{10}$$

The pressure ratio of Equation (9) can be converted to a difference of sound pressure levels.

$$SPL_s - SPL_r = 10 \log \pi f_o \delta$$

For example: If $f_o = 75$ cps, and $\delta = 0.025$

$$SPL_s - SPL_r = 10 \log \pi + 10 \log (75)(0.025)$$

$$= 5 + 3 = 8 \text{ db}$$

which means that for a given spectrum level (SPL per cps by definition of spectrum level) of random noise, the siren pressure must be 8 db less than the spectrum pressure level in order to generate equal rms stress responses.

3.2 RATIO OF CRITICAL DAMPING

The response of the linear system at resonance is determined by its damping. The damping is usually expressed as a fraction of the critical damping:

$$\delta = \frac{c}{c_c}$$

As there exists no analytical means for the calculation of δ, it must be determined during test of the structure. Investigators generally separate damping into its components for discussion. Structural damping is due partly to internal friction of the material (hysteresis damping), but is mostly due to slip between components of the structure, as for example, at riveted joints. Viscous damping of the air over the surface results in energy being radiated back to the surrounding medium; this is termed as acoustical damping. When the fraction of critical damping is measured, as in a siren test, the value is the agregate of these three but is usually dominated by one of the latter two.

BANDWIDTH METHOD

A commonly used method for determining damping is by measurement of the bandwidth at the half-power point on a stress-frequency plot. The relationship

$$\delta = \frac{c}{c_c} = \frac{\Delta f}{2 f_o} \qquad (11)$$

is valid at this point. See figure 6.

DECAY RATE METHOD

The accuracy of the bandwidth method is often limited by nonlinear stress-load behavior. However, use can be made of the classical relationship of the damping ratio to the decay rate of the response when the driving force is removed. This technique is often used, e.g., by Burgess, Reference 18. Figure 7a shows the trace of a decaying voltage on an oscilloscope, and figure 7b shows the same phenomenon on a level recorder.

The following characteristics of a decaying signal are known. (Reference 18.) The ratio of amplitude change per cycle

$$\frac{(y_{n+1})_o}{(y_n)_o} = e^{-\Delta} \qquad (12)$$

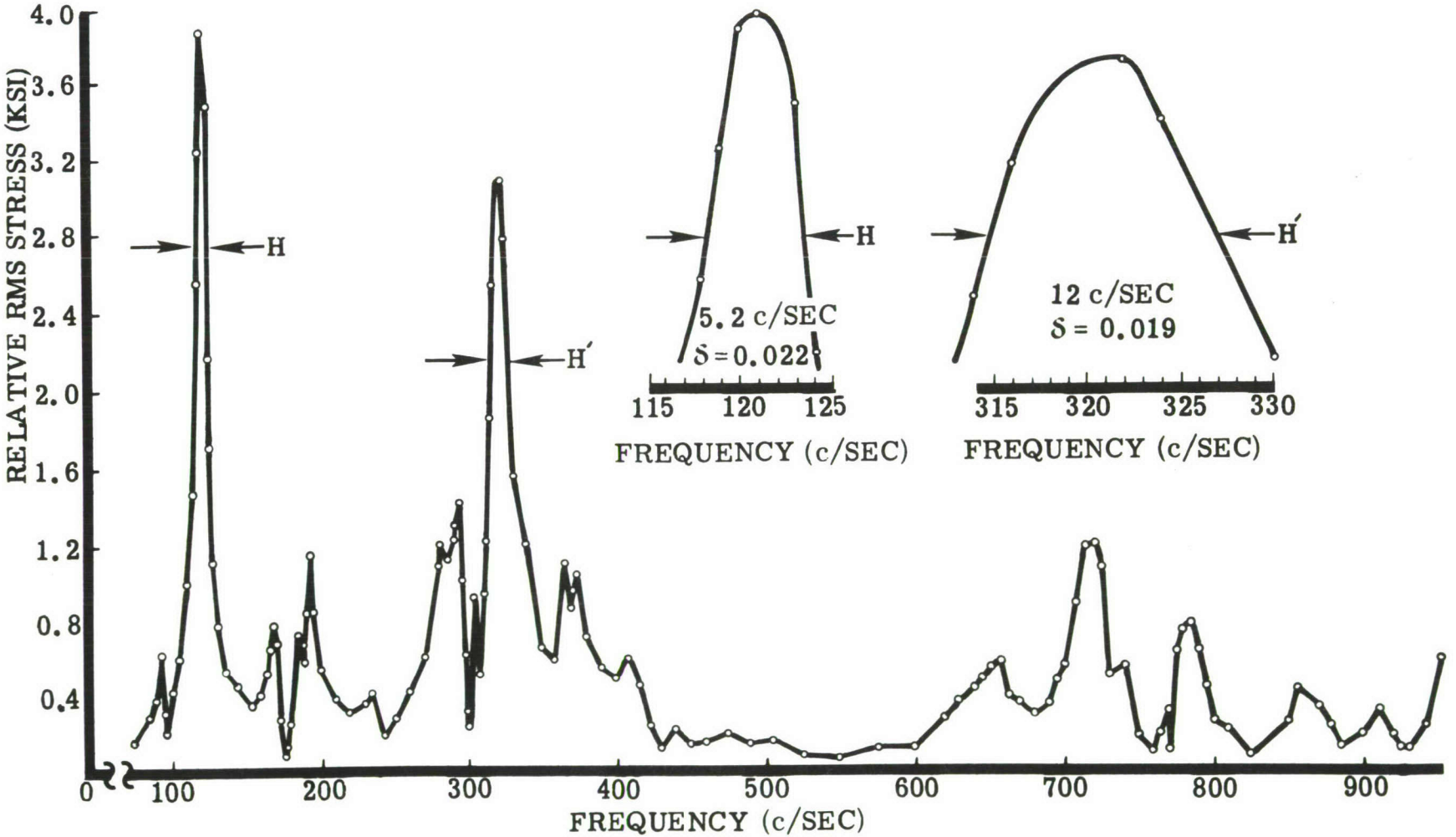

Figure 6 . Frequency Response Plot

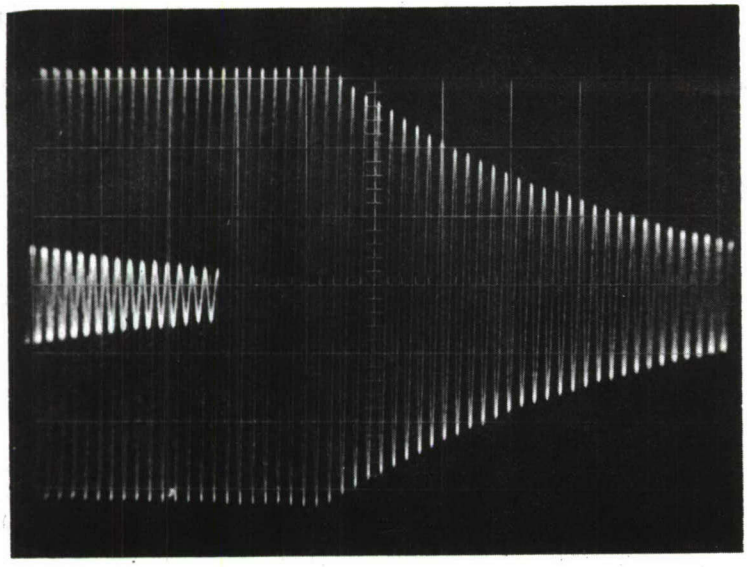

CHANGES IN DOUBLE AMPLITUDES FROM 5.8 TO 1.6 IN 31 CYCLES

AMPLITUDE DECAY = $\frac{20 \text{ LOG } \frac{5.8}{1.6}}{31}$ =

0.358 DB/ CYCLE

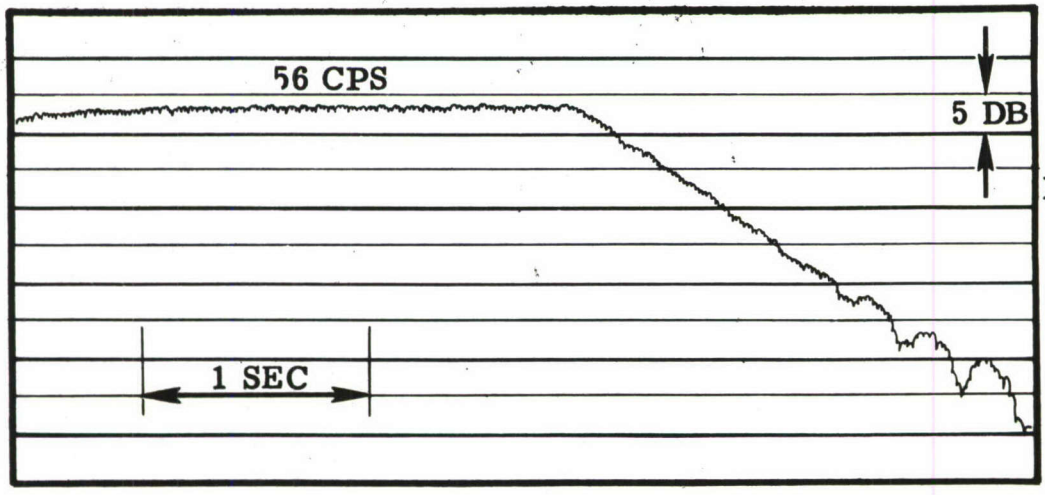

SIGNAL DECAY RATE = 21.5 DB/SEC

OR $\frac{21.5}{56}$ = 0.383 DB/ CYCLE

CALCULATED DAMPING COEFFICIENT RATIO = 0.0063 PER OSCILLOSCOPE
(Refer to Figure 8) = 0.0067 PER RECORDER

Figure 7 . Strain Gage Signal Decay Curves

$$\Delta = \frac{2\pi\left(\frac{c}{c_c}\right)}{1 - \left(\frac{c}{c_c}\right)^2} \qquad (13)$$

From this:

since $\frac{c}{c_c} \approx \frac{\Delta}{2\pi}$ as $\left(\frac{c}{c_c}\right) \ll 1$

Equations 12 and 13 are transformed into charts in figures 8 and 9 with amplitude ratios in db per cycle added for convenience.

3.3 NONLINEAR STRESS RESPONSE

Conventional skin-stringer construction exhibits nonlinearity in its stress response, often at relatively low stress levels. Sandwich construction because of its high bending stiffness, usually has a stress-load behavior which is approximately linear. The reason for the nonlinear behavior of the former is the diaphragm action which limits the amplitude of deflection of the vibrating plates. Thus, increases in sound pressure do not result in linear increases in the stress level of the panel.

Two observations could be made simultaneously during a response survey, using siren excitation, in order to determine the degree of nonlinearity in the behavior of a specimen. Figure 10 shows a composite plot of the information needed. Response in relative level of decibels is plotted against excitation level in figure 10. Linear conditions are shown as straight lines at 45-degree inclination; any deviation therefrom clearly indicates nonlinearity. In figure 10, the same response observation is plotted against the frequencies of excitation. At low excitation level, 100 db in the example shown, which produces a response that is approximately linear, the frequency plot shows the usual resonance peak at each modal frequency. As the excitation level is raised, to 140 db for instance, the resonance peaks for the modes exhibit drastic changes with different amounts of slope. Such apparent widening in response bandwidth, however, does not indicate an increase in damping, since the true response peak, unobtainable practically, should take the form 1-0′ -2-3 shown for the 1st mode in figure 10. One might intuitively consider an effective bandwidth to be obtainable from the equivalent linear system 1-0-3, point 0 being elevated in the same ratio as the increase in excitation level, in this case 40 db.

The above technique is useful in exhibiting the character of nonlinear response. For the purpose of calculating a correction factor to apply to the stress Equation (8), it is more convenient to plot the stress against sound pressure level, as in figure 11. A discussion of the curve and the calculation of the correction factor is included in Section V.

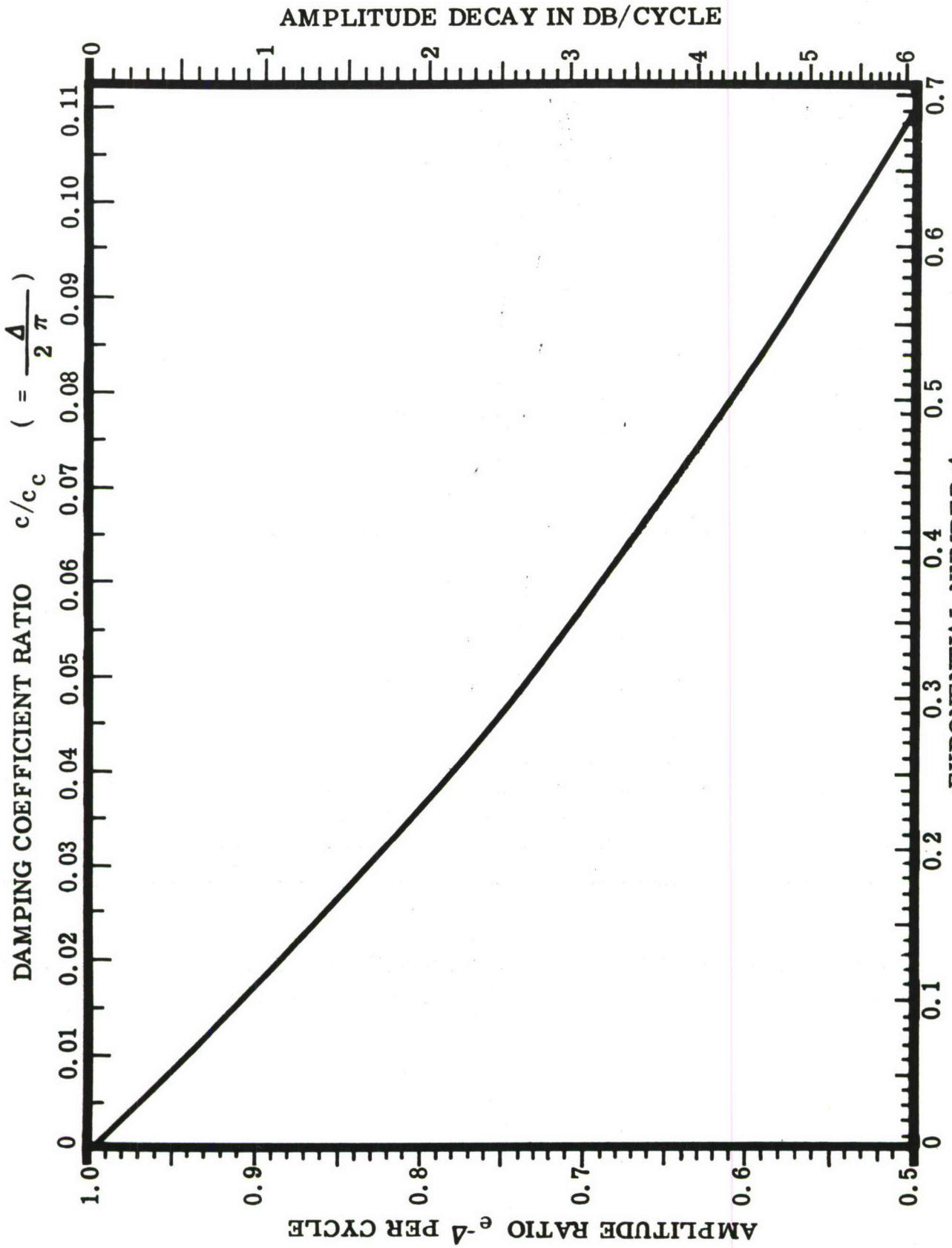

Figure 8 . Damping Coefficient Ratios

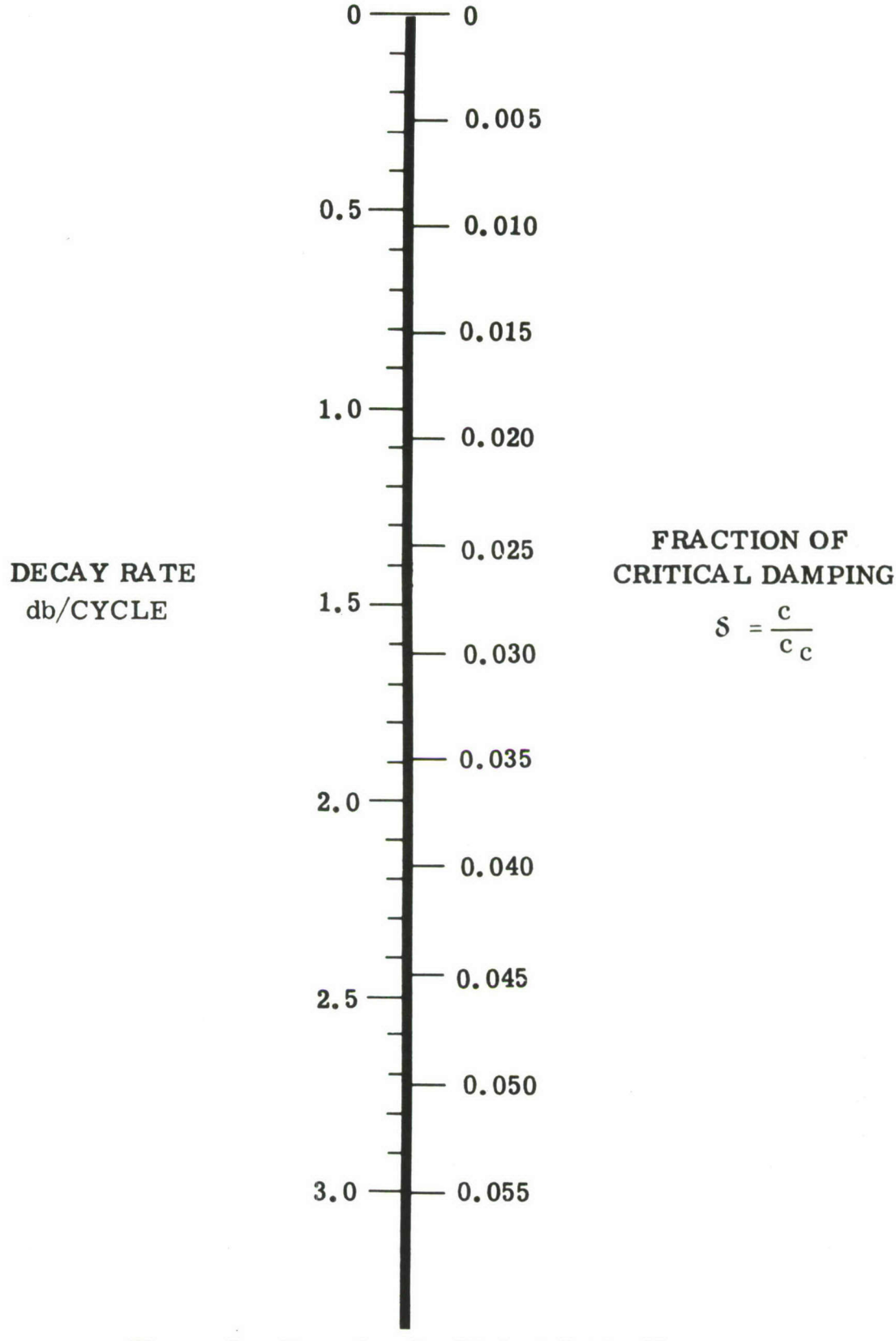

Figure 9 . Damping Coefficient Ratio Chart

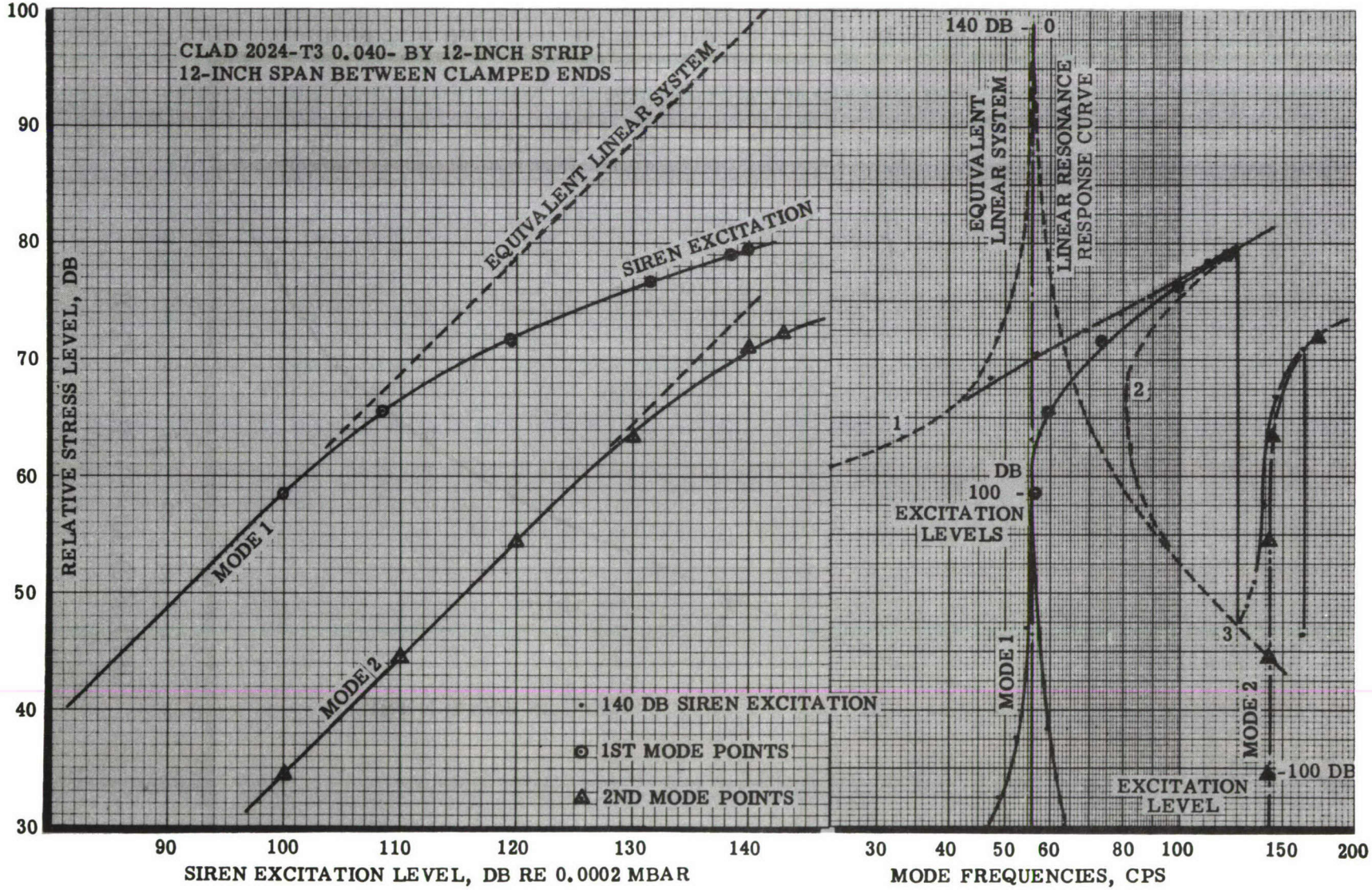

Figure 10. Nonlinear Stress Response

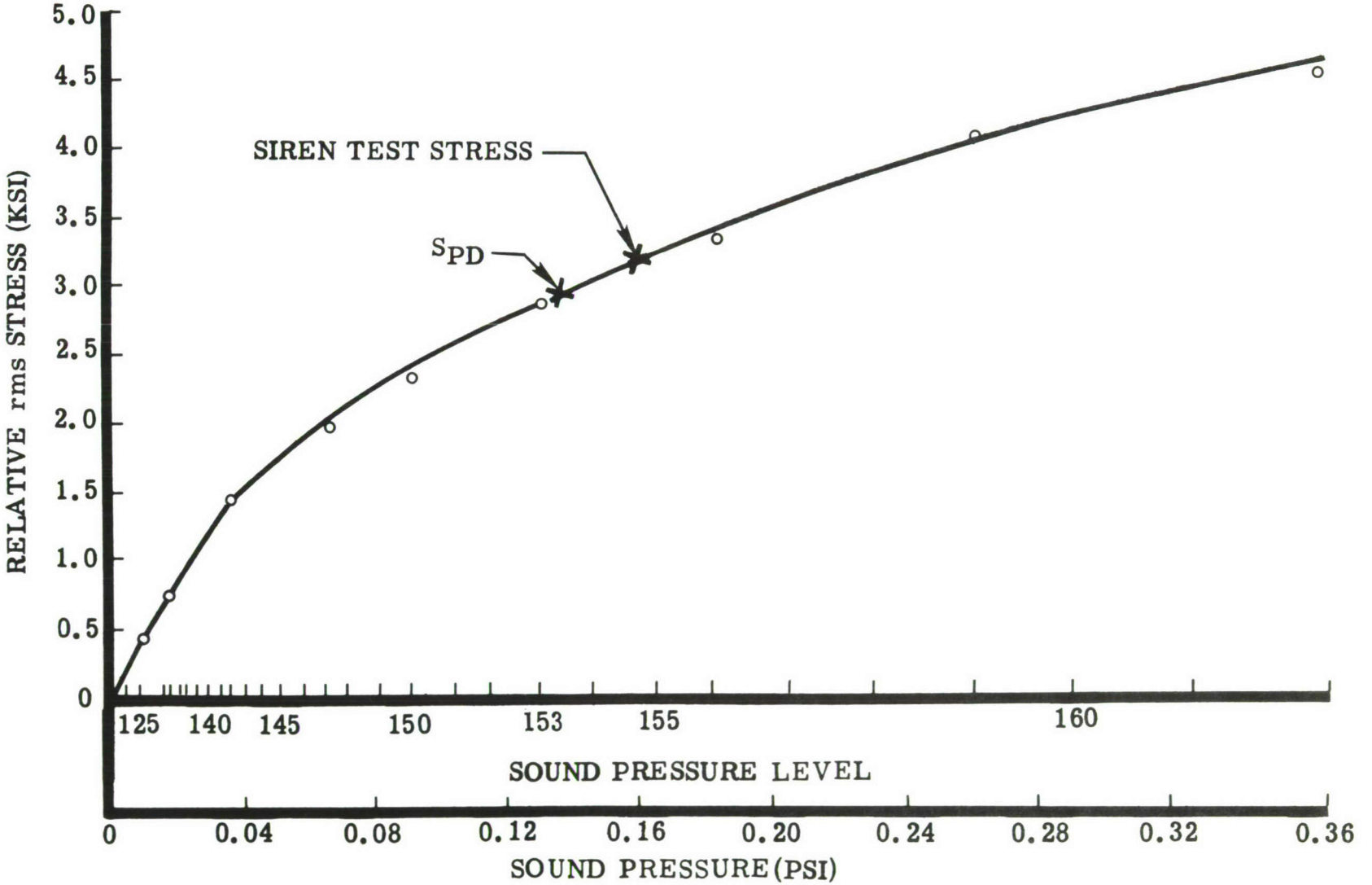

Figure 11. Power Response Plot

3.4 MULTIMODE RESPONSE

Typical air vehicle structure, especially of skin-stringer construction, often exhibits a tendency to respond significantly to excitations at frequencies other than the primary mode frequency. This tendency is demonstrated when a discrete frequency siren is used to perform a frequency sweep at constant-sound pressure level. Such a sweep is illustrated in figure 6 . At any specific location in the structure being tested, represented by the strain gage whose output is being plotted, it is possible for higher frequency modes to produce equal to or greater than those at the primary mode. Therefore, they are important in fatigue damage considerations. If this structure were subjected to a broad-band sound source, all significant modes would be excited simultaneously. Further, if the output of the strain gage were analyzed for frequency content, a response curve approximately the same as that obtained from the discrete frequency siren test would be plotted. This similarity is assured when the stress magnitudes are linear and damping is low. If the stress were non-linear and damping high, significant differences could occur.

When using actual strain-gage response data to correct Equation (8), an additional uncertainty exists if the strain gage is not located at the point of failure of the structure. The relative stress magnitudes of the different significant modes may change radically over a short distance on the structure. As pointed out in Reference 15, "it is probable that the greatest errors in the sine-random equivalence computation arise in the interpretation of multiple-mode data."

CORRECTION FACTOR FOR MULTIMODE RESPONSE

An approximate correction factor suggested by Belcher, Van Dyke, and Eshleman, Reference 15, assumes that the failure obtained in the discrete frequency life test resulted, in turn, at each mode significant enough to require test. It further assumes that the fatigue damage rate depends only on the total rms response stress which can be estimated as:

$$\overline{s_t^2} = \overline{s_1^2} + \overline{s_2^2} \ldots + \overline{s_n^2} \qquad (14)$$

The correction factor then is the ratio of the total stress to the modal stress

$$\gamma = \frac{\overline{s_t^2}}{\overline{s_i^2}} \qquad (15)$$

The stress at each mode is taken from a tendency response curve such as shown in figure 6.

3.5 DISTRIBUTION OF STRESS IN RANDOM LOADING

When the acoustic pressure forcing a structure having zero static stress varies in amplitude in a random manner, the instantaneous value of the stress response has been shown to vary with Gaussian distribution with the most probable value being zero. If the response is unimodal, each stress cycle is fully reversed and the distribution of the stress peaks is accurately approximated by the Rayleigh distribution function. (See figure 37.) However, if multimode response is evident, the distribution of the stress amplitudes is more significant. It has been shown by Schjelderup, Reference 25, that the distribution of the stress amplitudes is Gaussian. Either distribution can be used in fatigue calculations, as is shown in Section IV. Figure 12 shows random excitation traces of strain gage outputs for multimode and for single-mode response. The traces clearly show that the peaks are fully reversed when a single mode is dominant, whereas many peaks do not reverse themselves in the multimode case.

Pronounced nonlinearity in stress response will tend to distort the distribution of peaks away from that of Rayleigh. Since the distortion takes the form of suppression of the higher stress peaks assumed in the Rayleigh distribution, its use is then conservative.

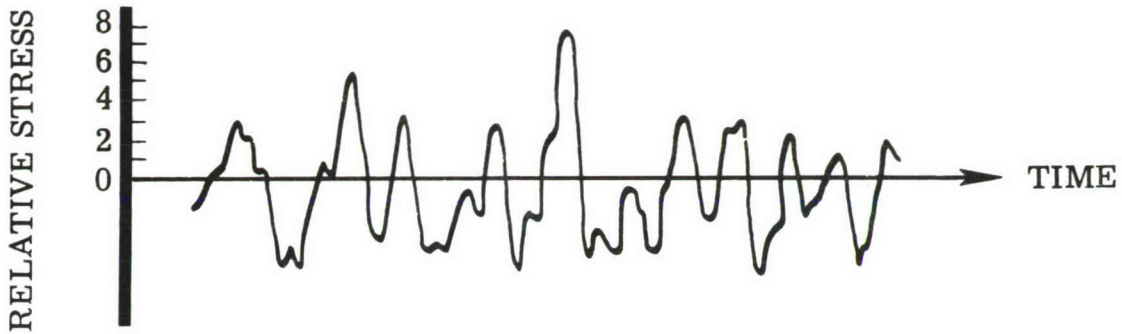

A. TYPICAL MULTIPLE - MODE RESPONSE TO JET NOISE

B. MEASURED STRESS RESPONSE TO JET NOISE SINGLE-MODE DOMINANT

Figure 12. Comparison Multiple Mode to Single Mode - Random Response

3.6 SPATIAL PROPERTIES OF PRESSURE AND RESPONSE

The one outstanding deficiency in the practice of acoustical fatigue analysis is the lack of an adequate treatment of the effects of the spatial properties of the acoustic pressures. This deficiency dwarfs, in its importance to the specification of mechanical response, accompanying stress, and resulting fatigue, the inaccuracies involved in the prediction of pressure levels and sine-random equivalence, including the multiple-mode correction, and scatter in fatigue behavior. Apparently, this is equivalent to saying, as will be argued in the following paragraphs, that the prediction of the detailed response of a general structure by analytical means is not now possible. Quite apart from the as yet inadequately treated question of the spatial distribution of pressure load, this is exactly why an empirical technique, siren testing, is the method most generally used, and why it is offered in this report.

Among the analyses of Powell, Smith and Junger, Dyer, and Tack and Lambert, References 19, 20, 21, and 22, are the elements of techniques necessary to specify the pertinent loading characteristics of both propagating acoustic waves and convecting decaying turbulence. The essence of the problem derives from the fact that each depends on a knowledge of the spatial characteristics of the responding structure.

Powell, for example, has applied his analysis to the determination of the total (all modes) mean square displacement response of a section of fuselage. (Compare Clarkson, Reference 23.) In this he uses tenable assumptions about modal behavior which, with the averaging of the effects of many modes, probably do not undermine the result drastically. But if the objective were stress at a point as is necessary for a fatigue analysis, rather than central displacement, the results would not prove very useful.

Figure 13, reproduced from the paper by Smith and Junger (Reference 20), illustrates the drastic dependence of response on the relationship of projected forcing wavelength to modal wavelength. Conventional skin and bent-flange rib structure provides a useful illustration of some of the implications of this figure:

1. If sound is propagating at grazing incidence in the direction parallel to the ribs, symmetrical modes, especially those involving the primary skin panel motions, should be more strongly excited; pressure is in phase over large areas of the assembly, and the details of spatial effects can be neglected.

2. If sound is propagating at grazing incidence in the direction perpendicular to the ribs, but there is only one panel (and two ribs), or the ribs are so much more rigid than the skins that little moment transfer from panel to panel can occur, then the Smith and Junger transfer function, or one like it for the appropriate boundary conditions, can be applied directly to the panel for the appropriate geometry.

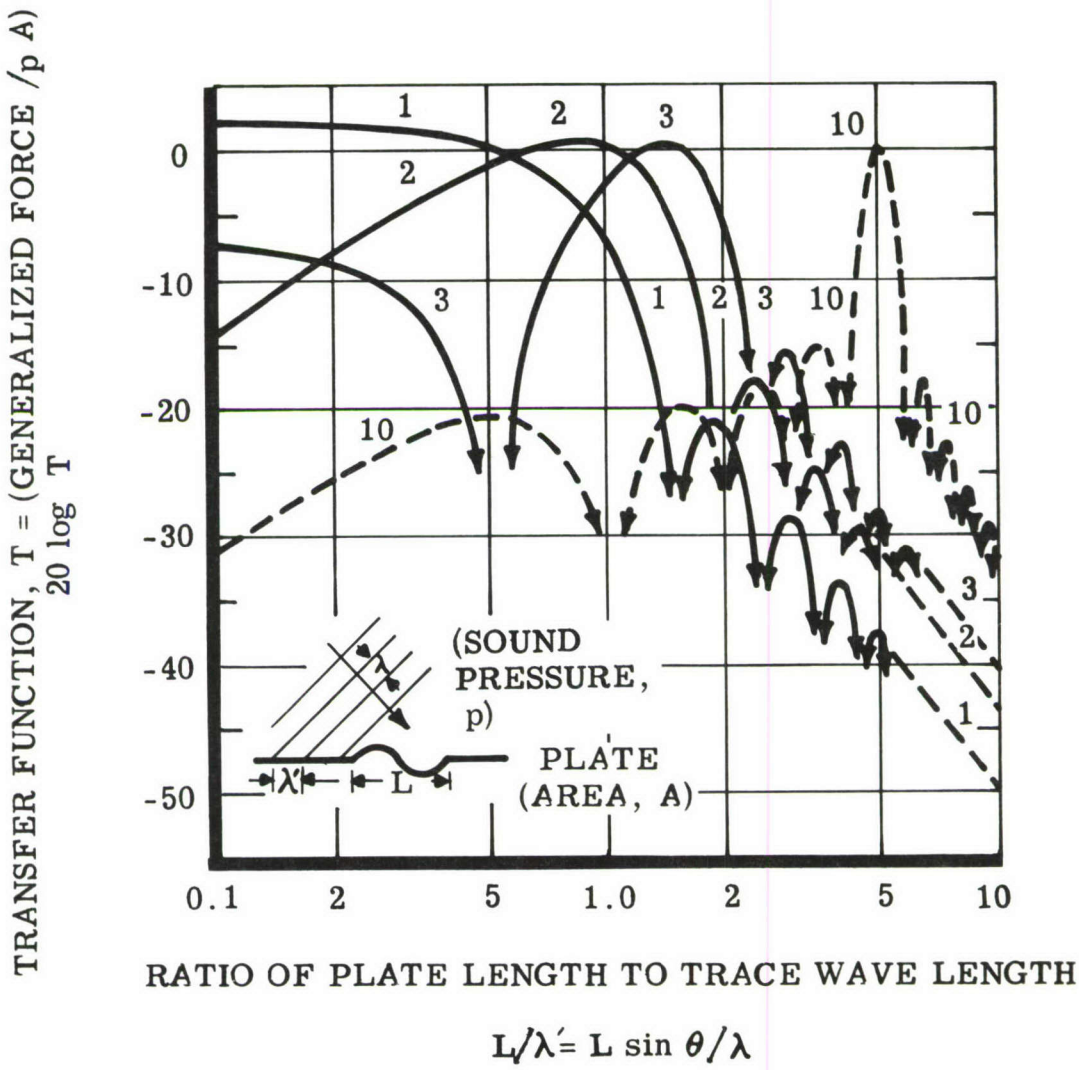

Figure 13. Transfer Function Diagram

3. The more frequently occurring case is similar to 2, but with many panels and highly flexible ribs. This is the major problem. Some approximations, mode by mode, can be made when the modes can be visualized and their relative contributions estimated. Beyond this, the best available tool is an effort at very close simulation of the spatial characteristics of the sound field, coupled with a conservative design approach.

Those who have worked with the multimodal, nonlinear behavior of conventional skin and bent-flange rib construction, which has dominated control surface structures until recently, may be requiring too much from response theories which might be developed, in view of the emergence of an encouraging trend. During the early period of effort in this field, it appeared that the potentialities of the analytical specification of response were limited by the difficulties involved in specifying the boundary conditions of plates. An accompanying problem, that of specifying modal shapes, became apparent when conventional skin-rib structure was viewed responding under stroboscopic light. However, several series of tests have been conducted recently on structure for high performance, supersonic air vehicles, dominated by configurations having comparatively long spans of surface between relatively rigid supports, the surface themselves having high local bending stiffness (e. g., honeycomb sandwich, corrugated inner-skin, etc). Not surprisingly, these structures demonstrated highly dominant responses in the primary panel mode, and these in an encouragingly linear manner. Perhaps technology will yet obviate the need for a single general treatment adequate for all types of structure. An example of just such a locally rigid configuration which did give way to an order-of-magnitude analysis of response under boundary-layer turbulence excitation is shown in Section VI, in an application of Dyer's treatment of convected turbulence (Reference 21). The approach used there, comparing the response under turbulence to a known response under sinusoidal excitation (or equivalently, random excitation using the sine-random equivalence), is a convenient and useful way of relegating the question of quantitative response and fatigue to the use of known or conventionally accessible data, thus isolating the real problem, the modal response character of the configuration.

Section IV

FATIGUE

4.0 GENERAL

The fatigue of structural components as a result of acoustic forcing occurred rarely before the introduction of rocket and jet engines. As a result of the high-sound pressure output of contemporary propulsion systems, an additional source of fatigue failure has been introduced. Except for the manner in which a structure is loaded, the end product of acoustical fatigue is no different than that caused by other cyclic loading mechanisms. Relatively speaking, the magnitude of acoustically induced stresses is not large. In addition to resonance amplification, what makes acousic loading critical for fatigue is the very high frequency of its load applications. Consequently, the area of greatest interest for the purpose of evaluating sonic fatigue damage is the lower range of the S-N curve.

4.1 FATIGUE CURVES

In any fatigue analysis, the primary tool of the structures engineer is the fatigue life curve. The fatigue life, or the S-N curve (S = stress, N = cycles of life) as it is most commonly referred to, is the basic method of tabulating fatigue test data. The S-N curve is obtained by cycle loading test specimens at different constant stress levels until failure. The fatigue life N will then be found to vary with stress as shown in figure 14 . The data for the S-N plot of figure 14 is for a completely reversed bending stress or an R factor of -1. R factor is used in fatigue work to denote the loading condition that was used in obtaining the data. It is defined as the ratio of the minimum to the maximum applied cyclic load. Figure 15 shows representation of some typical R factor loadings. It should be noted that an R = -1.0 load ratio can represent either a reversed-bending or a reversed-axial stress condition. As an illustration, a conventional single-skin panel would respond in a typical reversed-bending condition whereas the reversed-axial loading condition would represent face sheet failures of sandwich panels. Of the two loading conditions, the reversed axial loading is the more damaging. Some of the test variables other than R that will affect the shape and location of an S-N diagram are test temperature, material heat-treat, and stress concentrations. Stress concentrations, such as round holes and edge notches, are placed in the test specimens for the purpose of simulating acuities to be found in an actual structure.

By using collected fatigue data for various concentration factors, fatigue life of structural components containing built-in acuities can be evaluated.

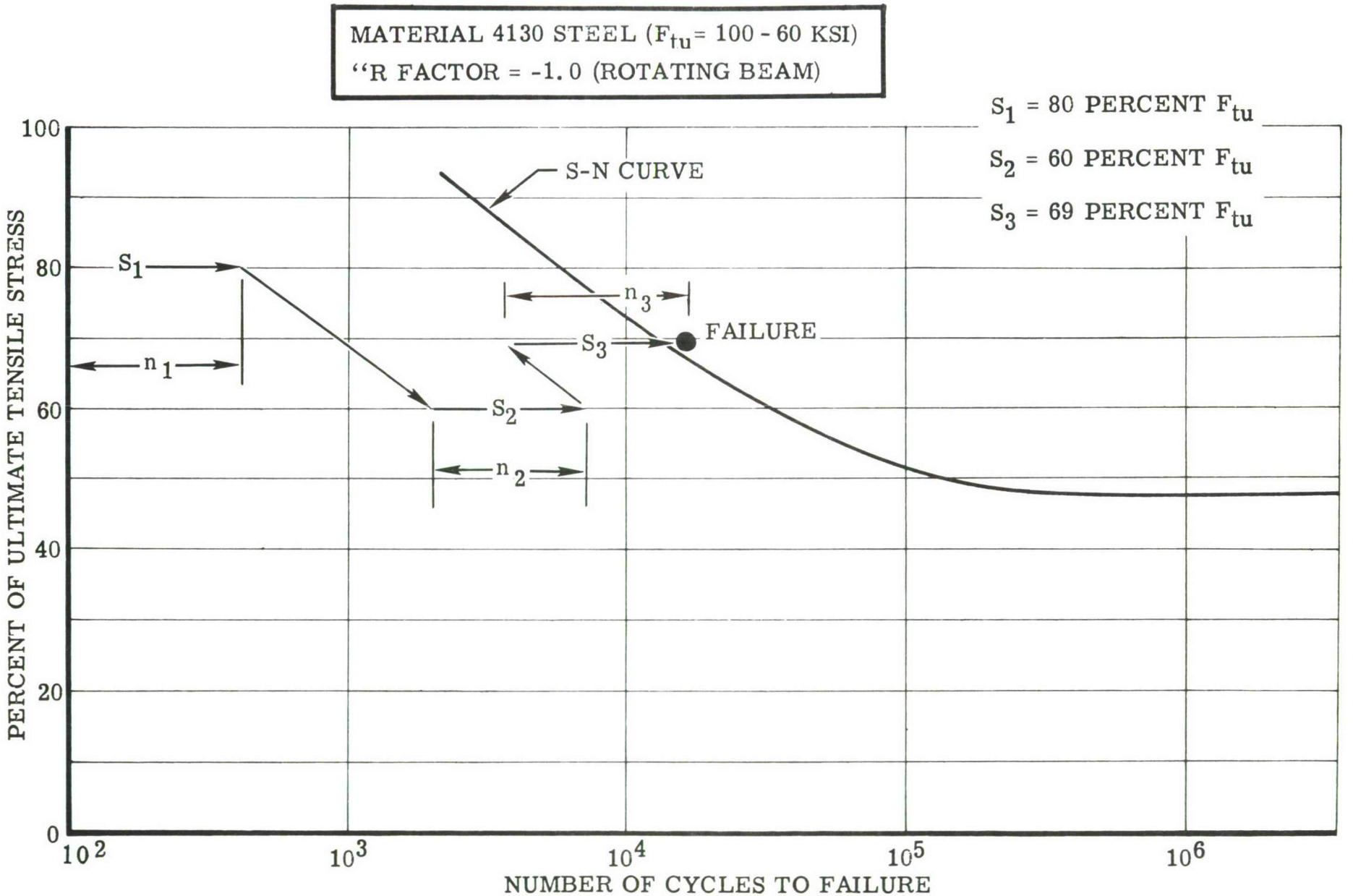

Figure 14 . Graphical Presentation of Miner's Rule

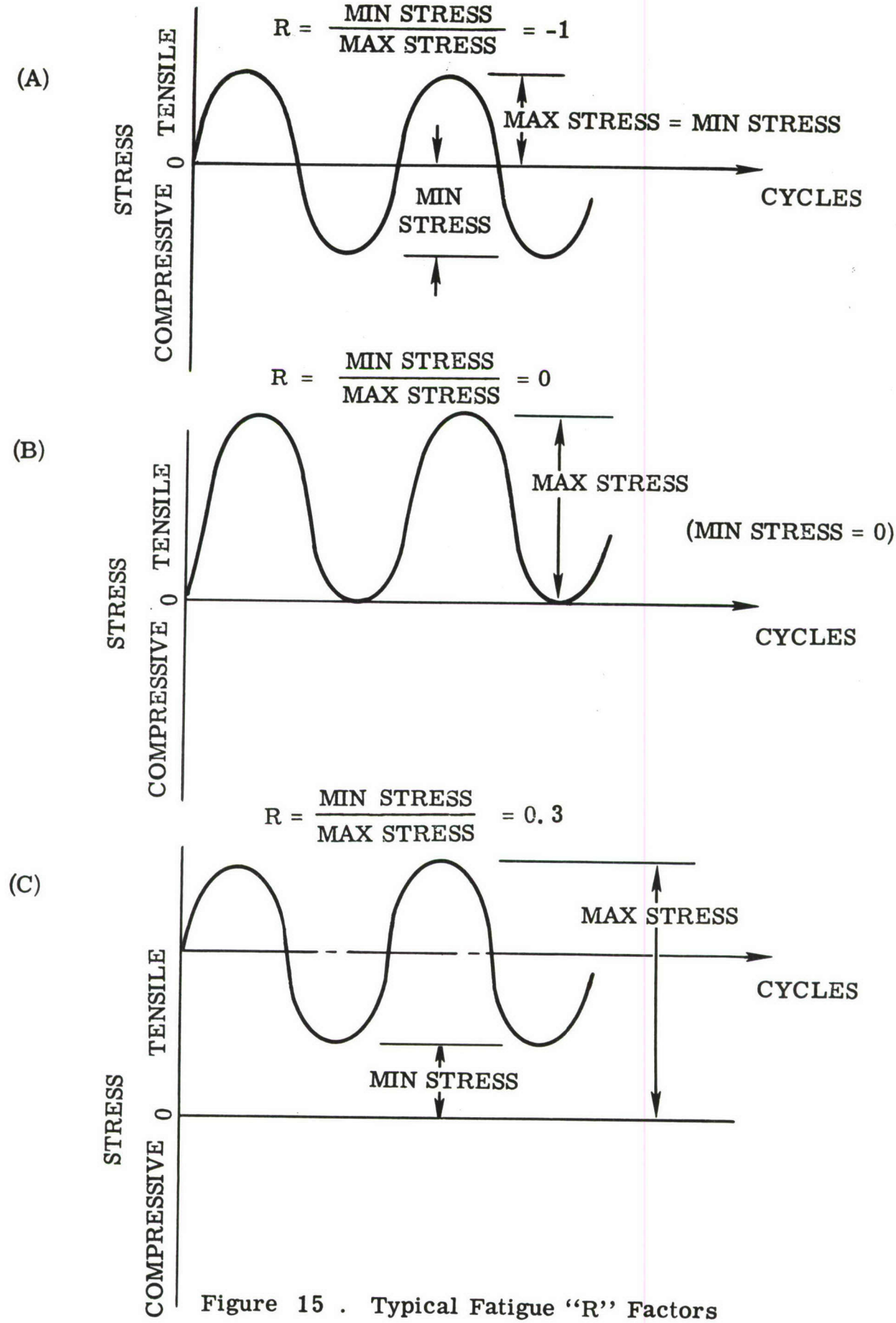

Figure 15 . Typical Fatigue "R" Factors

Once the concentration factor of the part to be analyzed is computed, by use of any of the accepted methods such as Peterson (Reference 14), the appropriate S-N curve can then be chosen. Although S-N curves are rarely available for all possible values of the geometric stress concentration factor, existing curves can be adjusted judiciously to account for nominal valves between $K_t = 1.0$ (polished) and $K_t = 4.0$. S-N data for a range of concentration factors is shown in figures 16 and 17 for three typical materials. To facilitate the use of S-N data, it is sometimes presented in the form of a modified Goodman diagram. The format of a Goodman diagram are stress ratio (R), mean stress, alternating stress, and maximum stress. Examples of modified Goodman diagrams are shown in figures 18 to 21. The primary advantage of using this plot is that a fatigue cumulative damage analysis (Reference, paragraph 4. 2) is simplified.

In acoustical fatigue, the material failures usually will be a result of stresses produced by the reversed bending of the structural components. That is, the stress picture will somewhat resemble the loading for R = -1 (figure 15), except that the stress peaks and their frequency of occurrence will be of a random nature. In Section V of this report, a detailed description is presented of a method for converting a standard S-N curve into a rms (root mean square) random allowable fatigue curve. These random fatigue curves will then be used as part of the analytical approach to acoustical fatigue. This approach to calculating a random S-N curve assumes that the frequency of occurrence of the peak stresses due to a random excitation can be described by a Rayleigh distribution (Reference, Section V). Calculated random fatigue curves for various materials are presented in figures 22 to 29. Also included with these basic material curves are random S-N plots for brazed honeycomb sandwich. These curves are for core shear fatigue. Recently, Schjelderup (Reference 25) has proposed that fatigue due to a random excitation is more correctly described by the variation in the mean and alternating stress as represented by a Gaussian distribution. The approach is simplified by accounting only for the distribution of the alternating stress, with no significant difference in the results. In the calculation of a Gaussian random S-N curve, use of a Goodman diagram is required so that the cycles to failure at alternating stress can be determined. Figure 30 illustrates a comparison of random S-N curves calculated by a Rayleigh and a Gaussian distribution. It is noted from the plot that the Rayleigh approach is the more conservative of the two. The conservatism is a result of assuming that the negative and positive stress peaks follow in succession (i. e., form complete stress reversals). Considering the inaccuracies encountered in fatigue life evaluation it appears that the use of the Rayleigh distribution is appropriate.

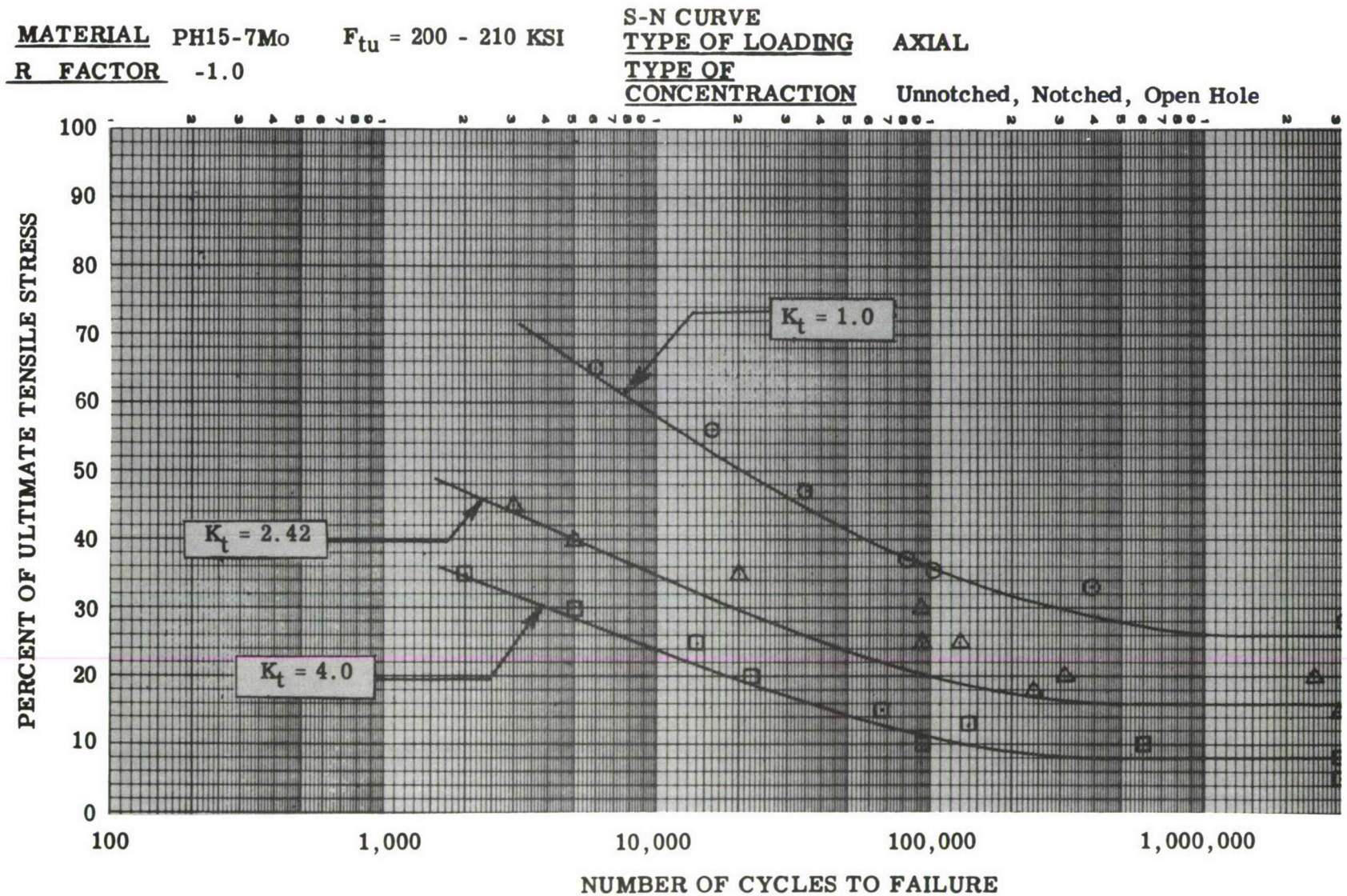

Figure 16. S - N Curve (PH15-7Mo Steel)

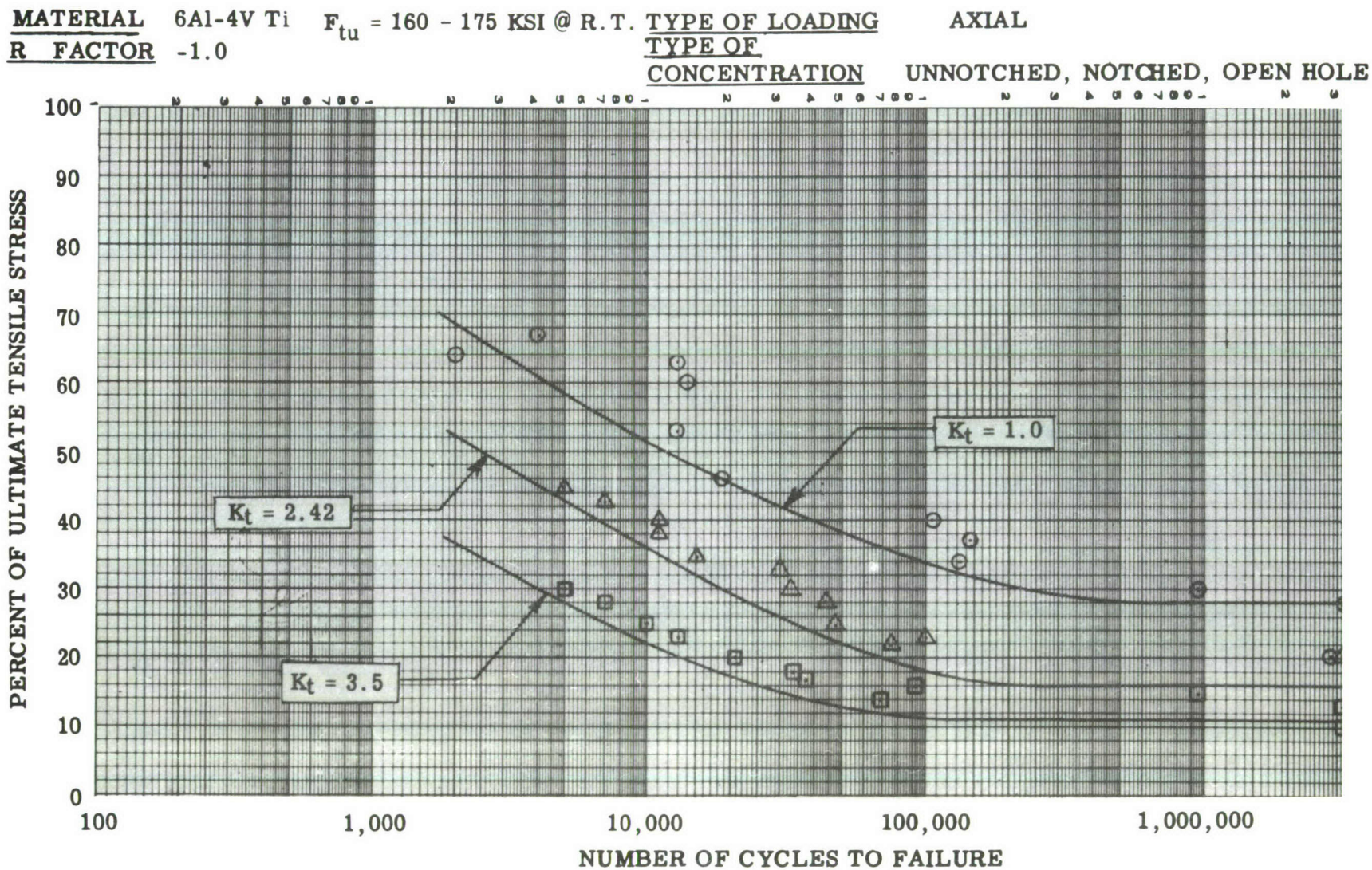

Figure 17. S - N Curve (6Al-4V Titanium)

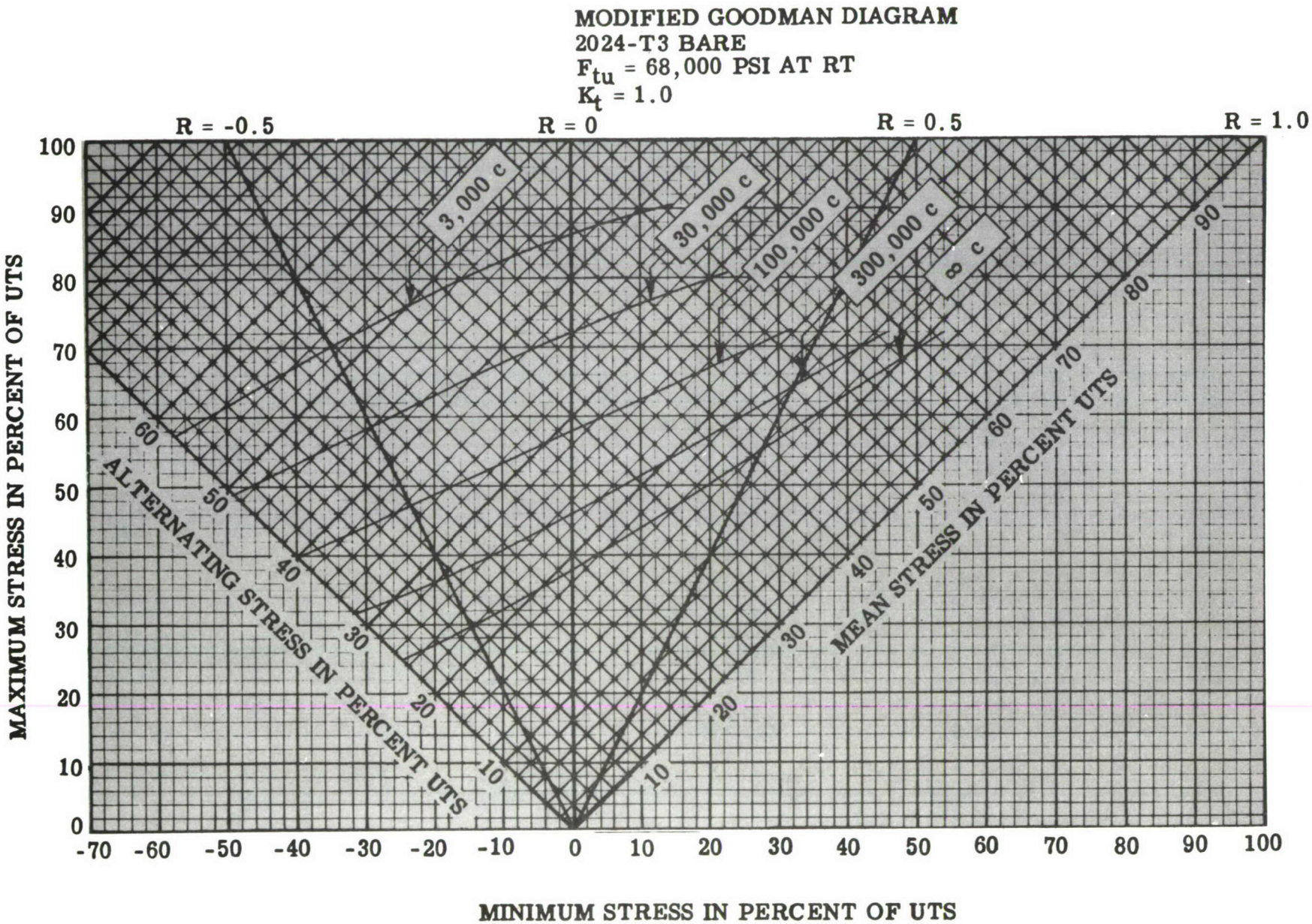

Figure 18. Modified Goodman Diagram (2024-T3 Bare)

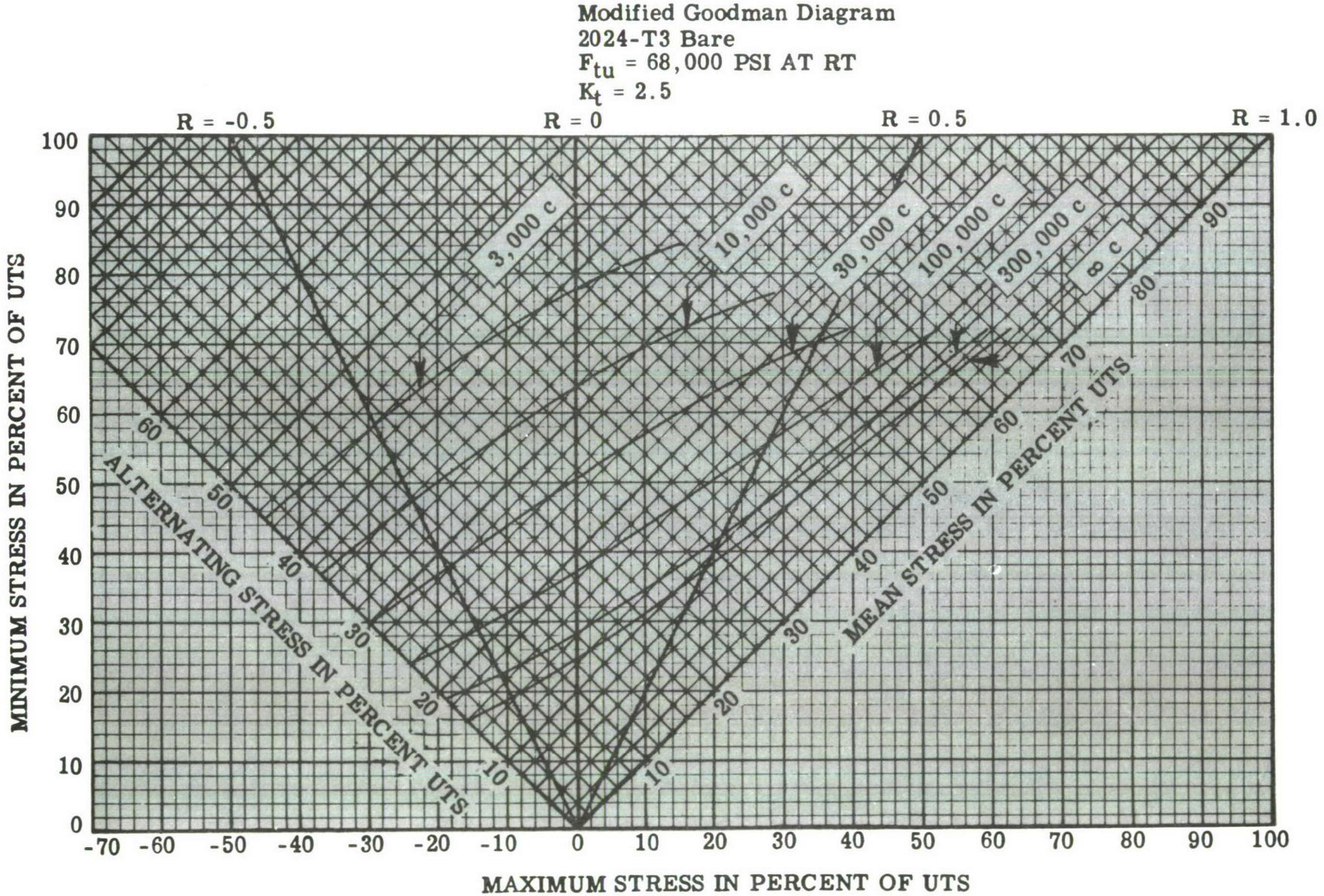

Figure 19. Modified Goodman Diagram (2024-T3 Bare)

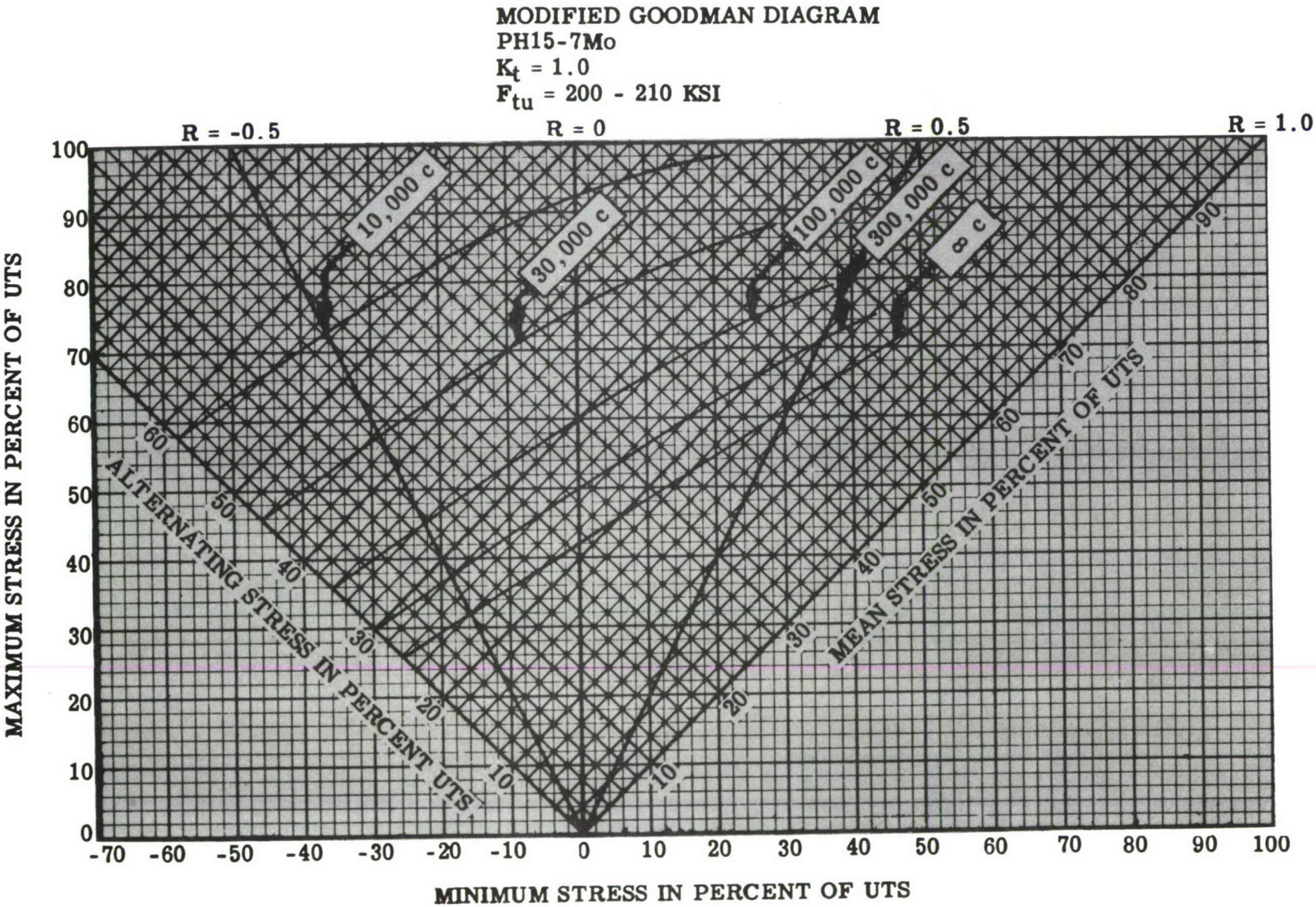

Figure 20. Modified Goodman (PH15-7N)

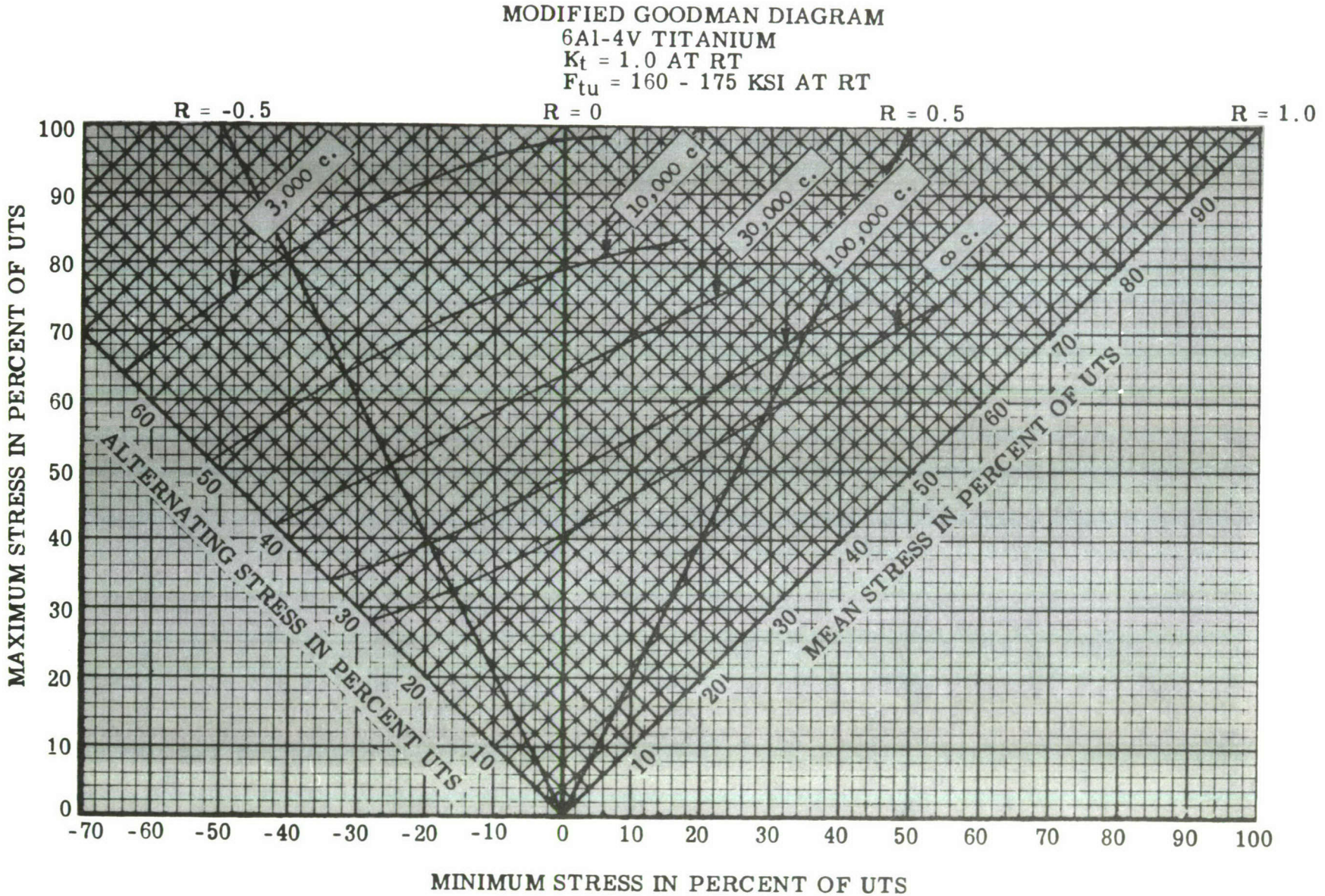

Figure 21. Modified Goodman Diagram (Titanium 6 Al-4V)

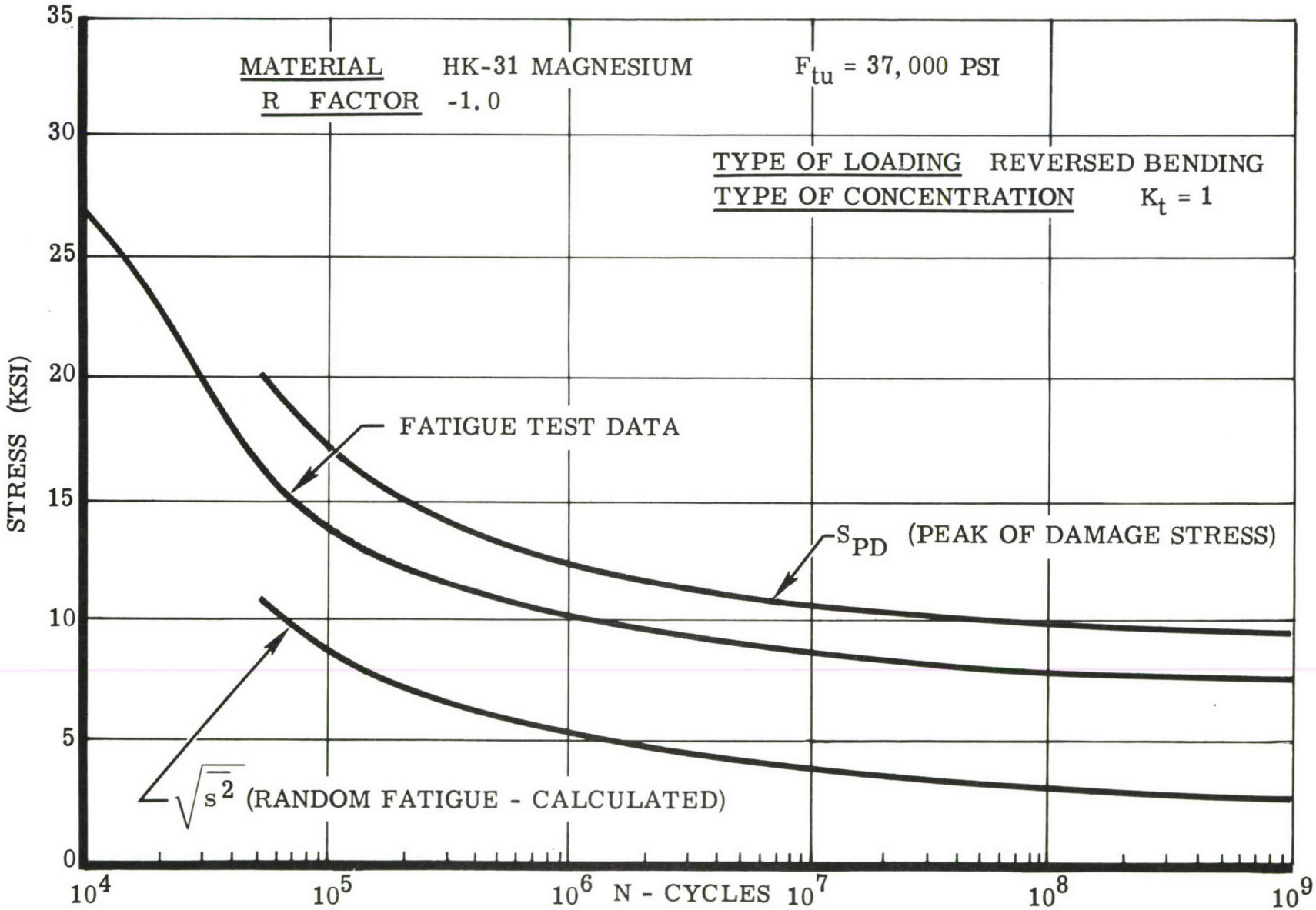

Figure 22. Calculated Random Fatigue and Peak Damage Curves

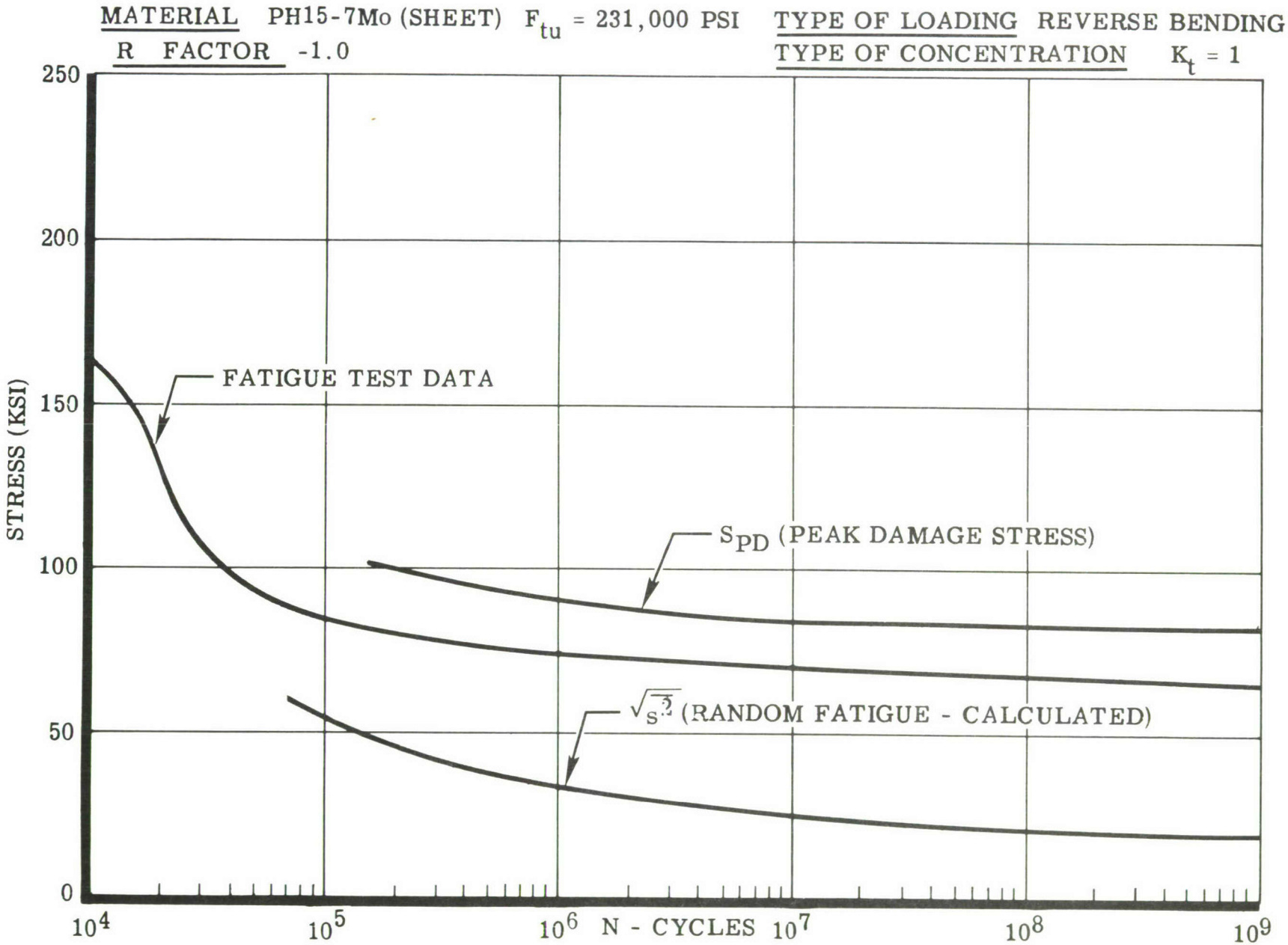

Figure 23. Calculated Random Fatigue and Peak Damage Curves

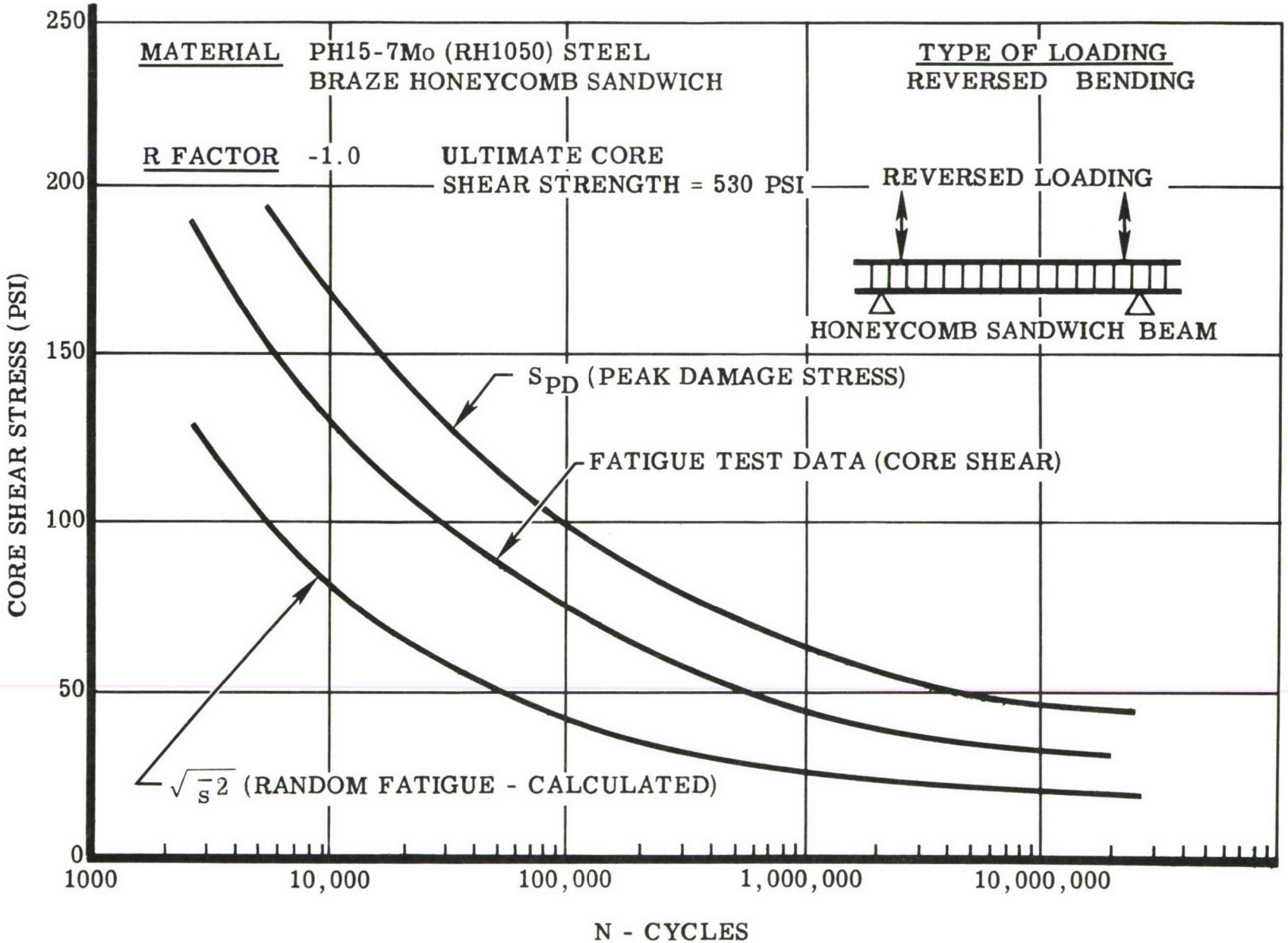

Figure 24. Calculated Random Fatigue and Peak Damage Curves

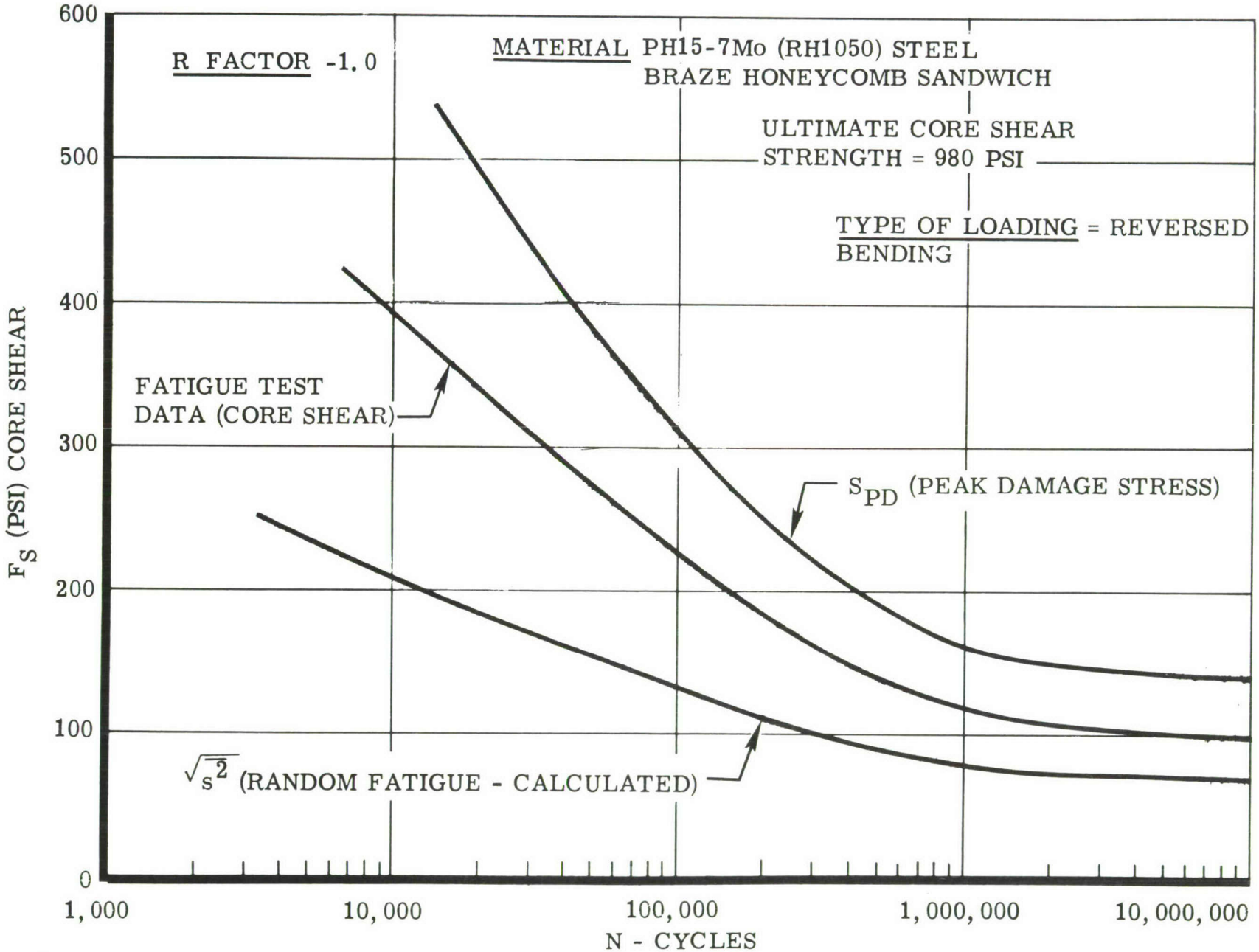

Figure 25. Calculated Random Fatigue and Peak Damage Curves

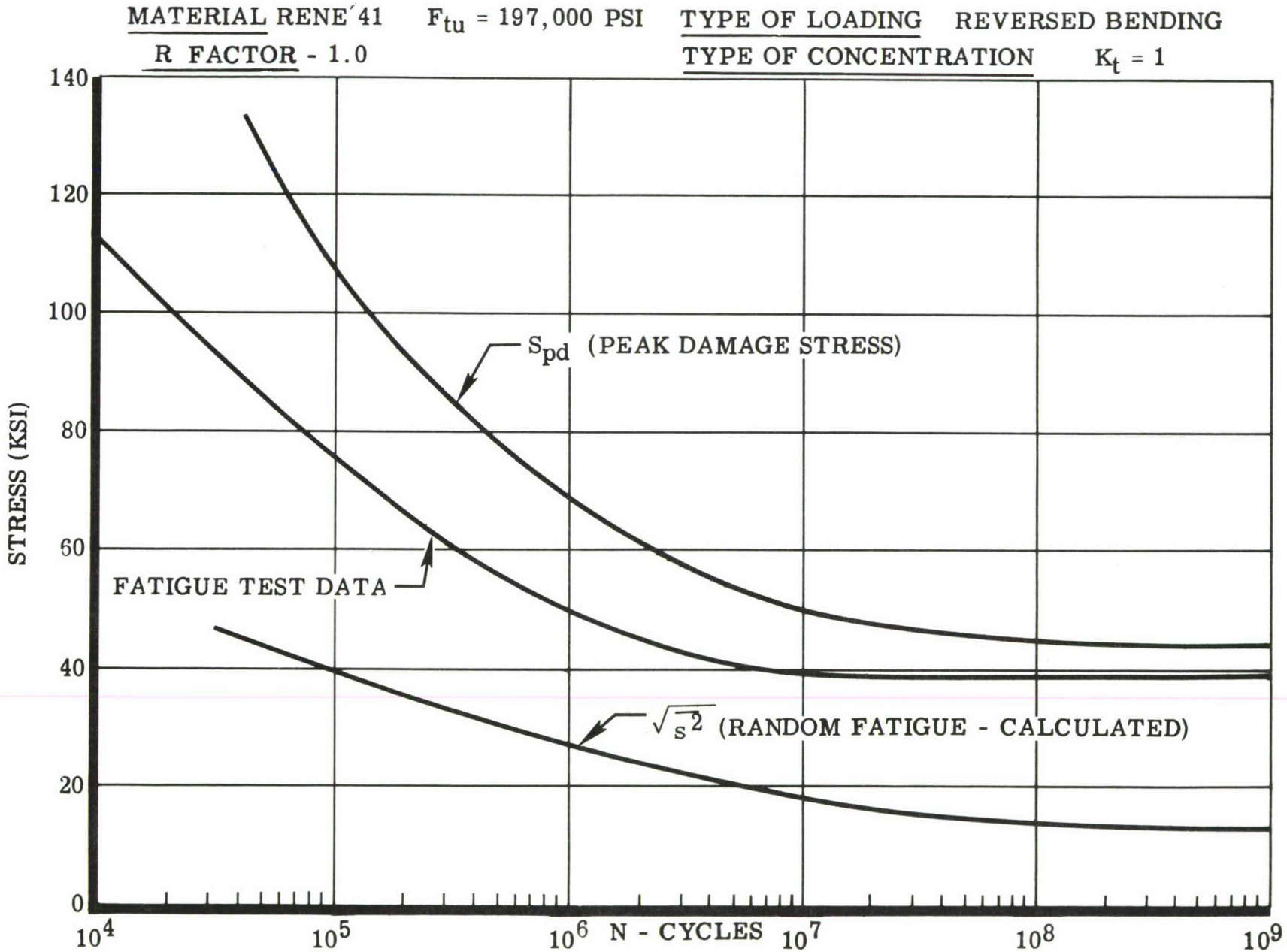

Figure 26. Calculated Random Fatigue and Peak Damage Curves

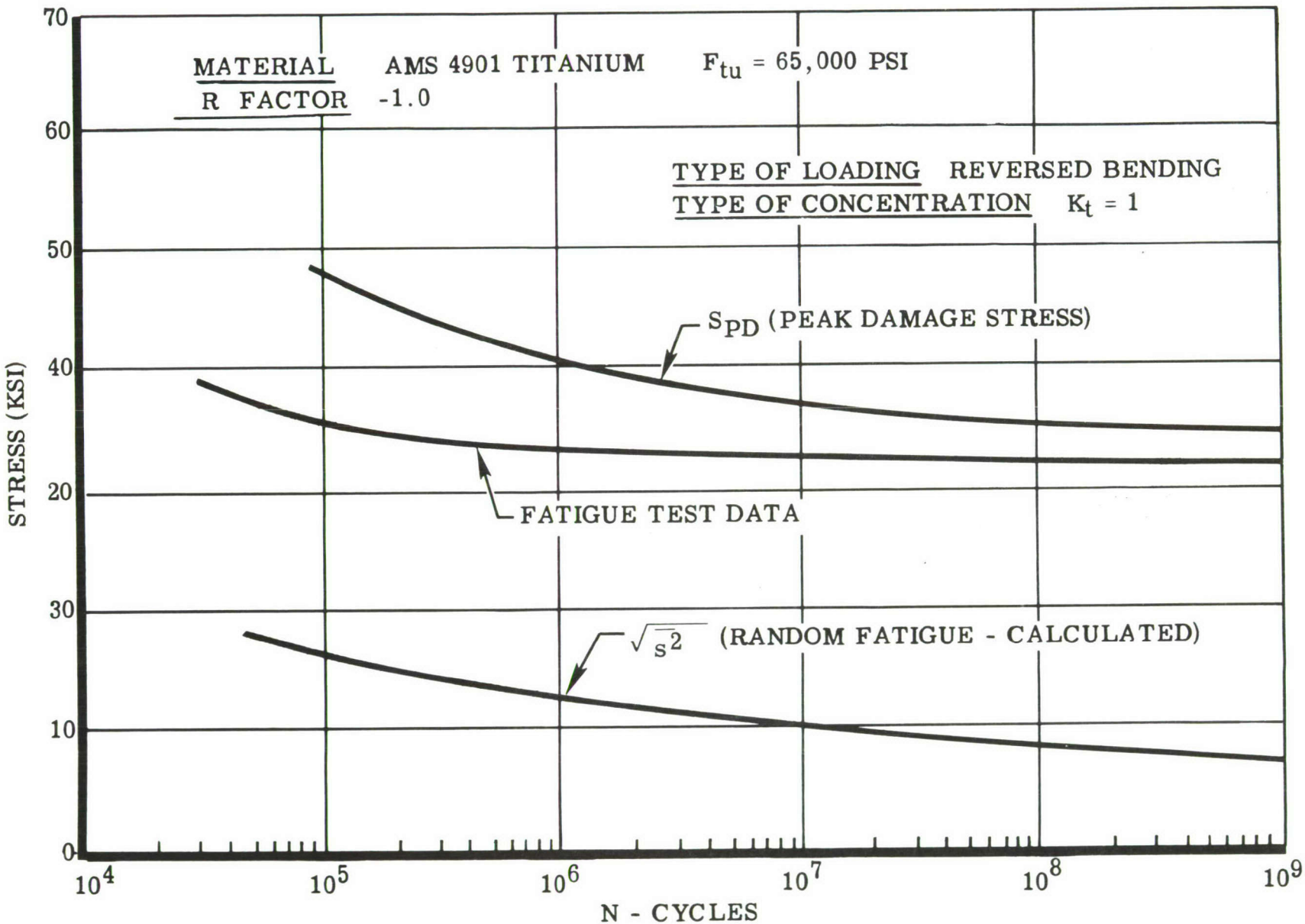

Figure 27. Calculated Random Fatigue and Peak Damage Curves

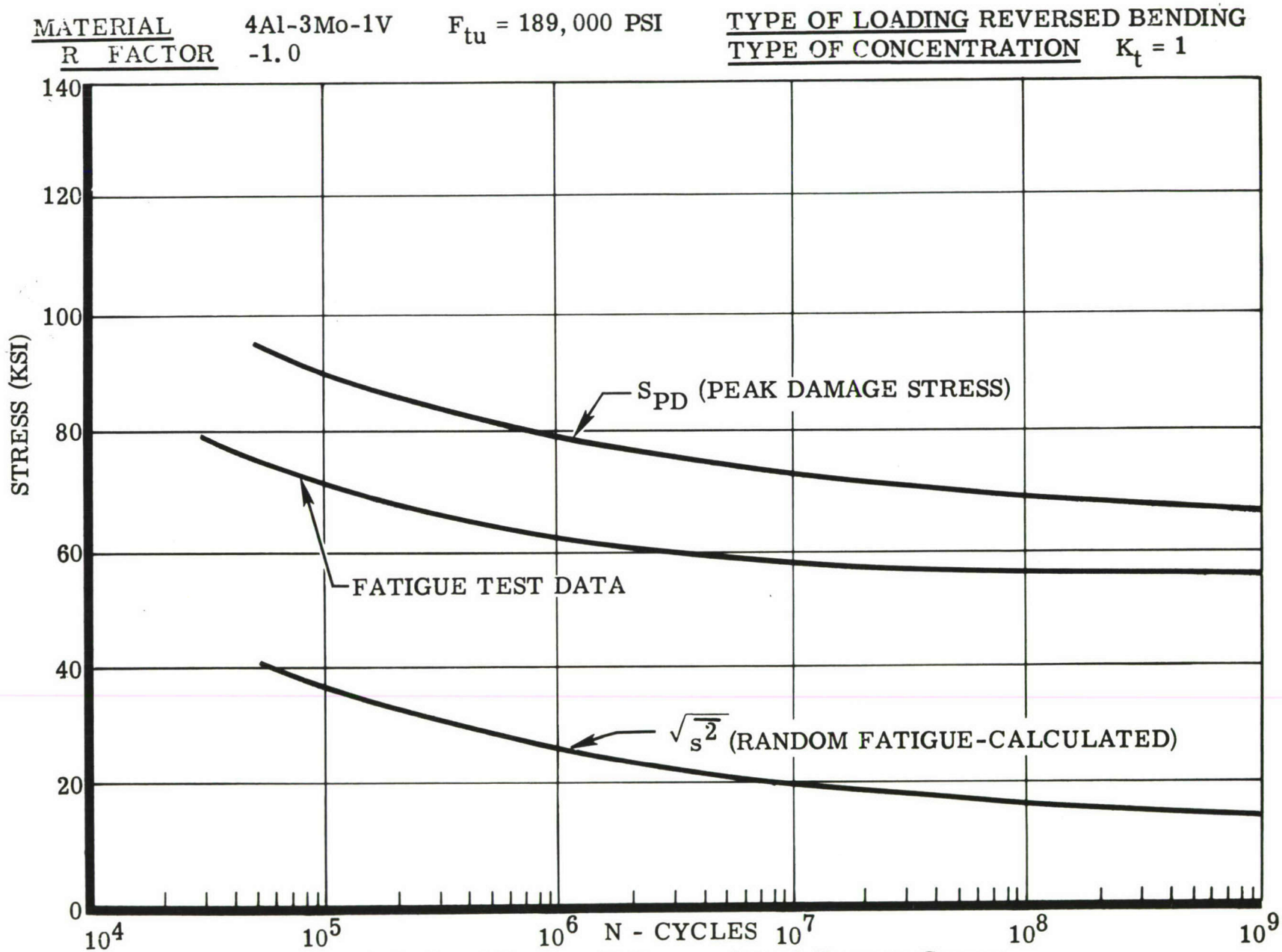

Figure 28. Calculated Random Fatigue and Peak Damage Curves

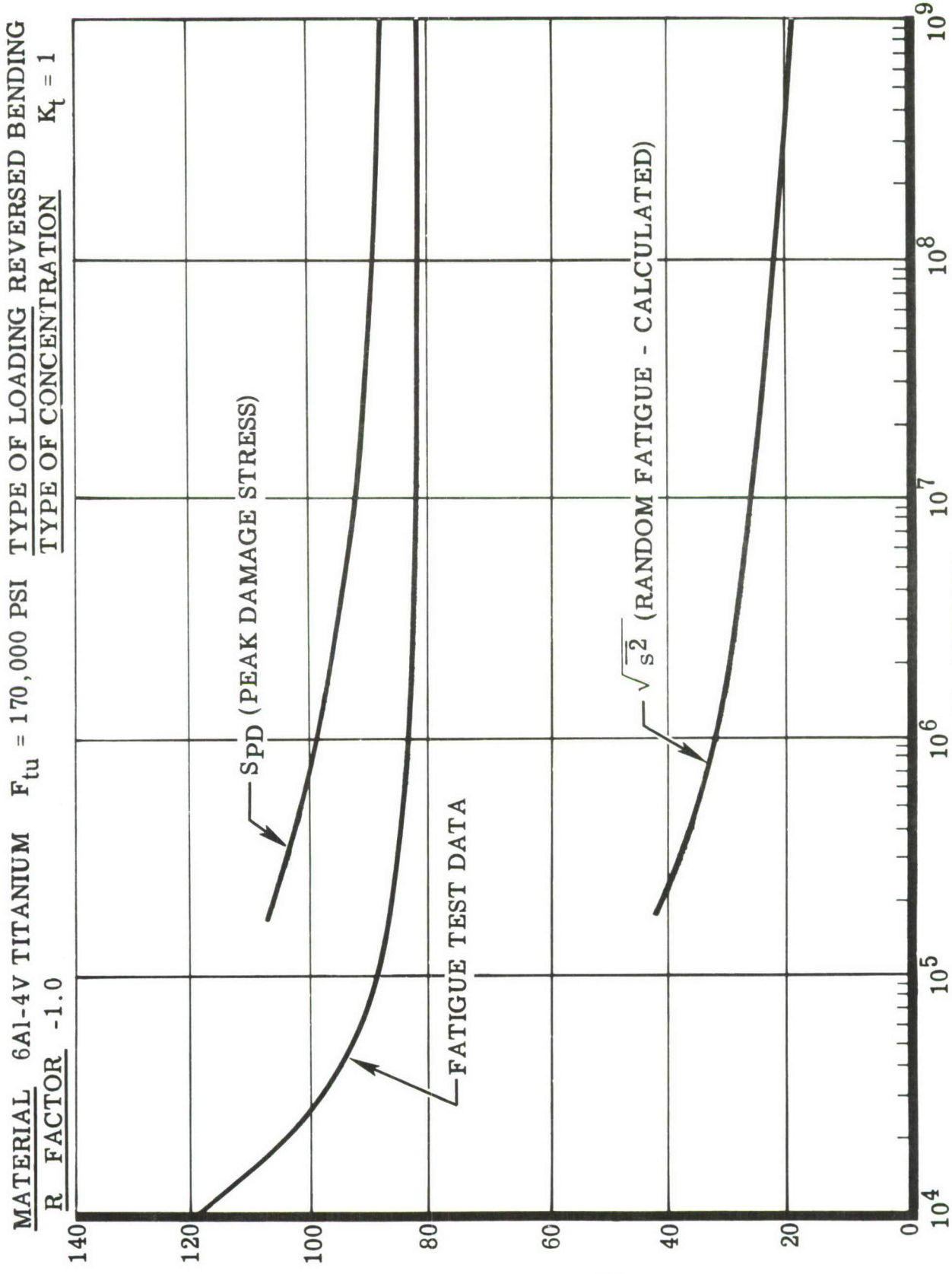

Figure 29. Calculated Random Fatigue and Peak Damage Curves

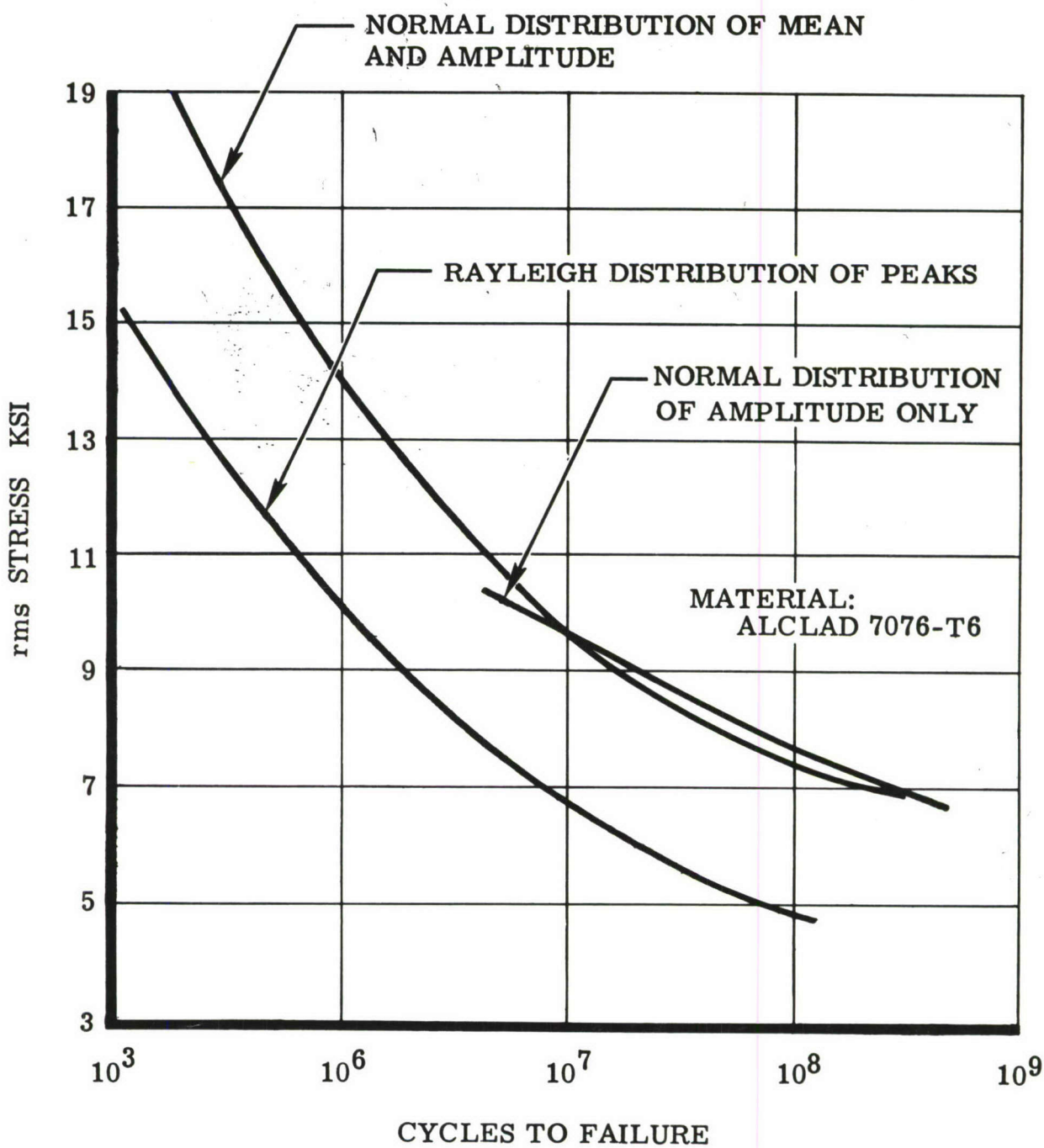

Figure 30. Comparison of Random Fatigue Curves Computed by Rayleigh and Gaussian Distributions

4.2 CUMULATIVE DAMAGE

It was not long ago that most aircraft structures were checked at one arbitrary fatigue load. The component was considered to be properly designed if it survived a specified number of cycles. This approach was usually conservative and at the same time yielded data that were of little practical significance.

Although considerable progress has been made in aircraft fatigue analysis, vehicle life prediction is still a difficult task. The difficulty is not only that of determining the magnitude and frequency of load application to be expected, but also of having a reasonable method of predicting fatigue life. Numerous damage theories have been postulated in an attempt to account analytically for fatigue damage incurred as a result of spectrum loadings. Palmgren (Reference 26) was the first to propose the cumulative damage concept, with Miner (Reference 27) suggesting its application to structural fatigue. Miner's approach is probably the most widely accepted and has been used successfully in designing many types of air vehicles. Most cumulative damage concepts, such as Miner's rule, have been applied mainly to fatigue analysis associated with primary structural loads. Recently, some damage methods have been specifically tailored for evaluating acoustic fatigue. Some of the prime requisites of a damage criteria are simplicity of approach, the ability to make use of the large quantities of available S-N data, and to predict fatigue life with reasonable accuracy. Some of the cumulative damage procedures currently in use are discussed in the following paragraphs.

LINEAR CUMULATIVE DAMAGE

Miner's linear cumulative damage rule states that the total fatigue damage is equal to the summation of the damages at each stress ratio. If the cycle ratios are equivalent to the damage ratios then at failure,

$$\Sigma \frac{n_i}{N_i} = \frac{n_1}{N_1} + \frac{n_2}{N_2} + \frac{n_3}{N_3} \cdots\cdots = 1 \qquad (16)$$

where n equals the number of cycles at stress S and N is the total allowable number of cycles at S. A graphic illustration of the use of the Miner's rule is shown in figure 14 .

In the example, three stress levels S_1 , S_2 , and S_3 were applied for n_1 , n_2 , and n_3 , cycles. Then, from the linear damage rule, $\Sigma \frac{n}{N}$ of the three load levels should equal unity at failure. The S-N curve used in the example was for a stress cycle ratio of R = -1.

Any number or combination of load ratios can be used with Miner's rule. The attractiveness of the cumulative damage method for engineering analysis is its simplicity. Further, the data required other than load spectrum are readily available in S-N curves. Since the damage theory was first proposed, numerous researchers have found that the variance from unity in $\Sigma \frac{n}{N}$ can be considerable. For example, in the application of Miner's rule to the prediction of life under random loading, Fralich (Reference 28) has found that the fatigue life was overestimated for the range of stresses considered. The test specimens used in the evaluation were notched SAE 4130 steel beams. This variance from unity or nonlinearity has been attributed to numerous factors, such as lack of randomness of the loading when duplicating a spectrum, the presence of stress concentrations, frequency of load application the order of load application (high load or low load first), and material characteristics. Of the factors noted, stress concentration factor (K_t) probably has the greatest effect on life prediction, but K_t will vary far more from the predicted values than $\Sigma \frac{n}{N}$ will vary from unity. Using the lower scatter band, life predictions by the linear damage method are generally conservative and fall within the limits of experimental data.

NONLINEAR METHODS

Various researchers have presented methods which attempt to account for nonlinearity in damage accumulation. Most of the approaches correct for nonlinearity by modifying the basic S-N curves. This is usually accomplished by use of statistical methods and/or by collecting new fatigue data which have been modified by some preload. Some of these nonlinear damage methods are:

- Freudenthal Method. Freudenthal's (Reference 29) cumulative damage method is expressly orientated toward fatigue damage due to randomly applied variable stress amplitudes. The approach attempts to account for both the statistical and the physical considerations of fatigue. Freudenthal utilizes Miner's linear damage concept, but accounts for nonlinearity by developing fictitious S-N curves. These fictitious S-N curves are obtained by simulating the conditions obtained under variable load conditions. Figure 31 illustrates a typical corrected S-N plot. An adequate amount of testing required to verify the theory has not as yet been accomplished. Other limitations for acceptance of the theory for practical usage are (1) complexity of the computations and (2) the large amount of new fatigue data that would be required to develop fictitious S-N curves.

- C. R. Smith's Cumulative Damage Method. C. R. Smith (Reference 30) suggested that Miner's cumulative damage approach would be adequate if it was used in conjunction with S-N curves for specimens

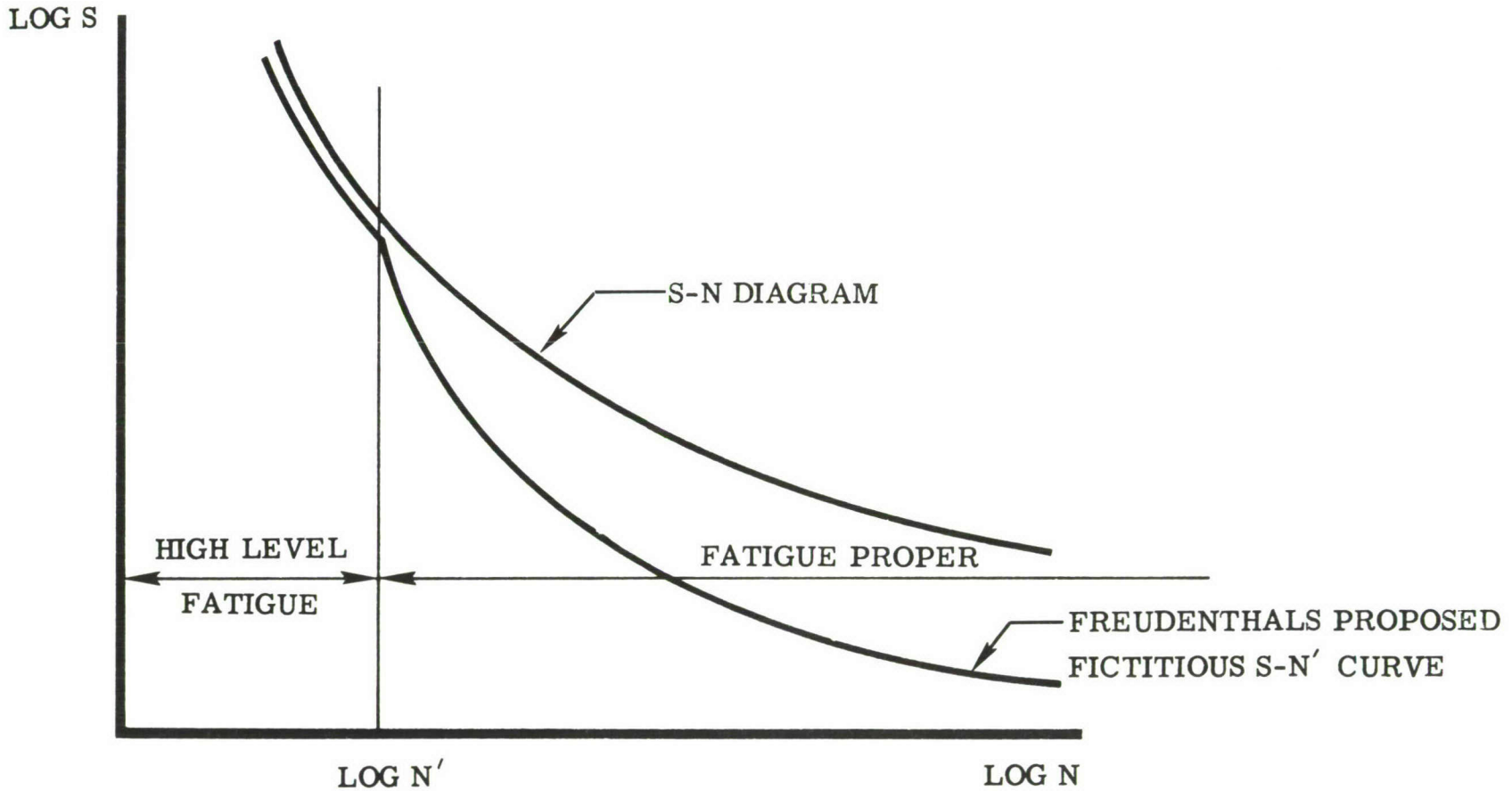

Figure 31 . Conventional and Fictitious S-N (N′) Diagrams

which had previous preload history. According to Smith the discrepancies in fatigue life prediction are primarily a result of residual stresses acquired at concentrations. The beneficial effects of high loads at stress concentrations are not always available, especially if the highest load does not exceed 30 percent of ultimate strength. Smith's corrected S-N curves are obtained by applying a preload that is equivalent to the highest statistically probable load that can be expected in the first 10 percent of service life. With these modified S-N curves, Miner's approach should yield safe life predictions. As yet, 7075-T6 aluminum has been the only material tested. Whether the effects shown for aluminum will be the same for other materials is not known. As in Freudenthal's method, new test must be acquired, as the available S-N curves are not usable in this analytical procedure. In fact, new S-N curves would be required whenever the load spectrum was changed.

- Shanley's Method. Shanley (Reference 31) proposes a method which avoids the use of an adjusted S-N curve, as proposed by Smith and Freudenthal. This is accomplished by the development of a formula which determines the effective stress of a spectrum loading. Shanley's cumulative damage method is evolved from ϵ-N (strain-cycle) fatigue diagrams which plot as straight lines on log-log paper. ϵ-N curves for various materials have approximately the same slope and lie within a narrow band. The equation for the effective stress is

$$S_{\epsilon} = \left(\frac{\Sigma S_i^x n_i}{n_i} \right)^{\frac{1}{x}} \tag{17}$$

where n_i is the number of cycles at stress S_i and x is the inverse slope on a log-log paper of the S-N curve; i.e., $\Delta \log N / \Delta \log S$. By the computation of the effective stress, a value is obtained which is equivalent to the spectrum loading in fatigue life. The required data for this method are the relationship between plastic strain and stress under dynamic fatigue conditions, and the true endurance limit under dynamically varying fatigue conditions. As in other nonlinear cumulative damage theories, additional unique fatigue test data must be obtained. At this time, test results adequate to corroborate Shanley's method are not available.

- Equivalent Fatigue Damage (EFD) Method. The equivalent fatigue damage method attempts to account for variables such as mean stress, temperature, frequency, waveform, stress concentration, etc, by relating life for a particular variable to a so-called standard condition. In the application of the EFD method, specialized fatigue test data for a family of spectrum stress levels must be collected. Equivalent fatigue damage plots for each loading condition are computed from

$$EFD = 1 - n_{sr}/N_s \tag{18}$$

where

n_i = load cycles at condition i (test variable)

n_{sr} = remaining cycles of life at a standard load condition after previous application of n_i cycles on test part

N_s = total cycles of life at a standard load condition

EFD plots for two load conditions are shown in figure 32 , with a typical $\frac{n}{N}$ life compution superimposed upon the curves. Failure of the part occurs when the summation along load condition curves A and B becomes unity or

$$\Sigma \frac{n_i}{N_i} = \frac{n_{a1}}{N_{a1}} + \frac{n_{b1}}{N_{b1}} + \frac{n_{b2}}{N_{b2}} = 1. \qquad (19)$$

The primary disadvantage of the EFD method is the extensive amount of test data required, without recourse to available S-N data.

- Modified Henry's Method. Henry's equation (Reference 32) is modified by the addition of the term D_c , which yields

$$\frac{D}{D_c} = \frac{n/N}{1 + \frac{S_E}{S-S_E}\left(1 - \frac{n}{N}\right)} \qquad \text{(Reference 33).}$$

where

D = fatigue damage

D_c = critical fatigue damage (damage at which part fractures completely)

S_E = endurance limit stress

S = maximum applied stress

The D_c term allows for the accounting for a load application which exceeds the residual strength of the test specimen. Life calculations are performed by the same process as used in the EFD method (figure 32). The n/N increments are summed along the damage curve, when $D/D_c = 1$ failure occurs. Prior to modification, Henry's equation

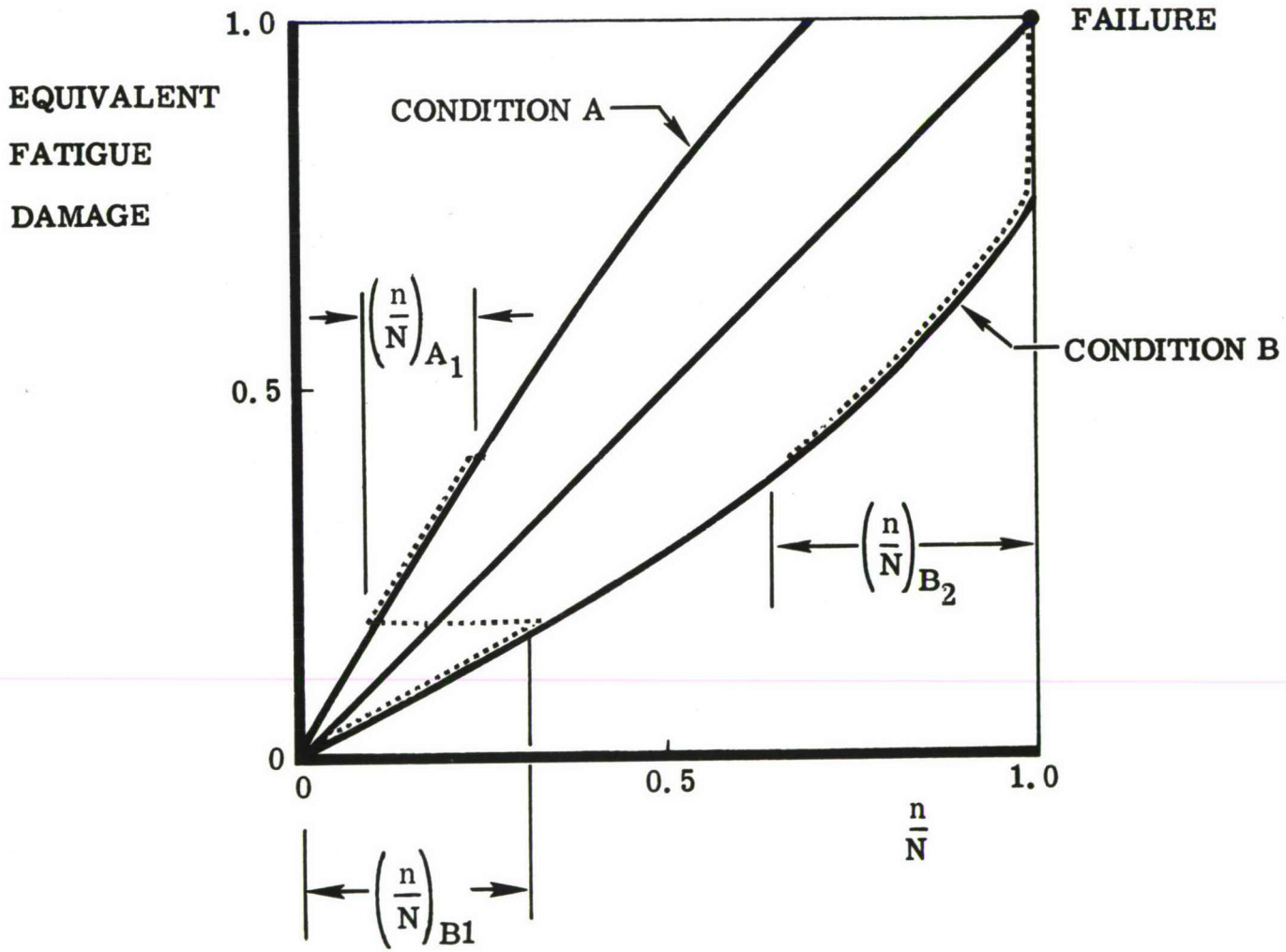

Figure 32 . Equivalent Fatigue Damage Computation

only required S-N curves and a load spectum, whereas additional test data are now necessary in order to obtain fatigue damage D_c. Another limiting factor of Henry's theory is that it is inapplicable to materials like aluminum which have no defined endurance limit.

CONCLUSIONS

From the survey of some of the better known cumulative damage concepts, it is apparent that each of the methods contains some desirable improvement over Miner's original proposal. However, when making a comparison of the basis of each method as a whole, Miner's linear rule is the obvious choice for use in cumulative damage analysis at this time. The primary reasons for the choice of Miner's rule are (1) The method is simple in concept and application and, (2) the data required, in the form of S-N curves, are numerous and readily available. Although Miner's damage concept does yield results which can vary considerably, the consistency of results of the other methods is not significantly better, considering their complexity. A comparison of test and predicted spectrum life (Reference 33) for four cumulative damage methods is shown in table 20.

Because of the assumption of linear damage in Miner's rule, approaches to already complex acoustical fatigue analysis are simplified. Although the two methods proposed in References 25 and 34 for developing random fatigue curves differ, the method of evaluating the damage is still Miner's rule.

4.3 SCATTER

The inconsistency or scatter of fatigue results will always plague the design engineer. Fatigue life evaluation, unlike the degree of accuracy accomplished in static strength computation, leaves much to be desired in the way of consistency. The incomplete understanding of the basic mechanisms of fatigue damage relegates life prediction to an empirical approach. Although important advances have been made in improving fatigue life computations, additional problems, such as the interrelationship of creep and fatigue at elevated temperatures, have been introduced. Fatigue life determination is not as forbidding a problem as it first appears, if the designer is aware of the variation to be expected and knows how to account for them. Some of the primary factors which influence fatigue life are: variability of material, environment, design details, and load history. Material variability, such as heat treat, surface conditions, and grain direction, can have a strong effect on fatigue scatter, especially if they are not accounted for during the collection of or use of S-N data. For example, the endurance limit of H-11 steel with transverse grain is 70 percent of longitudinally grained H-11. The order of fatigue loading on a part (e.g., high load first or low load first) can also cause a large variation in fatigue life. In some instances, an increase in life by a factor of ten has been observed.

Table 20

COMPARISON BETWEEN ACTUAL AND PREDICTED SPECTRUM LIFE

Material: PH15-7Mo (RH950)

Stress concentration: $K_t = 2.33$

Test Life (In Spectrum Blocks)
93 + (maximum)
70 + (average)
50 + (minimum)

	Predicted Life (In Spectrum Blocks)			
Preload	Miner's	EFD	Modified Henry's	Mean Damage Rate
None (1)	30.2	-	26.9	25.3
Simple (2)	41.3	-	37.1	35.3
Assumed (3)	63.9	44.8	55.8	51.4

(1) "Normal" S-N data
(2) S-N′ data with previously applied simple preload
(3) S-N″ data with assumed additional prior load history

The trend at present is toward the collection of S-N data on a statistical basis. Because of cost or time requirements, a useful statistical analysis is not always possible. Usually, the S-N curve is conservatively drawn through the lower envelope of the test points. Even with good, statistically developed fatigue curves, large errors can be introduced because of the inability to compute the stresses in the region of built-in structural acuities. Because of the many variables and the empirical nature of fatigue, it appears that fatigue evaluation will depend to a large extent on past experience.

In order to estimate the effect of fatigue scatter on the calculation of allowable sound pressure levels from a Rayleigh random S-N curve, a material was chosen for which considerable test data were available. (See figure 33.) S-N curves were drawn for the upper and lower range of the test data. Random fatigue curves were then calculated for each of the two S-N curves. The difference in allowable sound pressure level in db, at 2,000,000 cycles was found to be 2.8. Consequently, if a random curve was desired for a material for which limited fatigue data were available, the variation in allowable would not be great. It should be re-emphasized that a conservative factor is introduced in acoustical fatigue computations by the use of a Rayleigh distribution with Miner's linear damage rule.

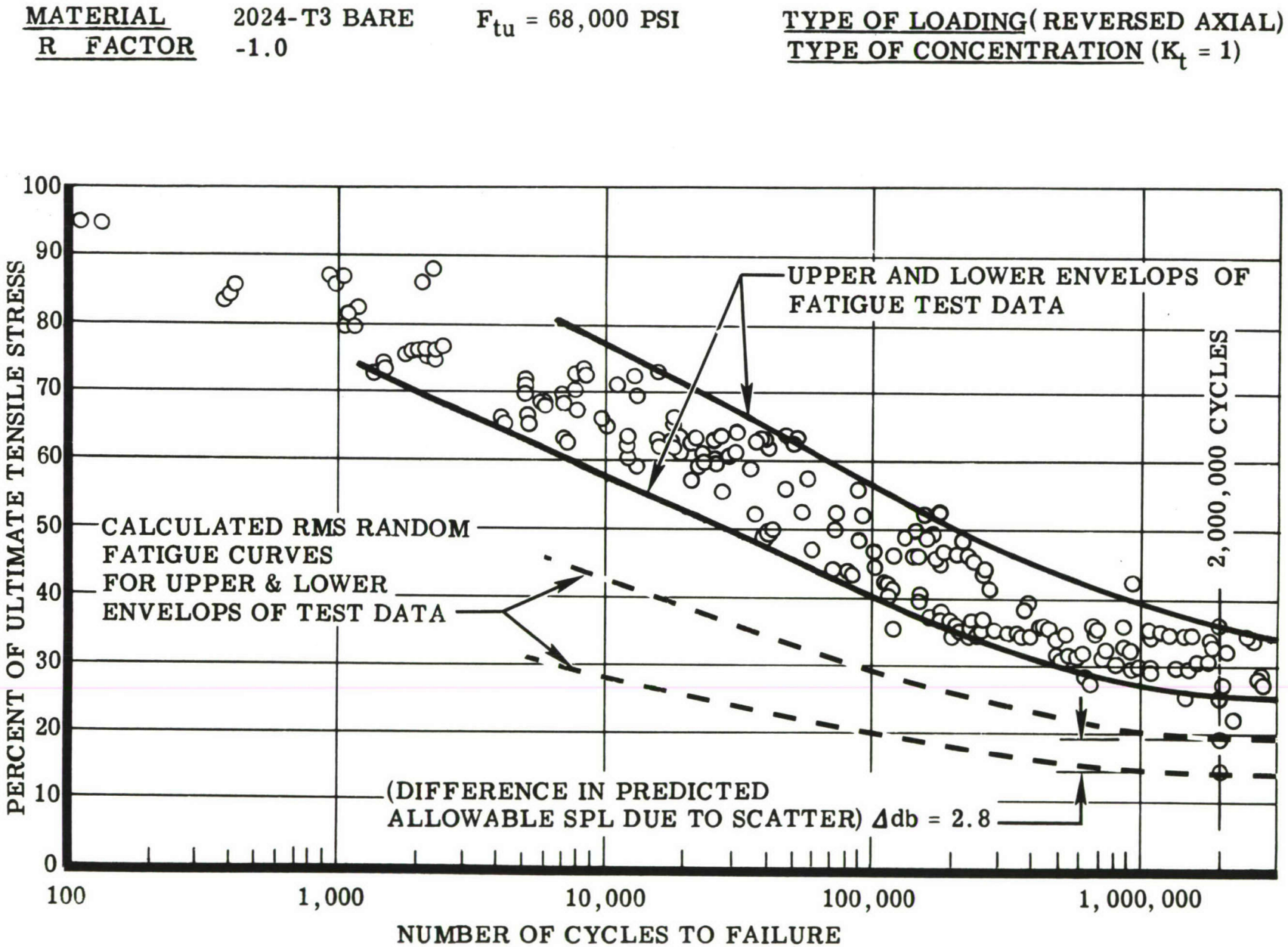

Figure 33. Effect of Fatigue Data Scatter on Allowable Sound Pressure Level

Section V

ANALYTICAL APPROACH TO DESIGN CRITERIA

5.0 ANALYTICAL APPROACH

The combination of the acoustic environment, its duration, the response of the structure, and basic material fatigue data can be brought together in a manner to permit analytical solution. The solution is in the main, dependent on the same assumptions as those used in solving primary-load fatigue problems. The principal distinction between the acoustical fatigue problem and that of primary-load fatigue lies seemingly in an imprecise knowledge of the stress magnitudes being imposed at the point of a failure in the former. The practical solution to this gap in dynamic stress analysis is reliance on test. Logically, these data could be collected in tests of simulated structure with either discrete frequency sirens or with broad-band sound sources. However, keeping in mind the afore-mentioned imprecision which exists for either sound source, discrete frequency testing offers obvious advantages. A random test cannot be empirically related to basic S-N curves; thus, a valuable source of fatigue data would be unavailable to help solve the problem. It is not economically feasible to test sufficient numbers of specimens of various structural configurations to recreate basic fatigue data in random source form. The random test, conceivable more accurate, can be utilized to advantage for proof-testing completed structural designs. For design development work, the discrete frequency siren appears to be more practical. Therefore, siren testing with constant sinusoidal sound pressure levels is offered as a rapid, economical procedure to obviate the need for the missing stress response information and to complete the analytical approach to design criteria. The method and techniques are essentially those developed by Belcher, Van Dyke, and Eshleman (References 15 and 34), and were used successfully in the design development of the DC-8.

5.1 DERIVATION OF ANALYTICAL APPROACH

STRESS RESPONSE

The stress response equations for sinusoidal and random excitation from Section III,

Sinusoidal:
$$\overline{s_s^2} = \left(\frac{1}{2\delta}\right)^2 s_o^2 p_s^2 \qquad (7)$$

Random:
$$\overline{s_r^2} = \frac{\pi}{4\delta} f_o s_o^2 p_r^2 \qquad (6)$$

Ratio sine-random:
$$\frac{\overline{s_r^2}}{s_s^2} = f_o \frac{p_r^2}{p_s^2} \qquad (8)$$

show that the stresses induced in structures can be related to the sound pressure levels which excite their surface panels. By relating these same stresses to fatigue life and comparing cycles to failure, the problem can be sufficiently simplified to permit a reasonable solution.

RANDOM-STRESS FATIGUE-LIFE PREDICTION

The fatigue life of a panel subjected to sinusoidal stress reversals, s_s, can be predicted simply by using an S-N curve for fully reversed bending or testing (R factor = -1) for the appropriate material and stress concentration factor. Utilizing cumulative damage methods, in this case Miner's Rule (refer to Section IV)

$$\text{Damage, } D = \Sigma \frac{n_x}{N_x} \quad \text{(equals 1 at failure)}$$

(n_x and N_x are applied and allowable number of cycles) and a probability density function of random stress peaks assumed to be that of Rayleigh (refer to Section III),

$$P(x) = xe^{-\frac{x^2}{2}}$$

where

$P(x)$ = fraction of the total number of cycles of stress level x

x = relative stress

the fatigue life for a given rms value of random stress peaks can be calculated. The most probable (or frequently) applied stress level is the rms stress level.

$$\text{Random cycles, } N_R = \frac{1}{\int_0^\infty \frac{P(x)dx}{Nx}} \tag{20}$$

RANDOM S-N CURVE

The solution of this equation for various values of $\overline{s_r^2}$, the random rms stress, will, when plotted, yield an S-N curve which is called the "random fatigue curve." The ordinate is the rms stress and the abscissa N, number of cycles, is the total number of random stress cycles at all stress levels. Figure 34 is an illustration for 2014-T6 aluminum alloy of the point-by-point construction of a random S-N curve. The significance of this curve lies in its use, together with a discrete frequency siren test to failure, in predicting

$$D = \Sigma \frac{N_x}{N_x} = 1 \quad \text{AT FAILURE}$$

$$P(x) = xe^{-\frac{x^2}{2}}$$

$$x = \frac{S_M}{\sqrt{\overline{s^2}}}$$

$$N_R = \frac{1}{\int_0^\infty \frac{P(x)\,dx}{N_x}}$$

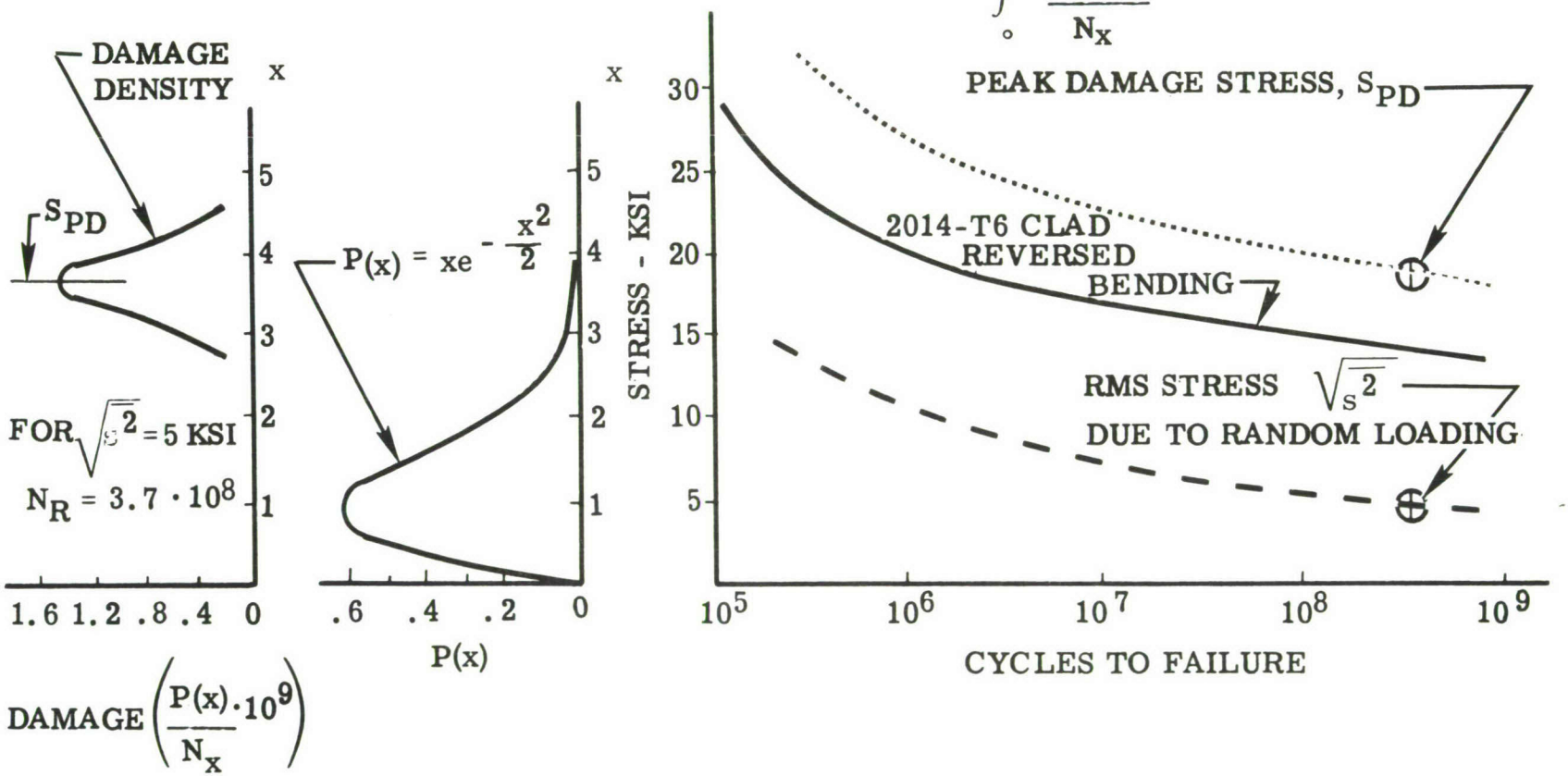

Figure 34. Computation of Random S - N Curve

either the life at a specified random spectrum sound pressure level or the random sound pressure level for a specified life. Random S-N curves for various materials are presented in Section IV.

The construction of the random S-N curve (figure 34) reveals the interesting and conceptually useful phenomenon of "peak damage stress." When a cumulative damage solution is performed using a smooth distribution such as that of Rayleigh, the neighborhood about a single load level turns out to contain nearly all of the significant damage. Mathematically stated, the $\frac{n \text{ (peak damage)}}{N \text{ (peak damage)}}$ term is the largest term in the summation:

$$\text{(damage)},\ D = \Sigma \frac{n_x}{N_x}$$

The peak damage stress in the example (figure 34) is almost four times the rms stress. This means, as seen in examining the Rayleigh distribution curve, that a very small number, compared to the total, of high stress peaks do most of the damage. The peak-damage stress concept then is an analytical explanation of the "acceleration nature" of a siren test, which is normally conducted at a sinusoidal stress near in magnitude to the peak damage stress, S_{PD}. The siren can apply, in a few minutes time, sufficient numbers of sinusoidal stresses near the S_{PD} to fail a panel which would require hours of random excitation or years of service experience.

CORRECTION FACTOR FOR NONLINEAR STRESS

The concept of peak damage stress allows a simple, first-order correction for nonlinearity. Figure 47 shows stress versus sound pressure level. It is necessary to make this correction only because the sinusoidal test stress, s_s, is likely to be of different magnitude than the peak damage stress, S_{PD}. As shown in the figure 47, the correction factor is simply the ratio of slopes at the two stress levels.

$$\lambda = \left(\frac{\alpha \text{ PD}}{\alpha \text{ TEST}} \right)^2 \tag{21}$$

CORRECTED STRESS RATIO EQUATION

The factors or correction added to equation (8) yields:

$$\frac{s_r^2}{s_s^2} = \pi f_o \delta \frac{p_r^2}{p_s^2} \lambda^\gamma \tag{22}$$

where λ is the nonlinear stress correction and γ is the multimode correction (both from Section III). The solution to this equation can be reduced to a

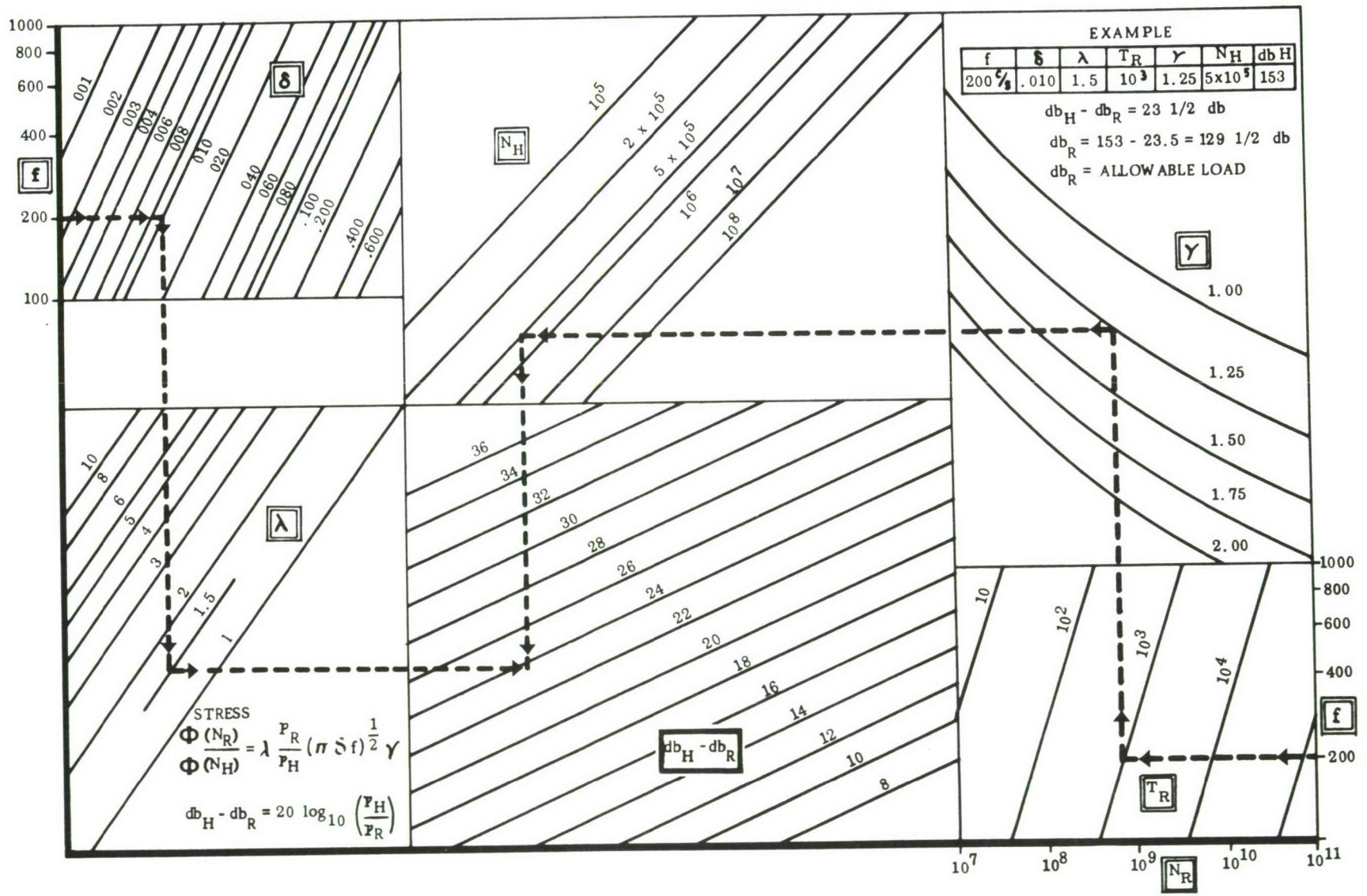

Figure 35. Conversion Chart Discrete Loading to Random Loading

STEP 1 CONSTRUCT RANDOM S-N CURVE

DETERMINE:

S_s FROM S-N CURVE AT N_S

$\sqrt{s_r^2}$ FROM RANDOM S-N CURVE AT N_R

(N_R = DESIRED LIFE $\times f_o$)

STEP 2 COMPUTE:

1. δ DAMPING FACTOR
2. γ MULTIMODE FACTOR
3. λ NONLINEARITY FACTOR

FROM SIREN TEST RESPONSE DATA

STEP 3 COMPUTE:

$\frac{p_r}{p_s}$ RATIO OF SOUND PRESSURE LEVELS

FROM $\frac{\sqrt{s_r^2}}{S_s} = \frac{p_r}{p_s} \left(\pi \delta f_o \right)^{1/2} \lambda \gamma$

STEP 4 COMPUTE:

db RANDOM FROM

$\Delta db = db_s - db_r = 20 \log \frac{p_s}{p_r}$

STEP 5 COMPARE:

db_r FROM STEP 4

WITH do ENVIRONMENT (SPECTRUM)

Figure 36 . Steps in Sine-Random Equivalence Calculation

nomogram (see figure 35) for rapid solution, however, the step-by-step process is favored for conceptual understanding. The steps are shown in paragraph 5.2 together with a detailed random S-N curve.

5.2 SINE-RANDOM EQUIVALENCE

The procedure, derived in the preceding sections, can be reduced to a step-by-step process (figure 36) for ease of conceptual understanding and performance by the structural designer. These steps assume that the vehicle acoustic environment has been completely described with the following data:

1. Over-all sound pressure levels
2. Frequency spectrum of SPL
3. Direction and distance from the sound source, i.e., a contour map of constant pressure (isobars)
4. Character of the noise source
5. Duration of the noise for the desired service life of the vehicle

In addition to environmental data, it is assumed that a siren test has been performed on a specimen which accurately simulated the vehicle structure. The data assumed extracted from the sinusoidal siren test are:

1. Total time to failure at specified sound pressure levels and frequencies.
2. A plot of frequency versus stress response from a frequency sweep. (See figure 6.)
3. Plots for each mode of sound pressure level versus stress response. (See figure 47.)
4. Description and location of the failure.
5. Knowledge of mode shape.
6. May include an amplitude decay rate curve. It is also assumed that standard S-N curves for the material in question at R FACTOR = -1, fully reversed loading, are available.

CONSTRUCTION OF RANDOM S-N CURVE

With the appropriate S-N curve for the test specimen at the point of failure, and an accurately drawn Rayleigh probability curve, figure 37, the random S-N curve can be constructed. The graphical solution is as follows: Select an arbitrary value of the random rms stress, $\left[\overline{s_r^2}\right]^{1/2}$. The solution then consists of solving for the total number of random cycles corresponding to the random rms stress, by using Miner's rule of cumulative damage. This is done graphically, using a cumulative damage table such as Table 21. Values of x, relative stress, are chosen at discrete intervals. At these values of x, P(x), the relative number of cycles, is read from the Rayleigh curve. N_x, the allowable number of cycles at each stress level, is obtained from the S-N curve at each stress level and which is equal to x times the rms stress chosen. Relative damage or damage density is the $P(x)/N_x$, in the last column. A plot of $P(x)/N_x$ versus x is called the damage density curve and reveals the peak damage stress level, S_{PD}. (See figure 38.) If all intervals of x, $0 \rightarrow \infty$, were included the table of $P(x)/N_x$, this column summed would be the integral of the area under the damage density curve. The reciprocal of the integral $\frac{1}{\int_0^{\infty} \frac{P(x)dx}{N_x}}$ is the desired number, the total random cycles, at all stress levels about the chosen rms stress which the specimen could endure. By repeating the calculation for a series of rms stress values, the curve of rms versus cycles, N_R, can be plotted. The curve of peak damage stress, S_{PD}, can also be plotted. Figure 39 shows a random S-N curve, a point from which corresponds to the damage density curve, figure 38, and the cumulative damage table, Table 21. The peak damage stress, which usually varies from 2 to 4 times the value of the rms stress, will be used in the calculation of a correction factor for nonlinear stress response.

The calculation of the random S-N curve lends itself readily to the high-speed digital computer, if desired. Since it need be performed once only for a given situation, the need is not readily apparent.

DEPENDENCE ON SIREN TESTING

The siren test, which is discussed in more detail in paragraph 5.2, must provide more data than just a failure at an applied sinusoidal stress level and a number of cycles realized. Even if the problem were considered completely linear in all respects, as discussed in "Stress Response" in Section III, one other result must be determined empirically, i.e., the damping factor or, equivalently, the amplification factor at resonance.

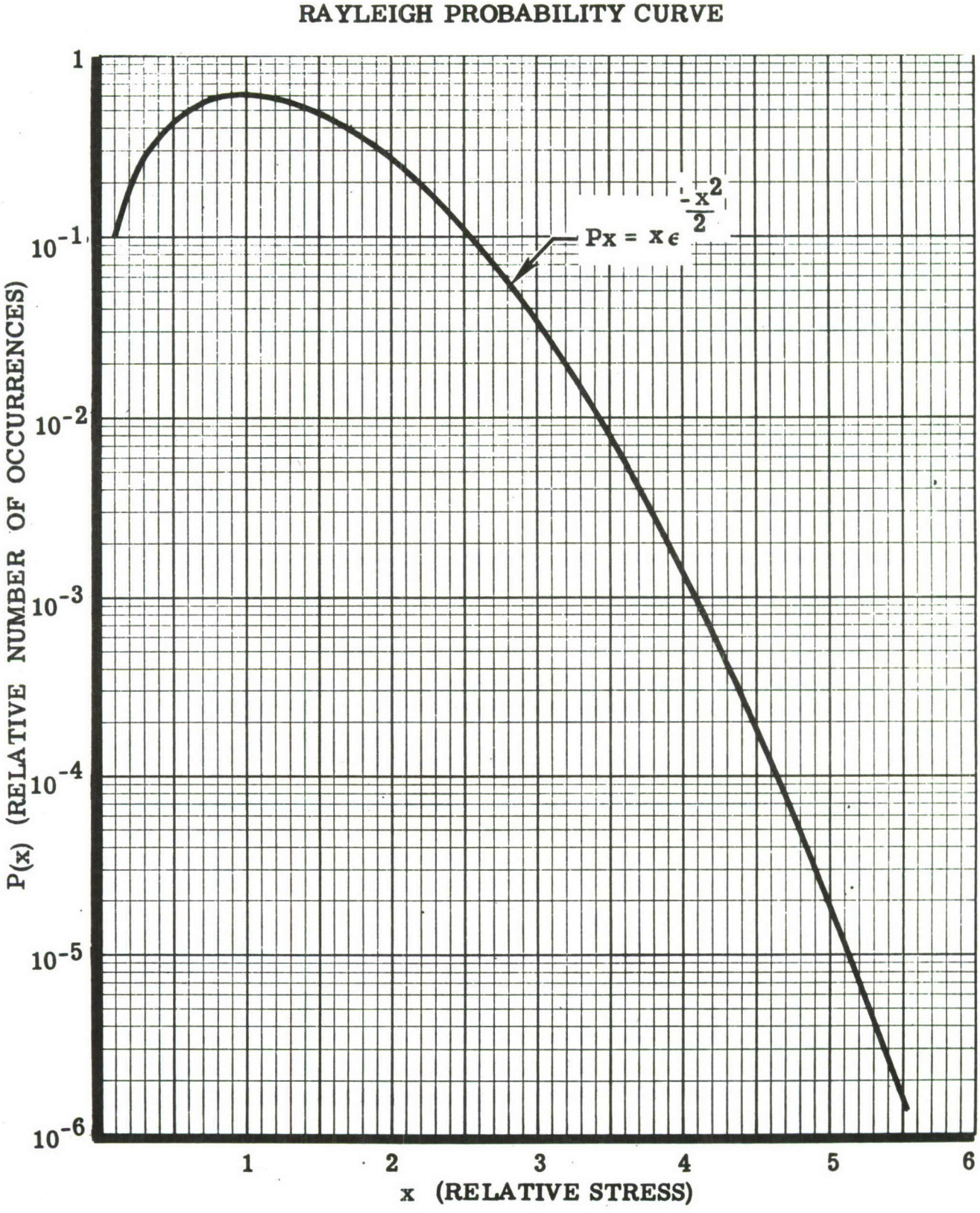

Figure 37. Rayleigh Probability Curves

CUMULATIVE DAMAGE TABLE FOR ANNEALED TITANIUM

$\sqrt{\overline{s_R^2}}$ = 15,000 PSI (ASSUMED)

x	P(x)	$N_{(x)}$	$P(x)/N_{(x)}$
2.2	$(1.95)(10^{-1})$	$(4)(10^{6})$	$(0.05)(10^{-6})$
2.4	$(1.34)(10^{-1})$	$(9.5)(10^{4})$	$(1.41)(10^{-6})$
2.6	$(8.8)(10^{-2})$	$(2.9)(10^{4})$	$(3.04)(10^{-6})$
2.8	$(5.6)(10^{-2})$	$(1.5)(10^{4})$	$(3.73)(10^{-6})$
3.0	$(3.5)(10^{-2})$	$(8.5)(10^{3})$	$(4.12)(10^{-6})$
3.2	$(2.0)(10^{-2})$	$(5.6)(10^{3})$	$(3.57)(10^{-6})$
3.4	$(1.05)(10^{-2})$	$(3.3)(10^{3})$	$(3.18)(10^{-6})$
3.6	$(5.5)(10^{-3})$	$(2.2)(10^{3})$	$(2.5)(10^{-6})$
3.8	$(2.8)(10^{-3})$	$(1.4)(10^{3})$	$(2.0)(10^{-6})$
4.0	$(1.5)(10^{-3})$	$(9.5)(10^{2})$	$(1.58)(10^{-6})$
4.2	$(6.2)(10^{-4})$	$(6.4)(10^{2})$	$(0.97)(10^{-6})$
4.4	$(2.7)(10^{-4})$	$(4.3)(10^{2})$	$(0.63)(10^{-6})$
4.6	$(1.2)(10^{-4})$	$(3)(10^{2})$	$(0.4)(10^{-6})$
4.7	$(7.5)(10^{-5})$	$(2.5)(10^{2})$	$(0.3)(10^{-6})$
Σ			27.48×10^{-6}

$dx = 0.2$

$$\Sigma \frac{P(x)}{N_{(x)}} = 0.2 \times 27.48 \times 10^{-6} = 5.496 \times 10^{-6}$$

$$N_R = \frac{1}{5.496 \times 10^{-6}} = 184,000 \text{ c}$$

Table 21. CUMULATIVE DAMAGE TABLE

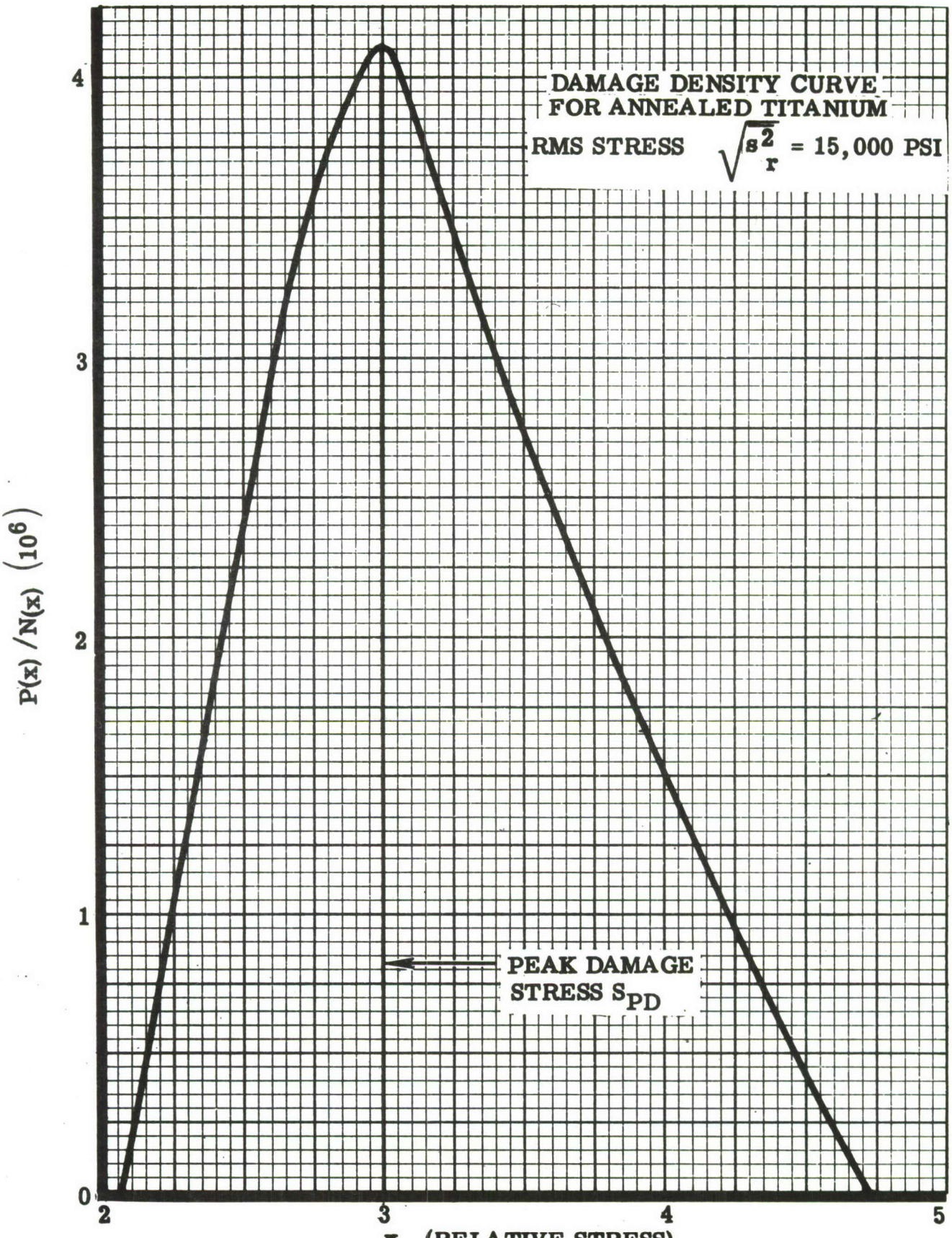

Figure 38. Damage Density Curve

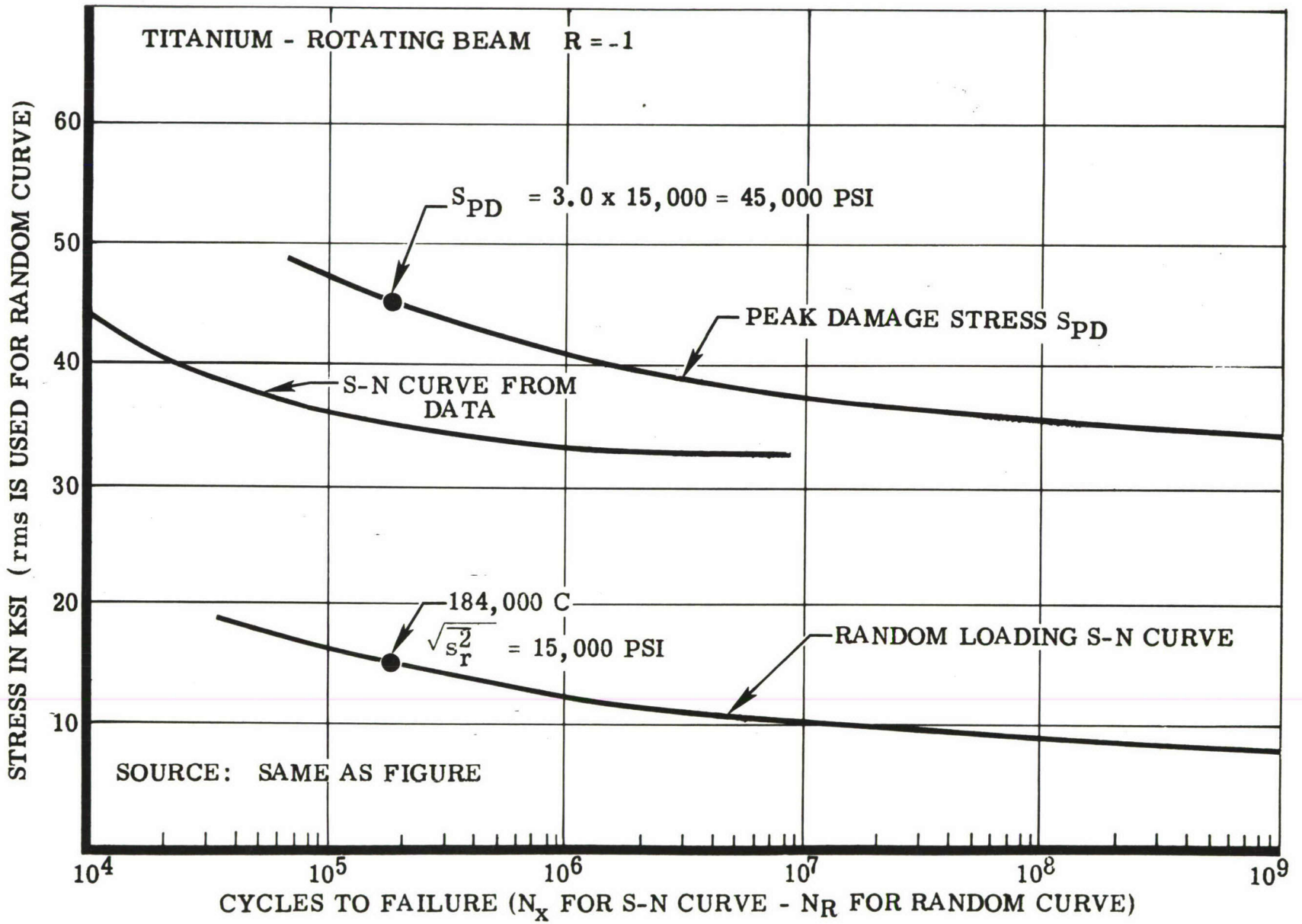

Figure 39. Comparison Between Actual and Predicted Spectrum Life

$$\text{Damping factor, } \delta = \frac{c}{c_c} \text{ ratio of critical damping}$$

$$\text{Amplification factor} = \frac{1}{2\delta}$$

The significance of the damping factor is revealed in the equation:

$$\frac{\overline{s_r^2}}{s_s^2} = \pi f_o \delta \frac{p_r^2}{p_s^2} \qquad (8)$$

which shows that damping has a different effect upon stress response to the two excitation pressures, sinusoidal and random.

5.3 SIREN TESTING

It is the purpose of this section to offer guides to the successful use of siren testing. This is necessary in the scope of this report only because sine-random equivalence is the approach selected.

Care must be exercised in choosing between a reverberant (normal) and progressive (grazing incidence) wave-sound field for a particular test. (See figure 40.)

More meaningful test results are obtained by testing structures in a sound field similar to that in which they are to be used. Also, there are instances in which a traveling-wave mode is excited in a progressive field and is the mode causing the greatest stress in the structure. This condition is not excited adequately in a reverberant chamber test; consequently, a reverberant test would produce unconservative results. It should be noted that this traveling-wave mode occurs only on specimens that are large with respect to the wavelength of the excitation source. (See Sections III and VI for more detail on spatial properties of sound sources.)

The siren facility must have sufficient control of frequency, either manual or automatic, to assure staying on resonance. For some structures initial failure is evidenced by relatively small changes (lowering) in resonance frequency.

TEST SPECIMEN SELECTION

Selection of typical structural specimens for test depends on many considerations, involving both the structural configuration and specific environment. Once the suspected problem areas of the vehicle have been determined, the

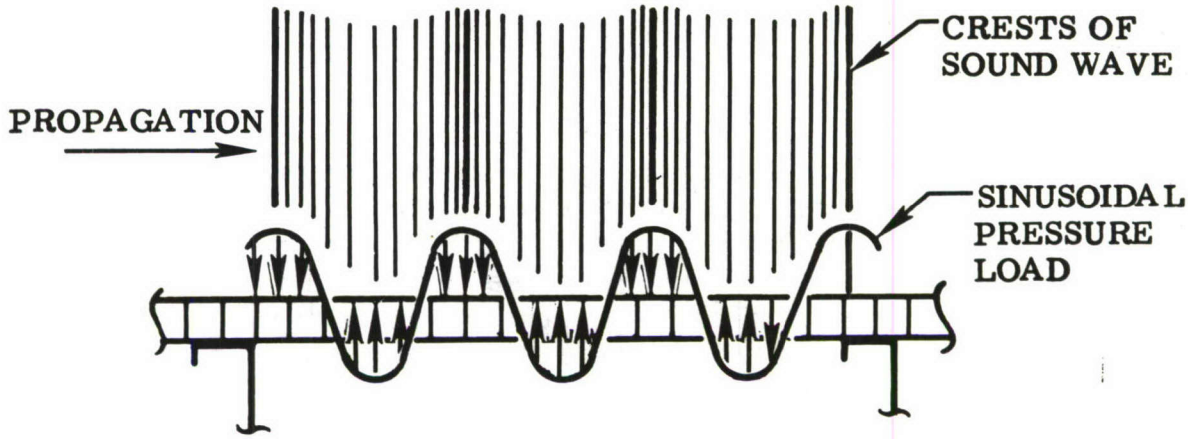

a. PROGRESSIVE (GRAZING INCIDENCE) WAVE

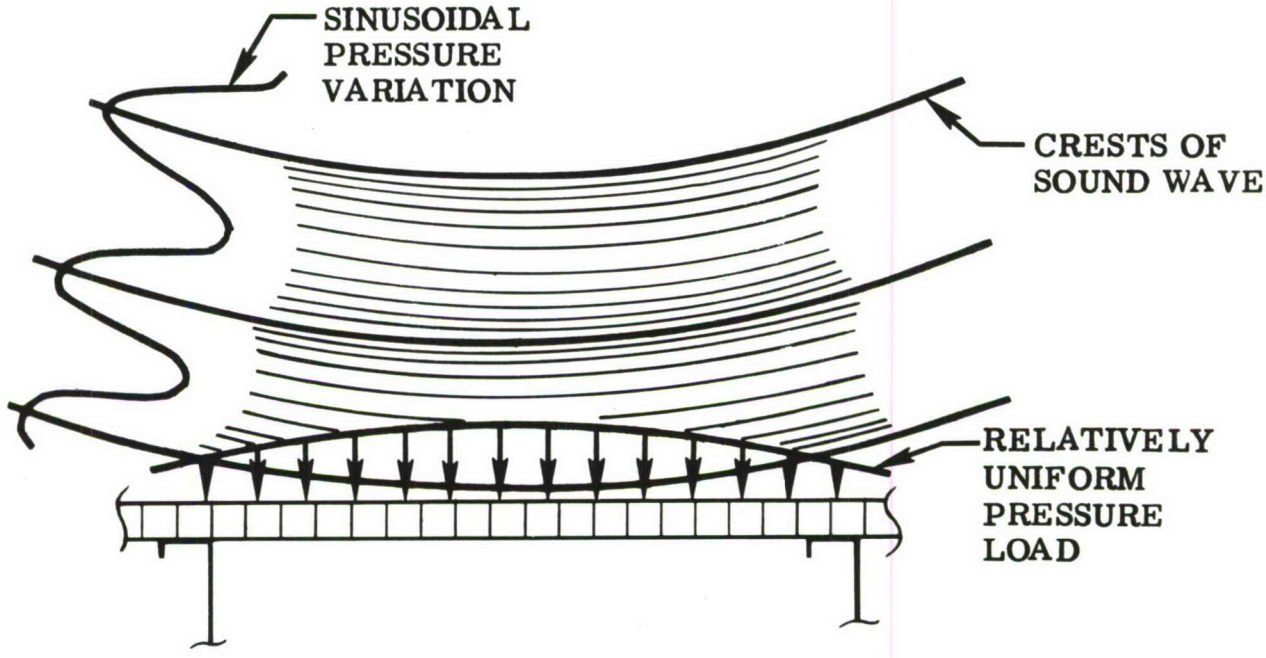

b. NORMAL WAVE

Figure 40. Normal Versus Progressive Wave

following precautions should be observed. (See Section VI for a practical illustration of these considerations.)

The test specimen should be representative of the sections having the largest unsupported panel areas. Rib webs or frames should be of representative depths.

It is also extremely important that the actual vehicle fastener configuration be used on the test specimen. If possible, production fastening techniques should be used. The fasteners have a large effect on the edge conditions and stress concentrations of the individual panels, and thus have great influence on both the natural frequency and stress response of the structure. It is also possible that different fasteners permit different slip rates at the joints of skin-stringer construction, thus affecting the structural damping of the specimen.

Great care must be exercised in determining the amount of substructure that must be part of the test specimen. For development work, early in a program, it may be desirable to test specimens consisting only of panel surfaces and that substructure which would have an effect on the end conditions.

Once a structural configuration has been defined, and it is necessary to conduct an evaluation for the specific vehicle environment, the specimen must be complete. Evaluation specimens must consist of production-type panels and substructure and must contain any electrical, hydraulic, or other fittings that would be attached to the panels or substructure. Although the actual performance of these fittings may not be of primary importance in the fatigue test, they may definitely influence the response of the structure through mass loading, stress concentrations, or changes in stiffness.

TEST SPECIMEN INSTALLATION

The effect of improper test specimen installation cannot be overemphasized. A test installation involving simple panels, rigidly clamped, may well provide useful comparative data, but the results would be difficult to analyze in terms of performance on an airframe.

The effects of edge attachment can be reflected in the mode shapes and natural frequencies of the structure under test. The point of maximum stress and the value of maximum stress are functions of edge attachment. As an example, the natural frequency of a 0.5- x 24- x 24-inch honeycomb sandwich panel changed from 310 cps to 280 cps when two out of ten attachment bolts vibrated loose during a discrete frequency test. The effect on mode shape and stress distribution is even more pronounced. Consequently, if a reasonably accurate structural analysis is to be made, the specimen edge attachment must approximate closely the actual air vehicle attachment.

An example of typical rib-skin structure is shown in figure 41. Note that the outboard bays are rigidly clamped, but that the central bays simulate the edge fixity of the actual air vehicle assembly.

Failures that developed close to the rigid supports possibly would not be indicative of what would happen in service; however, the response of the central bays would be similar to that under service conditions.

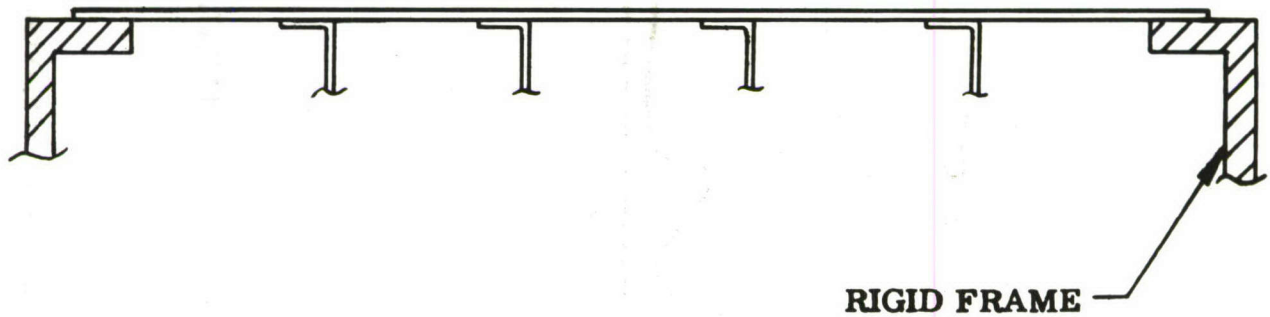

Figure 41. Typical Skin-Rib Test Panel

A frequency scan must be performed at some nominal constant sound pressure level (SPL) to determine resonance frequencies for life testing. A convenient method consists of plotting the output of a strain gage or a deflection measuring transducer as a function of frequency on an X-Y recorder. This display provides both a means of determining resonance frequencies and a measure of structural damping. The bandwidth at the 1/2 power points of the response curve is proportional to the damping coefficient (figure 42).

It should be noted that this method for determining the damping coefficient is valid only if the response of the structure is approximately linear, thus having an almost symetrical response curve. If the panel response is non-linear, other means are available for determining the damping coefficient. This subject is more completely discussed in the paragraph on "Test Data."

Determining the appropriate resonance frequencies for life testing of simple panels consists of choosing the frequencies which show the greatest stress response. This would normally include the fundamental bending mode. Viewing the specimen with a stroboscopic light is very helpful in defining the mode shapes at the various resonance frequencies.

Configurations with more complex responses, such as those of skin-rib assemblies require a more careful modal analysis for choice of test frequencies.

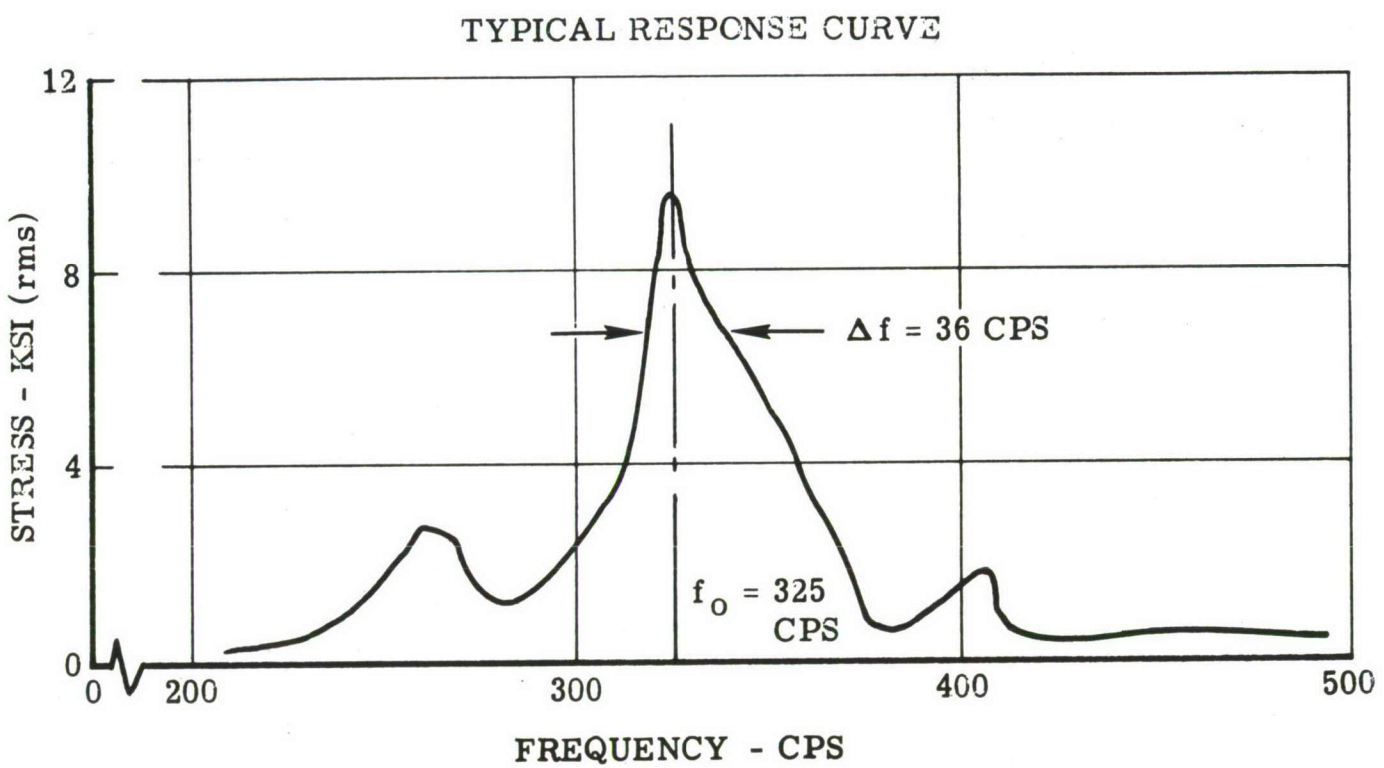

f_o = NATURAL FREQUENCY

Δf = BANDWIDTH AT HALF-POWER POINT

c/c_o = DAMPING COEFFICIENT (WITH RESPECT TO CRITICAL DAMPING)

$$c/c_o = \frac{\Delta f}{2 f_o} = \frac{36}{2 \times 325} = 0.055$$

Figure 42. Calculation of Damping Coefficient From Response Curve

LIFE TEST PROCEDURE

Simple comparative tests might be performed by testing several types of structures at the same SPL in similar modes. This procedure might be expanded to the point of testing several specimens each, of different configurations, at several SPL's and then plotting the results as test SPL versus time-to-failure (similar in shape to an S-N curve). Then, all other parameters being equal, the configuration with the highest curve would be the most desirable. Obviously, this technique would be quite expensive even if the test specimens involved more than just the simplest of structure. Also, the result is still only comparative in value unless a more comprehensive analysis is made.

A recommended procedure is to perform step-tests wherein a specimen is tested for some nominal time period at increased SPL increments until failure occurs. The test results are then equated to an equivalent time-to-failure and SPL by the cumulative damage method for comparative purposes and analysis. This technique permits the acquisition of as much data as possible from a limited number of specimens. In the extreme, it permits the complete proof-testing of a complex assembly with the use of only one specimen. This is, in fact, often done. Some loss of precision can be involved, but if the configuration shows adequate margin, the technique is satisfactory and the saving in time and resources can be highly significant.

TEST DATA

In order to equate the results of a discrete frequency test to an equivalent random application by the method outlined in paragraph 5.1, the following data must be obtained:

1. Test frequencies (and knowledge of the mode shapes)
2. Time-to-failure*
3. Sound pressure level*
4. Stress-load curves for each mode (see figure 43)
5. Stress versus frequency curve

*These values would be computed values if the step-test technique were used.

The stress versus frequency curve provides a means of calculating the damping of the structure. The stress-load curve is necessary for computation of a nonlinearity correction factor.

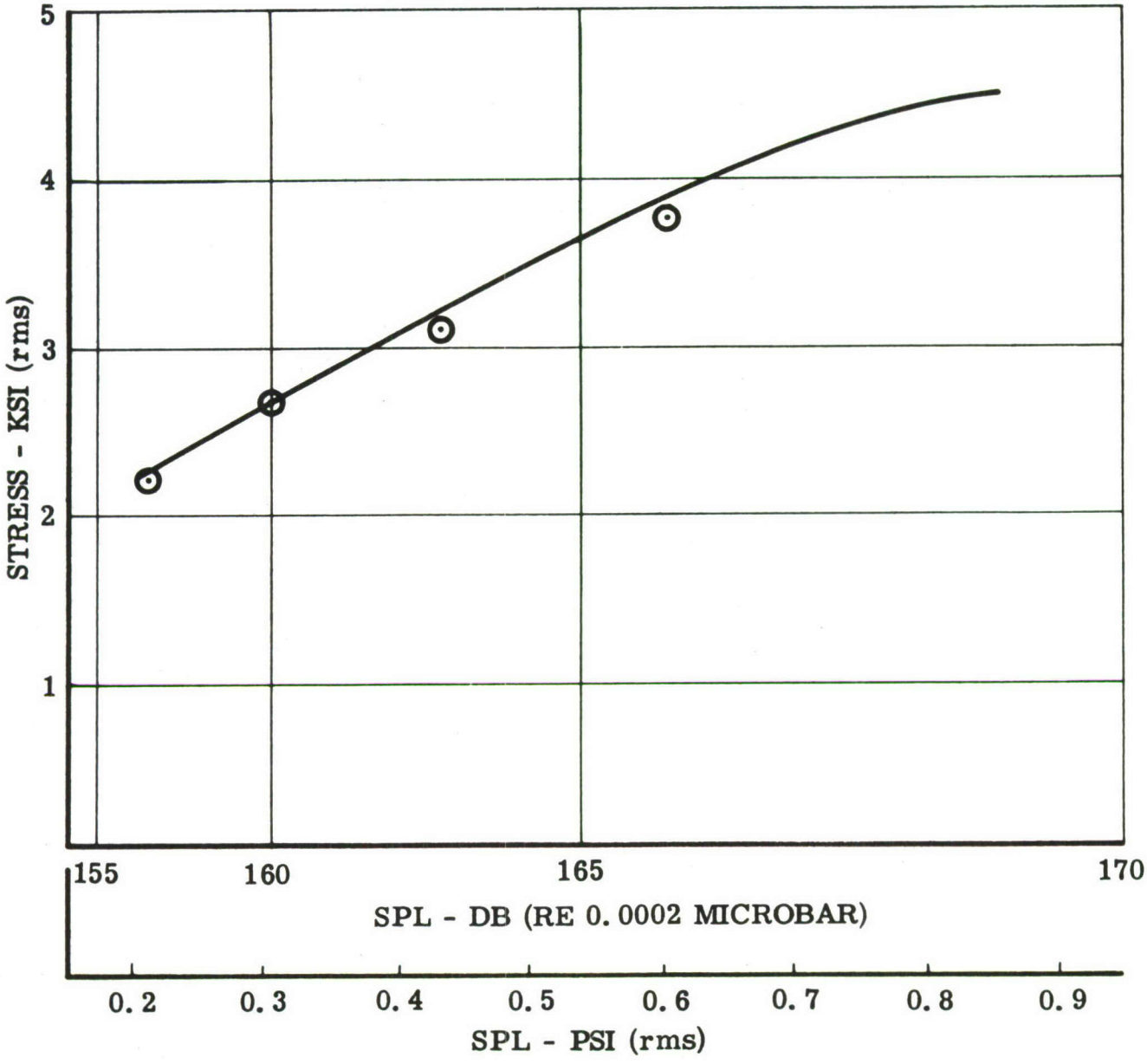

Figure 43. Typical Stress - Load Curve

It is suggested that the stress versus frequency curve be plotted at a sound pressure level low enough to avoid excitation of the specimen in its nonlinear range. If this is not possible, it is suggested that the structural damping coefficient be calculated from a decay curve.

This can be accomplished by exciting the specimen with a noise source such as a loudspeaker, removing the excitation, and recording the decay of a strain-gage voltage filtered to provide modal isolation. It is best to accomplish this procedure before the specimen is installed in the progressive wave-test section, as the slow reverberation decay of the test section may affect the decay rate of the specimen.

5.4 SOURCES OF ERROR

Quoted directly from Reference 34. "Comparison of test results under random and sinusoidal loading has been made for a number of specimens. (See Reference 35.) The variation between measured and computed stress ratios was found to be on the order of ±3 db. Some of the more obvious sources of error in computations for stress, and for fatigue life, not necessarily in the order of importance, are:

1. An error of one db in sound pressure measurement represents approximately 12 percent error in load.

2. If the siren excitation frequency is off resonance, a large nonconservative error in damage accumulation can occur.

3. Damping factors depend on how they are measured.

4. The propagation direction of the sound relative to the panel in a siren test and in an airframe application is not, in general, the same. (See References 15 and 17.)

5. Harmonics of the siren fundamental pressure wave may excite higher modes of the structure.

6. The nonlinearity of the structure depends not only on the design but also on the quality of fabrication, which is variable among specimens, e.g., skins which are tightly stretched begin to diaphragm at lower pressures than do loose skins. This can have a large effect on λ.

7. If there is more than one significant mode, additional effects which contribute to errors exist.

   (a) It is not necessary to know the actual values of stress for each mode, but the relative stress amplitudes must be known if the computed value of γ is to be meaningful.

(b) The possibility of obtaining misleading strain gage readings because of a nonzero geometric angle between the principal stresses must be considered.

(c) There is no certainty that the structural area which is critical when all modes are excited simultaneously (as by random noise) is the location of failure in the discrete frequency test.

(d) Coupling between modes, especially when there is little difference between the resonance frequencies, causes difficulties in measuring the damping factors and results in questionable interpretation of their physical meaning.

8. For a specified life, allowable stress varies as much as ±15 percent for a plain smooth specimen, and an additional variation of ±15 percent occurs for a notched specimen."

Spatial correlation, one of the possible sources of error, is discussed in more detail in paragraph 3.6, Section III.

Unpublished results from Contract AF33(616)-7147, Siren - Random Fatigue Testing Study, show random S-N curves which are about one db above predicted random S-N curves. In this case, the predicted random S-N curves were not corrected for either nonlinearity or multimode effects, nor were they measured in the test program.

Section VI

EXAMPLE PROBLEM SOLUTION

6.0 INTRODUCTION

A hypothetical problem is presented here to illustrate use of the techniques advanced in this report.

The vehicle is assumed to be a Mach 3.0 intercept fighter having two engines, in the 30,000-pound thrust class, with afterburners. It has a delta planform with elevons for roll-and-pitch control and a movable vertical stabilizer for yaw control.

The solution will involve the specification of the sound spectra at representative positions on the vertical stabilizer as determined by the engines' operating characteristics for various ground and flight operations and the vehicle geometry. The proposed structure for the vehicle will be reviewed in terms of the applied spectra, and a representative section of structure will be chosen for experimental determination of acoustical fatigue strength. A test specimen representative of this section will be designed, a siren test will be conducted, and the results of the test interpreted in terms of the allowable applied random loads for the durations of these loads anticipated in the design mission.

Further, the primary air inlet system for the vehicle's engines will be investigated for verification of its integrity under the excitation of boundary layer turbulence.

6.1 EXAMPLE OF STRUCTURE EXCITED BY ENGINE NOISE

AIRFRAME GEOMETRY

Figure 44, a sketch of the vertical stabilizer, shows the geometry and dimensions of the surface and its location with respect to the engine exits.

MISSION ANALYSIS

Filled in mission outlines are shown in Tables 22 through 24. The design capability for Mach 3 cruise, which would be employed fairly often on long-range intercepts, dictated minor deviations in Mission A, Table 22, in order to describe better the flight life for this particular aircraft. The changes are only a resequencing of the legs which, in effect, makes the climb-to-combat altitude leg sequential with the initial climbout and makes the two descent

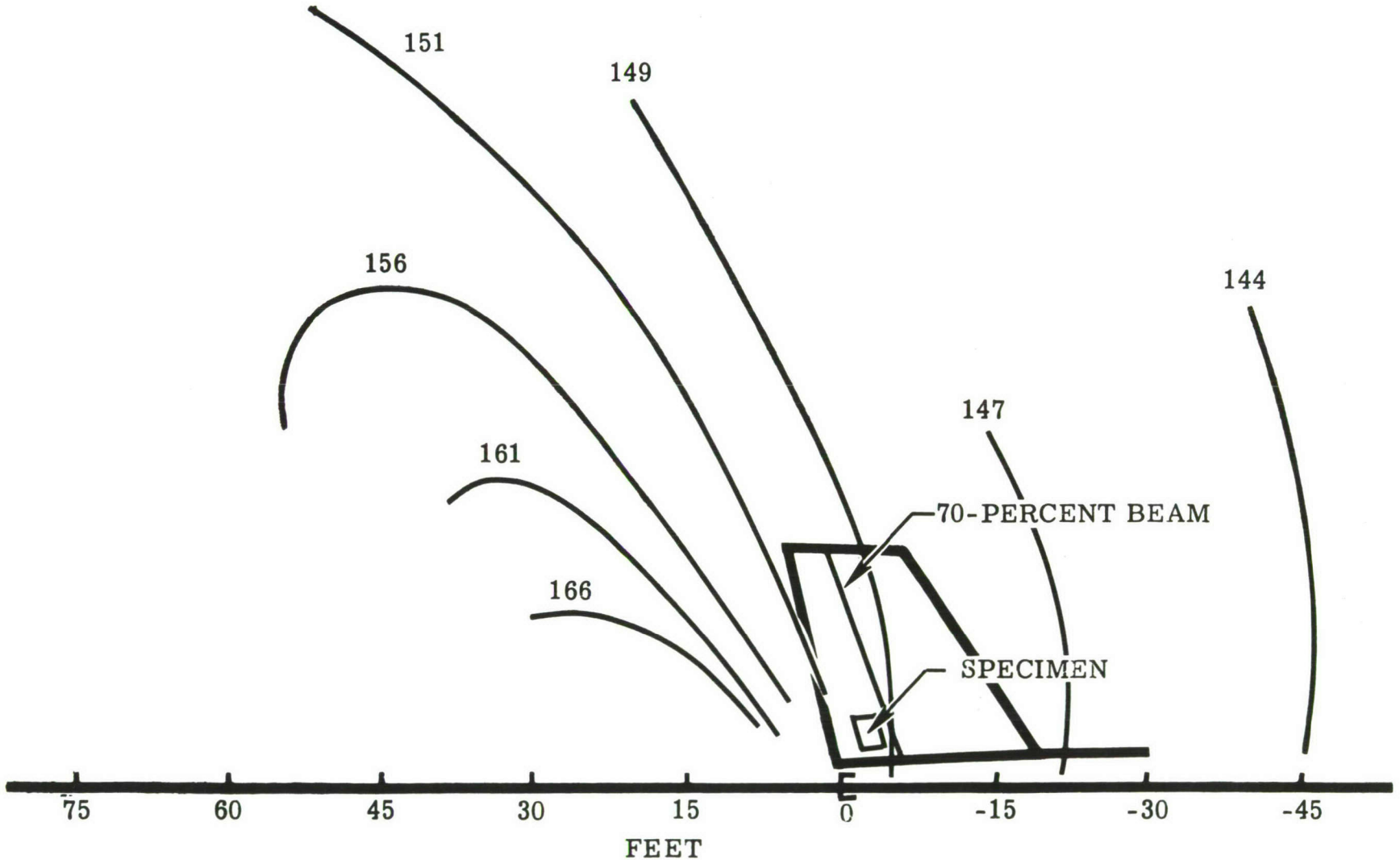

Figure 44. Over-all Near Field

EXAMPLE

INTERCEPT FIGHTER - MISSION A

HIGH-ALTITUDE INTERCEPT
WEAPONS LOAD ON 55 PERCENT OF THESE MISSIONS
WEAPONS RELEASE CYCLES ON 30 PERCENT OF THESE MISSIONS

Oper No. (i)	Operation Description	Power Setting (Note 1.)	Operation Min/Mission (t_{ai})	FT Mean Alt	KN Mean A/S	Operation Hr/1000 Flt Hr (Note 2.)
1.	Engine Start	IDLE	1.00	S. L.	0	8.47
2.	Taxi out + Taxi in and Park	IDLE	7.00	S. L.	0	59.2
		80 -90%	1.50	S. L.	0	12.7
3.	Power Check	MIL	0.05	S. L.	0	0.42
4.	Pre T. O. Interval	IDLE	2.00	S. L.	0	16.94
5.	Take off	MAX	0.50	S. L.	80	4.23
6.	Accelerate	MIL	0.50	S.L.	350	4.23
7.	Climb to Best Cruise Alt and A/S	MIL	4.6	18,000	560	39.95
8. 9.	Cruise - Climb	CRUISE	15.2	70,000	1721	128.8
9. 8.	Accelration and Climb to Combat Alt and A/S	MAX	4.2	40,000	1200	35.55
10.	Combat	MAX	5.0	70,000	1721	128.8
11. 12.	Descend to Best Cruise Alt and A/S	IDLE	10.6	59,000	650	89.8
12. 11.	Cruise - Climb	CRUISE	15.2	70,000	1721	128.8
13.	Descend for Landing	IDLE	8.2	20,000	350	69.45
14.	Landing	IDLE	1.0	S.L.	70	8.47
15.	Maintenance	IDLE	8.40	S. L.	0	71.10
		80-90%	0.40	S. L.	0	3.48
		MIL	0.40	S. L.	0	3.48
		MAX	0.40	S. L.	0	3.48
Mission A Flight Time ($T_{AF} = \sum_{5}^{14} t_{ai}$)			65.00			550
Mission A Total Oper Time ($T_{AO} = \sum_{1}^{15} t_{ai}$)			86.65			734

NOTES: 1. Max settings within all operating limits.
2. Operation hours per 1000 flight hours = (t_{ai}/T_{AF}) 550 hr = 8.47 (t_{ai})

Table 22. INTERCEPT FIGHTER - MISSION A

EXAMPLE

INTERCEPT FIGHTER - MISSION B

HIGH-ALTITUDE INTERCEPT
WEAPONS LOAD ON 50 PERCENT OF THESE MISSIONS
WEAPON RELEASE CYCLES ON 30 PERCENT OF THESE MISSIONS

Oper No. (i)	Operation Description	Power Setting (Note 1.)	Operation Min/Mission (t_{bi})	FT Mean Alt	KN Mean A/S	Operation Hr/1000 Flt Hr (Note 2.)
1.	Engine Start	IDLE	1.00	S. L.	0	3.85
2.	Taxi out + Taxi in and Park	IDLE	7.00	S. L.	0	26.90
		80-90%	1.50	S. L.	0	5.77
3.	Power Check	MIL	0.05	S. L.	0	0.19
4.	Pre T.O. Interval	IDLE	2.00	S. L.	0	7.69
5.	Take off	MAX	0.50	S. L.	80	1.92
6.	Accelerate	MAX	0.50	S. L.	350	1.92
7.	Climb to Best Cruise Alt and A/S	MAX	3.2	18,000	600	12.30
8.	Cruise - Climb	CRUISE	20.9	38,000	550	80.40
9.	Accelerate to Combat A/S	MAX	2.3	40,000	850	8.84
10	High-Speed Turns	MAX	5.00	40,000	1146	19.22
11.	Decelerate to Best Cruise	IDLE	2.3	40,000	850	9.42
12.	Cruise - Climb	CRUISE	20.9	42,000	550	80.40
13.	Descend for Landing	IDLE	8.2	20,000	350	31.55
14.	Landing	IDLE	1.0	S. L.	70	3.85
15.	Maintenance	IDLE	8.40	S. L.	0	32.30
		80-90%	0.40	S. L.	0	1.54
		MIL	0.40	S. L.	0	1.54
		MAX	0.40	S. L.	0	1.54
Mission B Flight Time $(T_{BF} = \sum_{5}^{14} t_{bi})$			65			250
Mission B Total Oper Time $(T_{BO} = \sum_{1}^{15} t_{bi})$			86.65			333.5

NOTES: 1. Max settings within all operating limits.
2. Operation hours per 1000 flight hours = (t_{bi}/T_{BF}) 250 hr = 3.845 (t_{bi})

Table 23 . INTERCEPT FIGHTER - MISSION C

EXAMPLE

INTERCEPT FIGHTER - MISSION C

TRANSITION

Oper No. (i)	Operation Description	Power Setting (Note 1.)	Operation Min/Mission (t_{ci})	FT Mean Alt	KN Mean A/S	Operation Hr/1000 Flt Hr (Note 2.)
1.	Engine Start	IDLE	1.00	S. L.	0	2.22
2.	Taxi out + Taxi in and Park	IDLE	7.00	S. L.	0	15.55
		80-90%	1.50	S. L.	0	3.33
3.	Power Check	MIL	0.05	S. L.	0	0.11
4.	Pre T. O. Interval	IDLE	2.00	S. L.	0	4.44
5.	Take off	MAX	0.50	S. L.	80	1.11
6.	Accelerate	MIL	0.50	S.L.	350	1.11
7.	Climb to Best Cruise Alt and A/S	MIL	4.6	18,000	560	10.23
8.	Cruise - Climb	CRUISE	75.2	40,000	550	167.0
9.	Descend for Landing	IDLE	8.2	20,000	350	18.22
10.	Landing	IDLE	1.0	S.L.	70	2.22
11.	Maintenance	IDLE	8.40	S. L.	0	18.67
		80-90%	0.40	S. L.	0	0.89
		MIL	0.40	S. L.	0	0.89
		MAX	0.40	S. L.	0	0.89
Mission C Flight Time ($T_{CF} = \sum_{5}^{10} t_{ci}$)			90			200
Mission C Total Oper Time ($T_{CO} = \sum_{1}^{11} t_{ci}$)			111.65			248

NOTES: 1. Max settings within all operating limits.
2. Operation hours per 1000 flight hours = (t_{ci}/T_{CF}) 200 hr = 2.22 (t_{ci})

Table 24 . INTERCEPT FIGHTER - MISSION C

legs consecutive. The performance data shown are based on design studies and reflect reasonable values for a Mach 3 interceptor design.

The summary tabulation made from these mission outlines is shown in Table 25, pages 109 and 110. The first page of the summary shows total engine ground-run times by power setting and then the complete breakdown by power and ambient temperature, using the temperature distributions from Table 2.

From this mission analysis, the following conclusions were reached:

1. The only significant engine noise conditions for the vertical stabilizer are static running at maximum afterburner power and ground roll for takeoff at the same engine power.

2. Engine operation at this power setting during initial climb does not add to the damage potential of the above condition except for extremely nonlinear structures, none of which will be found in the vertical stabilizer.

3. The utilization summary (Table 1) indicates that the combination of maximum static and takeoff time is about 7.25 hours per 1000 flight hours. Thus, for the design life of 3000 flight hours, the total exposure to maximum static thrust engine-noise, is about 22 hours.

4. Boundary layer turbulence does not provide sufficient excitation to be significant to the structural integrity of the vertical stabilizer.

The second page of the example utilization-summary table shows the in-flight conditions and times per 1000 flight hours as assembled from the three mission outlines. The takeoff operation appears again because it is a flight operation as well as a ground operation, but its time should not be added under both categories. Takeoffs, for this analysis, should be treated as a ground operation and broken up by ambient temperature distributions. The posttakeoff acceleration legs might also be treated as subject to the given temperature distributions, if the designer should determine that their effects on the total acoustic environment are significant. If this is done, it is likely that a closer breakdown by speed during these legs would be desirable to describe better the changing acoustic environment. One column of newly added information appears on this page of the summary; this is the mean dynamic pressure, "q," computed from altitude and airspeed for the assumed standard atmosphere.

ENGINE CHARACTERISTICS AND SOUND SPECTRA

The maximum acoustic environment is calculated for the vertical stabilizer of the hypothetical vehicle, with two afterburning engines, whose characteristics

UTILIZATION SUMMARY FOR A MACH 3 FIGHTER INTERCEPTOR

PART I - GROUND RUN TIMES IN HOURS PER 1000 FLIGHT HOURS TOTAL BY POWER SETTING:

Power	Idle RPM	80-90% RPM	Mil Power	Max Power (Static)	Takeoff Power
Hours	267.33	27.71	6.63	5.91	7.26

BREAKDOWN BY AMBIENT TEMPERATURES:

Pwr / Temp (°F)	Hot-climate Base					Cold-climate Base				
	Idle RPM	80-90% RPM	Mil Pwr	Max Pwr (Static)	T. O. Pwr	Idle RPM	80-90% RPM	Mil Pwr	Max Pwr (Static)	T. O. Pwr
113	9.35	0.97	0.23	0.21	0.25					
95	58.8	6.10	1.46	1.30	1.60	0.81	0.08	0.02	0.02	0.02
75	69.5	7.21	1.72	1.54	1.89	16.00	1.66	0.40	0.35	0.44
55	104.2	10.81	2.58	2.30	2.83	48.10	4.98	1.19	1.06	1.31
35	24.05	2.50	0.60	0.53	0.65	58.80	5.82	1.46	1.30	1.60
15	1.34	0.14	0.03	0.03	0.04	64.10	6.65	1.59	1.42	1.74
-5						53.40	5.54	1.33	1.18	1.45
-25						21.40	2.22	0.53	0.47	0.58
-45						4.01	0.42	0.10	0.09	0.11
-60						0.53	0.06	0.01	0.01	0.01

PART II - SPECIAL CONDITIONS

Weapon release cycles (bay openings):

507 cycles per 1000 flt hr at 1721 knots, 70,000 ft alt (169 missions)
231 cycles per 1000 flt hr at 1146 knots, 40,000 ft alt (77 missions)

Table 25. EXAMPLE UTILIZATION SUMMARY

UTILIZATION SUMMARY
FOR A MACH 3 FIGHTER INTERCEPTOR (CONT)

PART III - IN-FLIGHT OPERATIONS HOURS PER 1000 FLIGHT HOURS

Operation	Power Setting (Note 1)	Mean A/S (Knots)	Mean Alt (Feet)	Mean Dynamic Press. (Note 3)	Operation Hr/1000 Flt Hr
Takeoff (part of ground runs)		80	SL	21.7	(7.26)
Acceleration (Note 2)	Max	350	SL	416	1.92
Acceleration (Note 2)	Mil	350	SL	416	5.34
Acceleration	Max	850	40,000	605	8.8
Climb	Max	600	18,000	696	12.3
Climb	Mil	560	18,000	606	50.2
Climb	Max	1200	40,000	1195	35.5
Combat	Max	1721	70,000	590	42.3
Combat	Max	1146	40,000	1098	19.2
Cruise (heavy)	HS cruise	1721	70,000	590	128.8
Cruise (light)	HS cruise	1721	74,000	488	128.8
Cruise (heavy)	Cruise	550	38,000	278	163.7
Cruise (light)	Cruise	550	42,000	229	163.7
Deceleration	Idle	850	40,000	605	9.4
Descend	Idle	650	59,000	141.5	89.8
Descend	Idle	350	20,000	221.5	119.2
Landing	Idle	70	SL	16.6	14.5

NOTES: 1. Max power settings within all operating limitations.
2. Further breakdown by speed and ambient ground temperatures if critical.
3. Incompressible q in psf for std atmosphere.

Table 25. EXAMPLE UTILIZATION SUMMARY (CONT)

are shown in the table below and with the flight profile shown in Table 22, by the six steps illustrated below:

Thrust = 30,000 pounds

Mass flow = 275 pounds per second

Exit diameter = 3 feet

Exit Mach No. = 1.5

1. Calculate the expanded exhaust velocity of the hypothetical engine:

$$V = \frac{tg}{w} = \frac{30,000\ (32.2)}{275} = 3500 \text{ feet per second}$$

2. Calculate the change in sound pressure level from the reference contours of Section I:

$$\Delta \text{ SPL} = 10n \log \frac{V}{1850}$$

$$\Delta \text{ SPL} = 10n \log \frac{3500}{1850} = 2.77\ n$$

n	Δ SPL	Δ SPL
4	11.1	11
5	13.9	14
6	16.6	17
7	19.3	19

The values in the table above are added to the appropriate contour of figure 2.

3. Multiply the dimensionless parameters in figure 2 by the jet diameter to adjust the contours to the vehicle geometry.

4. Calculate the downstream shift and apply it to the reference contours:

$$\Delta x = 6.5\ (D_e)\ .\left(M_e - 1\right)^2 = 6.5(3)\left(1.5 - 1\right)^2 = 4.9 \text{ ft}$$

5. Obtain $\Delta\phi$ from figure 3 for the calculated exhaust velocity, and rotate the reference contours:

$V = 3500$ feet per second, $\Delta\phi = 20$ degrees

6. Calculate the spectrum shape at $\frac{X}{D} = 0$ from figure 4, using the following:

V = 3500 feet per second, D = 3 feet

OCTAVE (cps)	MID FREQUENCY (cps)	$\frac{fD}{V}$	db re OA SPL
20-75	53	0.455	-22
75-150	106	0.091	-18
150-300	212	0.182	-14
300-600	425	0.364	-10
600-1200	850	0.728	-6
1200-2400	1700	1.46	-6
2400-4800	3400	2.92	-7
4800-9600	6800	3.84	-9

By applying the preceding calculation, steps 1 through 5, to the reference contours of Figure 2, the free-field sound pressure levels for maximum A/B during static ground operation are obtained. They are shown in figure 44.

Each contour in figure 44 is increased 3 db to account for the effect of the structure in the sound field and an additional 3 db to account for two-engine operation. This gives a total of 6 db which is added to each contour in figure 2 for static ground operation with two engines. The maximum SPL occurs on the lower aft portion of the vertical stabilizer. It is obtained by extrapolation of the 156 db free-field contour in figure 44, resulting in a maximum over-all sound pressure level of 156 + 6 = 162 db.

The octave band spectrum shape does not vary appreciably over the surface of the vertical tail. It is shown in figure 45 as calculated in step 6.

The maximum acoustic environment occurring during ground runup will decrease as the vehicle attains speed and altitude. Soon after liftoff, 3 db can be subtracted because of reduced ground effect. An additional decrease caused by increased altitude and flight speed is calculated by the following formula:

$$\Delta SPL = -10 \log \left(\frac{V_e}{V_e - V_f}\right)^n \left(\frac{1}{1 - M_F}\right)^2 \left(\frac{P_{as}}{P_{aF}}\right) \left(\frac{T_{aF}}{T_{as}}\right)^{1/2}$$

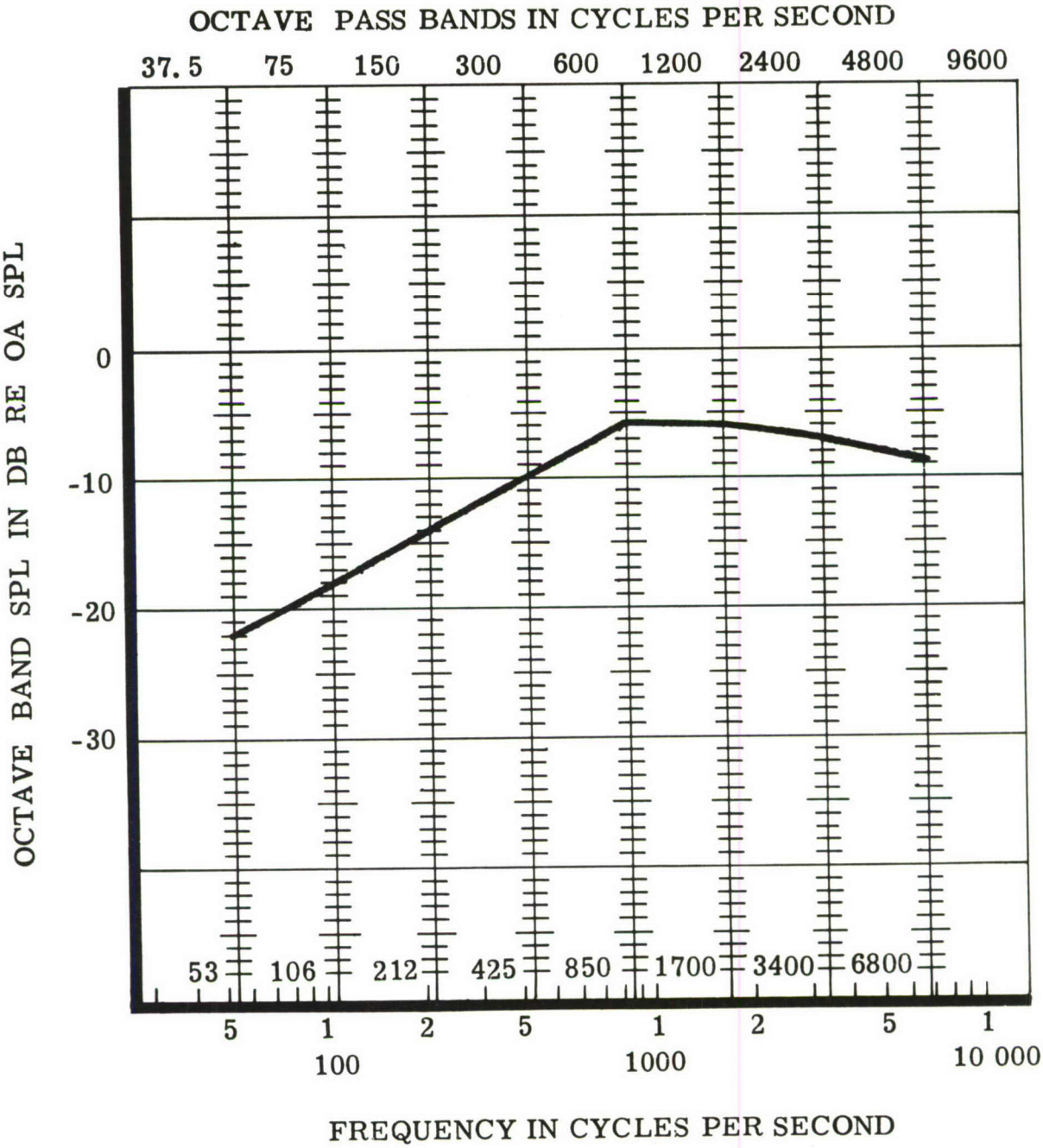

Figure 45. SPL Spectrum - Vertical Stabilizer

The decrease in sound pressure level from the maximum value, due to increased speed and altitude, is calculated in the following equation. The altitude and flight speed are obtained from the mission profile shown in Table 22.

Altitude - sea level

Velocity (avg) - 350 knots or 592 feet per second

Mach number -

$$M = \frac{V}{a} = \frac{592}{1116} = 0.53$$

$$\Delta SPL = -10 \log \left(\frac{3500}{3500 - 592} \right)^4 \left(\frac{1}{1 - 0.53} \right)^2 \quad (1) \quad (1)$$

$$\Delta SPL = -10 \log \ (2.07) \ (4.54) \ (1) \ (1) = -9.7 \text{ db}$$

The total decrease on the vertical stabilizer, forward of the nozzle exhaust for this flight condition, would be

$$\Delta SPL_{total} = -9.7 + (-3) = -12.7 \text{ db}$$

As higher speeds are attained and the maximum q condition on the mission profile is approached, the aerodynamic turbulence increases. At the maximum q flight condition, the over-all turbulence pressure level for the hypothetical vehicle would be

$$SPL_{OA} = 83 + 20 \log 1195 = 145 \text{ db}$$

The over-all pressure level on the vertical stabilizer, due to the turbulence of unseparated boundary layer flow, is lower than that of the engine noise during ground runup at maximum engine power. Because of the poorly correlated character of boundary layer turbulence, the effective pressure for exciting the structure is lower than the predicted pressure level previously shown, reducing the effective pressure to a value much lower than that of the engine noise. It is assumed then that the steady, unseparated, shock-free boundary layer is insignificant compared to engine noise in determining the response of the vertical stabilizer of the hypothetical vehicle.

Open bomb bays, wheel wells, oscillating shocks, and separated boundary layer flow cause large increases in pressure over those of the normal flow conditions on which the preceding calculation was based. A great amount of maintenance annoyance has attended failures caused by these pressure sources. It is highly desirable, therefore, that these effects be held to a minimum or eliminated entirely by the designer.

The sound pressure level during ground operation is dependent upon engine operating procedure and ambient conditions. The extreme range in ambient temperatures expected for ground operation is shown in Table 25 as a function of time per 1000 flight hours for various engine power settings for an operational aircraft. Individual engine operating procedure, as a function of ambient temperature, can be evaluated by the designer to obtain the effective exhaust velocity and to compute the corresponding sound pressure.

STRUCTURAL CONFIGURATION AND SPECIMEN LOCATION

The primary loads of the vertical stabilizer are carried by structure forward of and including the 70-percent beam. Although the structure both forward and aft of this plane is of brazed stainless-steel honeycomb sandwich panels, mechanically attached to ribs or beams having corrugated titanium webs welded to caps of the same material, the structure aft of this plane is of secondary load-bearing capacity and, hence, is significantly less strong. The problem of locating the specimen is then reduced to determining the area of the aft box which has the lowest ratio of acoustical fatigue strength to acoustic load. For the example, it is assumed that the aft 15 percent of the stabilizer is constructed of full-depth honeycomb, and that the section properties of the aft box are uniform in the spanwise direction except for the upper and lower terminations; the lower termination achieving much greater rigidity through a gradual taper of sandwich face and web gages. In the chordwise direction, box depth, sandwich section depth, and sandwich-face gages taper. The 70-percent joint and the 85-percent joint are so constructed as to present no acoustical fatigue problem. The area of maximum over-all pressure for the aft box lies in the area of constant spanwise section properties (figure 44). This is the area from which the specimen is taken. It is expected that the structure will prove adequate, that no redesign will be required and, therefore, that testing of a specimen from this one area will qualify all areas of the aft box.

SPECIMEN DESIGN

Specimen design is inevitably a compromise. In this case, size limitations of the test chamber control the number of bays of the panel and its chordwise extent. Inevitably, some artificiality arises at three of the four edges. If simulation breaks down here, it must be in a conservative way; but this too is a hazard, for if the means used to effect the conservatism result in a premature failure, it is difficult, if not impossible, to judge if the panel is adequate.

It is found that five spanwise bays of the panel can be handled. This is adequate. Adjustment of the end bays should be made to protect them from failure and to allow the specimen to behave as if the system were continuous beyond them. The object here is to cause the center bay and the two ribs which define it to be the primary specimen. Should failure not occur here, it

can still be reasoned that the test is conservative. The adjustment is as follows: The two end bays are shortened 30 percent, and the web and cap gages of the ribs are increased 30 percent. Experience has shown that these changes are adequate.

Size limitations in the chordwise direction will not allow use of the full section from the 70-percent to the 85-percent plane. As long as the chordwise length of the specimen is more than three times the individual bay width, response of the sandwich panels and their rib supports will not be reduced materially. In choosing which end (fore or aft) to shorten, a prediction of the probable nature of the failure is useful. It is expected that the sandwiches themselves will not fail. The attachments, the high-density honeycomb near the attachments, and the rib caps or webs near the welds which tie the caps to the webs seem the most likely sites. Therefore, the aft section is in need of more careful simulation; the sandwich thickness (and hence strength) is decreasing; and the reduced depth of the vertical stabilizer means that the ribs are less deep at the aft end, thus providing greater rotational restraint with consequent higher stressing of attachments, high-density honeycomb, and rib parts. (Had the sandwiches been of constant section, and primary concern been with the sandwich panels proper, it could be argued that the forward end should be accurately simulated, for the reduced rotational restraint of the deeper rib would allow greater bending deflection of the honeycomb.) Beyond all these considerations is the fact that the acoustic load is higher at the aft end of the panel.

The modification of the structure for specimen design is done by moving the simulated 70-percent beam back to the 75-percent plane, reducing its depth to match the section at the 75-percent plane, and making all ties of the panel to the beam, including the shear ties of the rib webs to the beam web, simulate the airframe design. At the aft end the sandwich and rib ties to the simulated aft closing channel should reproduce those of the airframe.

Since the flexural characteristics of the beam and closing channel are not judged to be important in the response, they can be of highly rigid construction and the mounting angles can be tied to them. The specimen is mounted with one face flush with an inner wall of the progressive-wave siren test chamber to provide grazing incidence, and with the ribs parallel to the direction of propagation of the sound. This orientation closely simulates the situation of the airframe.

As an alternative to this, it can be argued that since the specimen is also to qualify the aft box at every location along its span, and since the direction of propagation near the top of the stabilizer is not parallel to the ribs, that the specimen should be mounted in the test chamber and rotated in its face plane to provide a suitable direction of propagation. Doing so was, in fact, what limited the specimen size. Stress response curves from strain gages on each of the major components of the specimen should be taken at a low SPL

in each of a number of appropriate orientations of the specimen to determine if a substantial difference in response per unit load in any mode giving significant response is found. The results of this preliminary investigation showed that, for this part, the responses were not significantly different, and the orientation with the ribs parallel to the propagation direction was chosen for the test.

This result is not to be anticipated generally, for the relationship of half-wavelength to individual bay size can be very important in determining the acceptance of load from the sound wave. Papers by Powell (19) and Smith and Junger (20) can be of considerable assistance in making judgements on this question, as well as in illustrating the high magnitude of errors which can be encountered in improper simulation. The problem is intensified for our example by the fact that knowledge of the wave character of the sound forward of the engines (on the stabilizer) is inexact, as is that for the sound of the siren at a specimen test location close to the horn of the siren. It may be seen how much more involved the problem becomes with more conventional construction than the honeycomb assemblies, such as that widely used on aircraft from the DC-3 to the DC-8, skins on highly flexible bent-flange ribs, for which the forms of modes beyond the simplest and most obvious can be a source of amazement to the engineer when examined by strobelight. Spatial simulation of sound loading is still an inexact art at best.

THE TEST

Two identical specimens will be assumed to have been built, a modest number in light of the manifold contingencies they are intended to cover: a severe but possibly undetected flaw in one or both, premature failure due to an error in judgement in design of the terminations or mounting of the specimen, an accident during the testing, and, finally, the possibility of a limited redesign and rework of the second specimen, following a failure revealing an inadequacy in the design, are the more obvious ones.

Assume that the test was conducted on the first specimen, frequency scans were conducted at an SPL of 145 db for several strain gages having representative locations, and the specimen responses, plotted as stress versus frequency, appeared as shown on figure 46. The results of these scans would be used to determine the resonance frequencies for the life test and to calculate the damping ratios for the modes.

Assume that the specimen was "step-tested" for 15-minute periods in each of the two modes showing significant response, with the SPL increased 3 db per level, and that stress levels were recorded during each run in order to provide data for constructing stress-load curves for computation of the non-linearity factors (figure 47). This was assumed to have been done for most

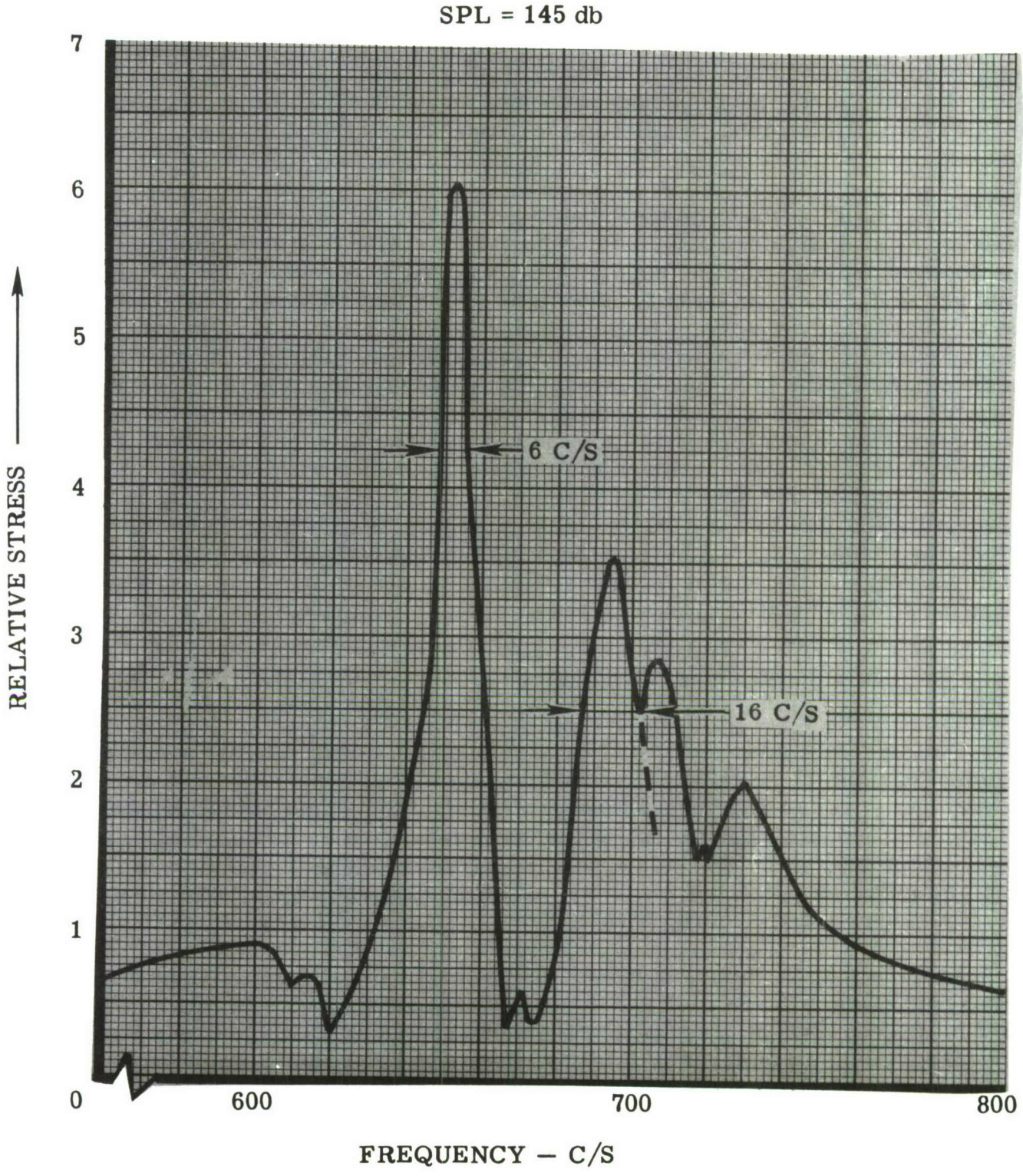

Figure 46. Stress - Frequency Curve (For Example Problem)

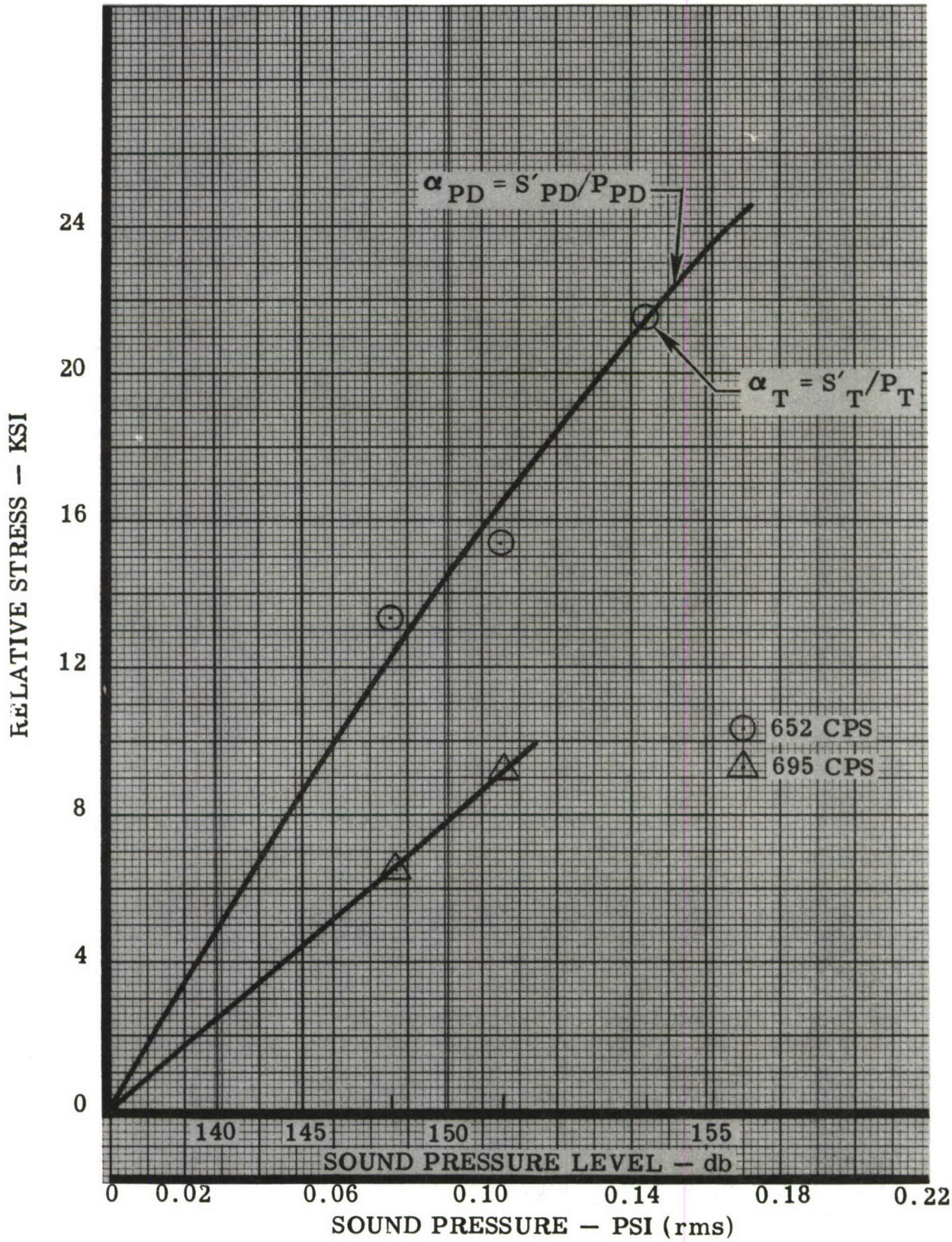

Figure 47. Stress - Load Curves (For Example Problem)

of the gages used in obtaining response curves, so that response and stress-load data for a gage near the failure location would be available for the interpretation calculation.

The hypothetical test results are tabulated as follows:

TIME (min)	SPL (db)	FREQUENCY (cps)	RELATIVE STRESS (psi)
15	148	652	13,200
15	148	695	6,500
15	151	652	15,300
15	151	695	9,200
3	154	652	21,700

Failures developed after 3 minutes of testing in the lower frequency mode at 154 db. The failures consisted of cracks along the web-to-cap welds of several rib webs. The data for the response and stress-load curves of figures 46 and 47 were taken from the output of a strain gage located near the failure and oriented at right angles to the line of failure.

TEST INTERPRETATION

Interpretation of the result for this specimen is particularly simple, characteristically so for most honeycomb assemblies, in that the contributions of modes other than the primary one are slight and little nonlinearity is found in the response.

In the following, the subscripts 1 and 2 refer to the 652-cps and 695-cps modes, respectively.

The equivalence equation for the i th mode is

$$\left(\frac{p_r}{p_s}\right)_i = \frac{1}{(\pi \delta_i f_i)1/2} \left(\frac{s_r}{s_s}\right)_i \frac{1}{(\gamma_i \lambda_i)1/2}$$

where the p's and s's are rms values.

Determination of Equivalent Load and Life

The 652-cps mode, the principal mode, had the following pertinent life experience:

15 min at 151 db	$n_{151} = 5.9 \times 10^5$
3 min at 154 db	$n_{154} = 1.2 \times 10^5$

Now since

$$\frac{n_{151}}{N_{151}} + \frac{n_{154}}{N_{154}} = \frac{n_e}{N_e} = 1$$

at failure, it is necessary only to find values of N_{151} and N_{154} which satisfy the equation. By trial and error, a value of $N_{154} = n_{154}$ was found. This means that only the exposure at 154 db contributed to the failure, provided that it was the 652-cps mode which caused failure. The proof is as follows: From the S-N curve for 6Al-4V Ti, the stress corresponding to $N_{154} = 1.2 \times 10^5$ is $S_{154} = 87,500$ psi. From the stress-load curve for the mode, $S_{151} = \frac{16,700}{21,710} S_{154} = 0.77\ S_{154} = 67,300$ psi. (Had the response been linear in this stress range, S_{151} would have been $0.707\ S_{154}$ for a 3-db change in load level would produce the same change in stress.) For S_{151}, $N_{151} = \infty$ and S_{151} does not contribute to failure. Clearly this is a trivial case; not all are.

Sine-Random Equivalence Computation

The required information: $p_{s1} = 154$ db, $\delta_1 = \Delta f/2f_1 = 0.0046$, $f_1 = 652$ c/s, $s_{s1} = 0.707 \times 87,500 = 61,800$ psi (rms value), $s_{r1} = 23,000$ psi (from the random S-N curve for the desired life of 22 hours, which is 5.2×10^7 cycles at 652 c/s), $\gamma_1^{1/2} = 1.06$ (see below), and $\lambda_1^{1/2} = 1.0$ (see below).

$$\gamma_i = \left(s_T^2 \Big/ s_i^2 \right)_i = \left(\sum_1^n \delta_i f_i p_i^2 s_{si}^2 \right) \Big/ \left(\delta_i f_i p_i^2 s_{si}^2 \right)$$

for p_s constant (as it is in the frequency response curve). The values of relative stress used here should be taken from the stress-load curves for a pressure level of 154 (or 151) db. However, with the approximately linear response, values from the frequency response curve at 145 db serve as well.

f	Δf	$\frac{\Delta f}{2f}$ =	S (relative	S^2	$\delta S^2 f$
652	6	.0046	6	36	108
695	16	.0015	3.5	12.3	12.8

$$\gamma_1 = \frac{121}{108} = 1.12$$

Note that a value of γ_i exceeding n (where n is the number of modes in the computation), no matter which mode is the basis of computation, would be artificially conservative.

$$\lambda = (\alpha PD / \alpha T)^2$$

$$= \frac{S'_{PD}}{P_{PD}} \Big/ \frac{S'_T}{P_T}$$

where $$S'_{PD} = \left(\frac{S_{PD}}{S_T}\right) S'_T$$

$$\lambda = \frac{S_{PD}}{S_T} \frac{P_T}{P_{PD}}$$

where the primes denote measured stresses (i.e., relative, as opposed to actual), the PD's denote peak-damage stresses or loads relating to the most damaging stress levels in the random application, either relative or actual, and the T's denote stresses or loads at failure in the siren test, either relative or actual.

S_{PD} = 90,000 psi (from the peak-damage curve for the desired random life of 5.2×10^7 cycles), S_T = 87,500 psi (from the original S-N curve at the test life), P_T P_{PD} = 0.145/0.151 from the stress-load curve, P_{PD} from a point on the curve whose stress is (90,000/87,500) S_T.

$$\lambda = .986 \simeq 1$$

The proximity of the two stresses illustrates how well the siren test, lasting but a few minutes, approximates the number of damaging cycles which the part experiences under random load in the life of the airframe.

For this example the γ correction amounts to one-half db and the λ correction is trivial. Note that had the desired random life been $\sim 10^9$

cycles with a test life of 1.2×10^5 cycles, or had the test life been $\sim 8 \times 10^4$ cycles for the desired random life of 5.2×10^7 cycles, λ would equal one, no matter how nonlinear the part is, for $S_{PD} - S_T$ for these two cases. Use can be made of this relationship when a nontrivial equivalent life, n_e, and a corresponding load level, P_e, must be calculated. If n_e is chosen (and P_e varied) to give a stress $S_T = S_{PD}$ for the desired random life, $\lambda \equiv 1$.

$$\left(\frac{p_r}{p_s}\right)_1 = \frac{1}{(\pi \delta_1 f_1)}\ 1/2 \left(\frac{s_r}{s_s}\right)_1 \quad \frac{1}{(\gamma_1 \lambda_1)}\ 1/2 = 0.114$$

$$20 \log_{10} 0.114 = -20 + 1.1 = -19 \text{ db}$$

$$\text{db}_{r1} = \text{db}_{s1} \quad -19 \text{ db} = 154 - 19 = 135 \text{ db}$$

This is the allowable random spectrum pressure for the desired life.

Margin Calculation

The maximum static OA SPL on the airframe part is 156 db. From figure 45, the octave level at 652 cps is approximately 149 db. The corresponding spectrum level (by definition, SPL in a one cps bandwidth), found by subtracting 13 + 3i db where i is the number of the octave containing the subject resonance, is approximately 149 -28 = 121 db. Therefore, the specimen shows for the 652 cps mode a 14 db margin (factor of 5 in stress) for the design life of the airframe.

A similar computation for the 695-cps mode yields a random allowable of at least 129 db. This is highly artificial for it assumes failure in this mode and, in fact, failure after 15 minutes at 151 db. If the relative values of stress indicated by the gage whose output is presented by figure 46 are a reasonable accurate representation of those at the failure point (the computation of γ_1 assumed this to be true), then it is highly unlikely that this mode would have resulted in failure at even 154 db. However, while this argument is plausible, the assumption about the gage output can be questioned. The conservative (and indicated) procedure is that this mode be excited during the fatigue test, as it was. The only means available for definitely improving the allowable for this mode, which, considering the margin of at least 8 db, is not indicated, is the running of a step test at this mode only, on the second specimen. In this test, one specimen gave adequate information; it did not give all possible information.

6.2 EXAMPLE OF STRUCTURE EXCITED BY BOUNDARY LAYER NOISE

Accurate evaluation of the dynamic response, and hence the fatigue performance, of structure excited by boundary layer turbulence is usually very difficult. The techniques introduced in the following example depend, as would any rational calculation, on knowledge of the mode shape of each significant mode. Structural configurations with very simple response character, such as rigid honeycomb panels on very stiff supports, submit to calculation with fair accuracy.

The example is the primary engine intake duct of the hypothetical interceptor. The construction is of one-inch thick brazed stainless-steel honeycomb panels on very stiff frames spaced 20 inches apart. From the mission analysis it can be concluded that the critical condition is at Mach 2.1 at 40,000 feet. Lumping all time in that condition range yields an exposure of about 55 hours per 1000 flight hours or 165 hours during the life of the vehicle. Since "q" and turbulence pressure are proportional, no other flight condition has pressures within 6 db (factor of 2) of this condition.

The inlet duct may be thought of as a device which converts the supersonic ram air to air of low-subsonic velocity at high pressure with high efficiency.

The following paragraphs to page 129 are taken from an analysis performed for the B-70 (Reference 36). (This quoted material is UNCLASSIFIED)

FLOW CONDITIONS

"Transients in flow demand, as would result from a change in engine demand or from maneuver, can initiate changes in the position of the normal shock. At high Mach-number cruise the duct normally operates in the condition termed 'maximum pressure recovery'; a normal shock is positioned in the throat and the boundary layer in its vicinity is bled. Should an inability of the duct or engines to pass all available flow arise, the shock may move to a position forward of the lip of the cowl, this condition being termed 'unstart', allowing spilling of subsonic air past the lip. If the surplus is uncorrected by a change of bypass and throat area the shock may remain in a position forward of the lip. This condition is termed (for the purpose of this discussion, and not in consonance with the terminology usually applied to ducts) 'stable unstart'.

PRESSURE CORRELATION

"Excitation of the surface walls of the inlet duct by turbulence depends not only on the pressure exerted, but on the spatial extent over which that pressure is coherent and in phase with the motion of the structural mode being driven.

It is therefore necessary to know the area of influence of the turbulence (correlation area), the mean rate at which the turbulence is convected (for comparison of convection frequency with modal frequency), and the mean rate of decay of the turbulence.

"Five transducers, arrayed in a line in the stream-wise direction aft of the throat (of a one-quarter scale model of the duct, operated in a wind tunnel), were used for simultaneous detection of the turbulence pressures during normal operation, steady unstart, buzz, and stead restart. These signals were to be analyzed by correlation reduction, cross-correlation with zero-time delay yielding the correlation area, and cross-correlation with variable time delay yielding the convection velocity and the decay rate." (Only zero time-delay data are used in this example.)

STRUCTURAL RESPONSE

"The following discussion on structural response is included to . . . . . demonstrate that turbulence is not a threat to the integrity of the duct structure.

"Perhaps the most useful manner of considering the magnitude of response to convected turbulence is in comparison to the corresponding response to an acoustic wave propagating at grazing incidence, having the same over-all rms pressure. This comparison, for the general mode, is not easily made. However, Dyer (Reference 21) has presented an order of magnitude solution for the response of a simply supported plate to convected turbulence from which it is possible to derive the turbulence-to-sound comparison for the first mode. In view of the construction of the duct, it is unlikely that any other mode of the duct walls is significant.

"From Dyer, the first mode response to turbulence for convection velocities less than the 'coincidence speed' in the plate is

$$\overline{w_t^2} \doteq \frac{\overline{p_t^2}\ A}{4\omega^2 M^2} \quad \frac{4}{L_x L_y} \quad I_{11}(0)$$

where

$$I_{11}(0) \doteq \frac{2}{a_{11}} \quad a_{11}\theta \ll 1;\ a_{11} = \frac{\eta \omega_{11}}{2} = \delta \omega_{11}$$

Thus

$$\overline{w_t^2} \doteq \frac{2\overline{p_t^2}}{\omega_{11}^3 M^2} \quad \frac{A}{L_x L_y} \quad \frac{\theta}{\delta}$$

Where $\overline{w_t^2}$ is the mean square displacement response to the turbulence, $\overline{p_t^2}$ is the over-all mean square turbulence pressure, A is the correlation area of the turbulence, ω_{11} is the first mode resonance frequency, M is the mass per unit area of the structure, L_x and L_y are the dimensions of the plate (L_x in the streamwise direction), $I_{11}(0)$ is a time integral for zero time delay, θ is the decay parameter of the turbulence, and δ is the proportion of critical damping (c/c_c).

"The stress response to a sinusoidal acoustic pressure is given by Reference 21 as

$$s_s^2 = \left(\frac{1}{2\delta}\right)^2 s_o^2 \; p_s^2 \; T^2$$

where the mean square sinusoidal pressure p_s^2 has been modified by the factor T^2 which accounts for the effectiveness of loading when the wave is not in phase over the entire panel. Now, since

$$s_s/w_s = s_o/w_o\,, \quad \omega^2 = k/M$$

and

$$w_o\, k = 1 \text{ (Hooke's Law)}$$

$$w_s^2 = \frac{1}{4\delta^2 \; \omega^4 \; M^2} \; p_s^2 \; T^2$$

where w_s^2, w_o^2, s_s^2, s_o^2 are mean square displacements and stresses, the subscript o referring to response to unit load, and k is the restoring force of the panel.

Equating displacements

$$\frac{p_s^2}{\overline{p_t^2}} = \frac{8}{T^2} \; \frac{A}{L_x L_y} \; \theta \, \delta \, \omega$$

"An estimate (to be adjusted to account for scaling effects in the section on that subject) of the comparison for a meaningful example can be made using a result from the correlation measurements. For the stable unstart condition a (zero-time delay) correlation value of +0.3 was found. This implies that the correlation length (distance to first zero crossing of a plot of zero-time-delay correlations versus transducer separation) is no greater than 2 inches. Correlation length l_c is related to a size parameter k by

$$l_c = \frac{\pi}{k}$$

"From Reference 21, consistent estimates for A and θ are

$$A = \frac{2\pi}{k^2}, \quad \theta \doteq 3\,\frac{\delta^*}{U_\infty}, \quad \delta^* = \frac{2}{k}$$

The coefficient 3 in the expression for θ applies to supersonic flow (which is probably the situation at these transducers during unstart), for subsonic flow it is replaced by 30. δ^* is the boundary layer displacement-thickness and U_∞ is the free-stream velocity of flow.

For this example, the following estimates are made:

$l_c \simeq 2$ in, $U_\infty \simeq 10^4$ in/sec, $T \simeq 1$, $L_x \simeq 20$ in,

$L_y \simeq 60$ in, $\delta \simeq 0.01$, and $\omega \simeq 3000$ rad/sec

From these,

$$\left[\frac{p_s^{\,2}}{p_t^{\,2}}\right]^{\frac{1}{2}} \simeq 10^{-2} \text{ or } -40 \text{ db}$$

"For a corresponding subsonic case, θ would increase by a little more than 10, yielding a corresponding result on the order of -30 db.

SCALING

"A quantitative examination of the question of scaling is not required in view of the conclusion of the previous paragraph. It is necessary only to establish the orders of magnitude of the adjustments required in using the model results in design of the airframe.

"The mean square turbulence level is determined by the dynamic pressure (Reference 21), which is preserved in the model.

"The octave analyses of the primary-duct pressures are in most cases fairly flat or gently rising (figure 48). If these data were replotted as pressure in one cycle-per-second bandwidths, a 3 db decrease per octave adjustment would appear in the shape. The spectra would be approximately flat or gently falling as were those of turbulence observed in wind tunnels by Willmarth (Reference 37) and Harrison (Reference 38). These authors have noted a cutoff frequency above which these approximately flat spectra drop very sharply. This frequency is given by

$$\omega \simeq \frac{U_\infty}{\delta^*}$$

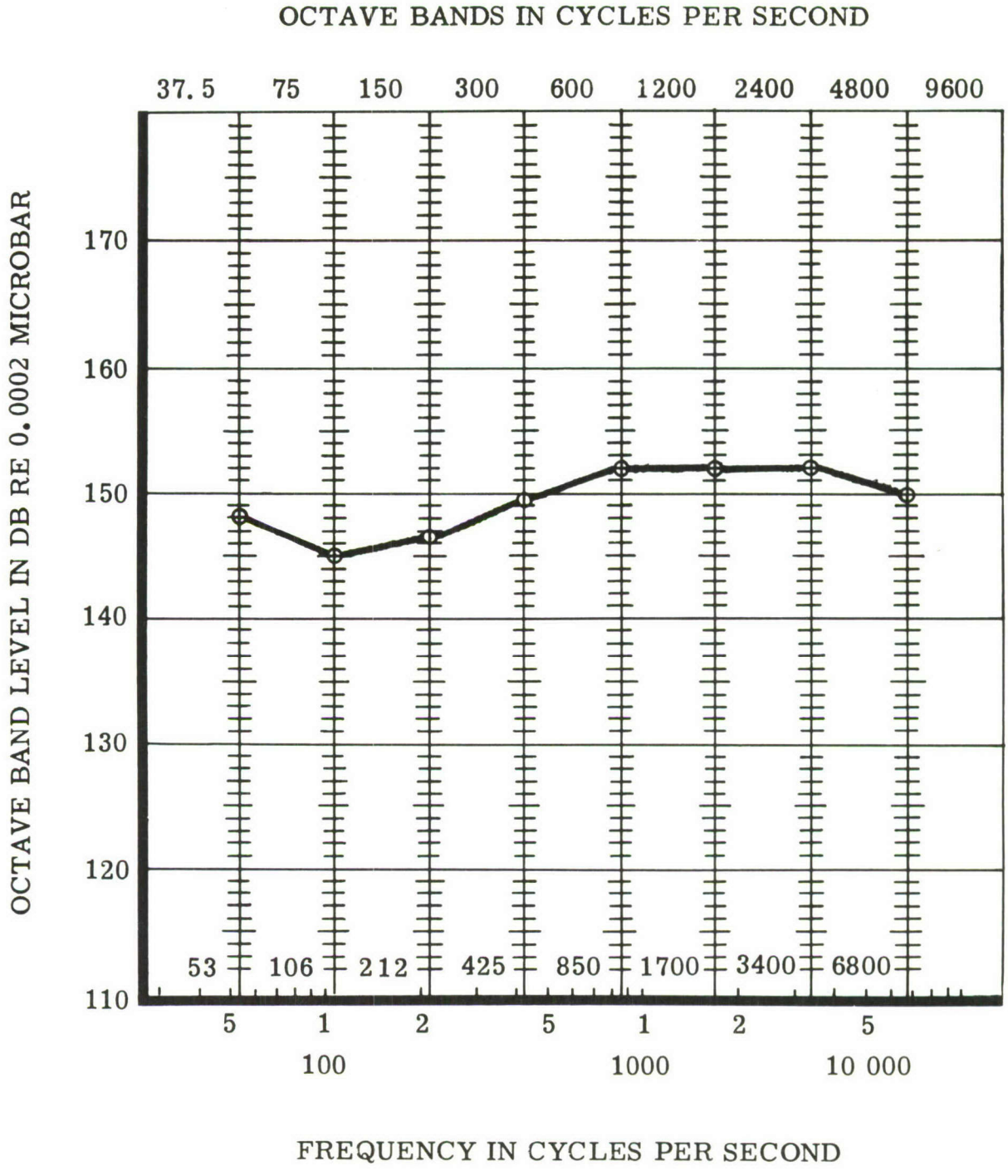

Figure 48. Turbulence Pressure Levels - Duct

"Using the approximation of correlation length of 2 inches, as before, a cutoff frequency in the neighborhood of the upper frequency limit of accuracy of these measurements is found. Reference 39 notes that boundary layer thickness, (and hence, displacement thickness), depends directly on distance of build-up for the layer, and inversely on the local Reynolds number to the one-seventh power. Reynolds number is four times as large for the airframe, for local Reynolds number per foot is preserved in the model. Therefore, δ^* should be about 3.3 times as thick for the airframe as for the model. It is reasonable to consider the layer as initiated at the aft end of the bleed, near the throat.) Thus, it is probable that the airframe will have spectra flat at least to 1500 cps, and flat or dropping off sharply above this frequency.

"The turbulence parameters A and θ depend on the displacement thickness δ^* as

$$A \sim \frac{1}{k} \sim \delta^{*2}, \quad \theta \sim \delta^*$$

Thus,

$$\left[\frac{p_s^2}{p_t^2}\right]^{\frac{1}{2}} \simeq A\theta \sim (\delta^{*3})^{\frac{1}{2}}$$

An adjustment to the estimates of -40 and -30 db of the preceding section is therefore required to account for a factor of 3.3 in the boundary layer thickness of the airframe as compared to that of the model.

$$(3.3)^{3/2} \simeq 6 \simeq 15.5 \text{ db}$$

A sinusoidal acoustic wave of pressure level 15 to 25 db lower than the turbulence pressure levels measured in correlated regions (figure 48) is not of sufficient magnitude to fatigue the (rigid honeycomb) duct structure." (End of quote from Reference 36.)

Honeycomb structure of this thickness and span has an allowable sinusoidal load for a siren test life simulating the life of the airframe exceeding 170 db. The applied turbulence load in the neighborhood of 480 cps, from figure 48, is about 150 db octave level, which is 125 db spectrum level. Subtracting the minimum turbulence-to-sinusoid correction of 15 db yields 110 db effective sinusoidal level, for a positive margin exceeding 60 db.

Section VII

SUGGESTIONS AND RECOMMENDATIONS FOR FUTURE WORK

7.0 GENERAL

The sonic fatigue problems described herein include many facets, some of which are known only empirically. Sound source descriptions of sufficient detail and accuracy to proceed with the stress and fatigue analysis must be determined by microphone surveys. The stress response cannot be determined with any reasonable accuracy without an empirically determined damping factor. Even with the damping factor known, calculation of the stresses at a given point (at which fatigue failure might occur) is highly speculative without a knowledge of panel edge conditions and a knowledge of the possible multimodal shapes of response. Fatigue, thus far, is almost completely an empiracal phenomenen. It is interesting to speculate that the basic fatigue portion of the solution with all its empiricism and traditional wide scatter of data is probably the least unknown of all the sonic fatigue problems, except for, perhaps, the mission analysis portion. To gain further knowledge of these problems, the research projects in the following paragraphs suggest themselves.

7.1 SOUND SOURCE DATA

It is difficult to see how substantial improvements can be made in prediction of the sonic environment, without simply collecting more empirical data from the principal sound sources, propulsion system, and boundary layer. Displaced microphone surveys of full-scale jet and rocket engines in the free field and in the presence of typical, simple fuselage and aerodynamic surface bodies are suggested. The almost limitless variability of body presences should not discourage a straightforward attack on this problem. Aerodynamic surface cruciforms forward and aft of the jet exhaust nozzle will cover the buried engine and the "caravelled" engine pod. Whereas, wing pod-mounted engines can be treated by a single aerodynamic surface attached to an adjacent fuselage body. These surveys could be economically conducted on existing operational vehicles at low cost in a manner similar to that used in the B-66 surveys.

7.2 CONFIRMATION OF SIREN TEST APPROACH

It is anticipated that most sonic fatigue life tests will be conducted in discrete frequency test facilities for the next several years for reasons outlined in Section VI.

Consequently, one of the most important aspects of the sonic fatigue problem is to determine an accurate method of correlating discrete frequency test results to actual service conditions. The sine-random equivalence technique, which is considered to be as advanced as the present state-of-the-art, is presented in Section V of this report. However, it is recommended that a carefully controlled test program be instigated, subjecting specimens to both discrete frequency and random excitation, to substantiate the validity of this method.

7.3 ANALYTICAL DETERMINATION OF STRESS RESPONSE

Existing techniques of stress analysis can be brought to bear upon the problem of a panel responding to acoustic excitation. The variables most likely to cause poor prediction results are damping and panel-edge support conditions. Solution of the stress distributions in the panels for a variety of edge fixities and assumed damping coefficients would allow a complete solution upon experimental determination of these two unknowns. The results of stress prediction calculations can be utilized to advantage in the over-all sonic fatigue problem in many ways. For example, it would allow prediction of the location of ultimate failure, which state-of-the-art at present is a guessing game. It is expected that such solutions would point the way to more accurate multimode correction factors without involving complex mathematical processes.

7.4 CREATION OF DESIGN TYPE CHARTS

Finally, the surest method of assisting the designer-analyst in an early solution to sonic fatigue problems is with preprepared design charts for different types of construction. Random sound source testing is required to produce accurate charts of this type. However, the siren test analytical procedure outlined in this report could be used to produce curves with attendant loss of assurance of accuracy. The approach herein offered, once confirmed by either a test program as suggested in paragraph 7.2, or by service usage, could be used to produce design charts with sufficient accuracy to warrant the cost. ASD PR 147870, now in the competition stage, appears to be aimed at this problem.

REFERENCES

1. WADC TR 58-343, "Methods of Flight Vehicle Noise Prediction," P.A. Franken, et al

2. C. M. Harris, Handbook of Noise Control, McGraw-Hill Book Company Inc, N.Y., N.Y., 1957, Chapter 33

3. WADC TR 52-204, Handbook of Acoustic Noise Control, Vol I, Supplement I

4. NACA TN 3018, "A Theoretical Study of the Effect of Forward Speed on the Free Space Sound Pressure Field Around Propellers," I. E. Garrick

5. M. J. Lighthill, "On Sound Generated Aerodynamically," Proceedings of the Royal Society of Aeronautics, Vol 211 and 222, 1951 and 1953, pp 564-587, pp 1-32

6. A. Anderson and J. Johns, "Characteristics of Free Supersonic Jets Exhausting Into Quiescent Air," Jet Propulsion, January 1955

7. H. R. Hull, "Effect of Jet Structure on Noise Generation by Supersonic Nozzles," The Journal of the Acoustical Society of America, Vol 31, February 1959, pp 147-149

8. NASA TN D-21, "Near Field and Far Field Noise Surveys of Solid-Fuel Rocket Engines for a Range of Nozzle Exit Pressures," W. H. Mayes

9. NACA TN 3763, "Near Field of a Jet Engine Exhaust," W. L. Hawes and H. R. Mull

10. NACA TN 3187, "The Near Noise Field of Static Jets and Some Model Studies of Devices for Noise Reduction," L. Lassiter and H. Hubbard

11. NOR-60-26, "Structural Vibration in Space Vehicles," Norair Division of Northrop Corporation, Hawthorne, California, H. Eldred, W. Roberts, and R. White (Unpublished)

12. University of Southampton, U.S.A.A. Report No. 131, "Boundary Layer Noise Research in the U.S.A. and Canada", a critical review, E. Richards, M. Bull, and J. Willis, February 1960

13. WADC TR 59-676, WADC University of Minnesota Conference on Acoustic Fatigue, March 1961

14. NACA TN 3764, "Near Noise Field of a Jet Engine Exhaust, II - Cross Correlation of Sound Pressures," E. Callaghan

15. Belcher, P. M., Van Dyke, J. D., and Eshleman, A. L., "Development of Aircraft Structure to Withstand Acoustic Loads," Aero/Space Engineering, Vol 18, No. 6, June 1959

16. Miles, J. W., "On Structural Fatigue Under Random Loading," The Journal of Aeronautical Science, Vol 21, No. 11, pp 753 - 762, November 1954

17. Powell, A., "On the Fatigue Failure of Structures due to Vibrations Excited by Random Pressure Fields," The Journal of the Acoustical Society of America, Vol 30, No. 12, pp 1130 - 1134, December 1958

18. WADC TR 59-676, "Quick Estimation of Damping From Free Damped Oscillograms, J. C. Burgess

19. Powell, A., "On the Response of Structures to Random Pressures and to Jet Noise in Particular," Random Vibration, edited by Stephan H. Crandall, Chapter 8; The Technology Press, Cambridge, 1958

20. Smith, Jr., P.W. and Junger, M. C. "Sound Induced Vibrations," Journal of Environmental Sciences, pp 9 - 14 October 1959

21. Dyer, Ira, "Sound Radiation Into a Closed Space Fron Boundary Layer Turbulence," Report No. 602, Bolt, Beranek, and Newman, Inc, Cambridge, Massachusetts, December 1958

22. WADD TR 60-188, "Influence of Natural Frequencies and Source Correlation Fields on Random Response of Panels," R. F. Lambert and D. H. Tack, University of Minnesota, July 1960

23. B. J. Clarkson and R. D. Ford, "Random Excitation of a Tailplane Section by Jet Noise," University of Southampton, Report A. A. S. U. -171, March 1961

24. Peterson, R. E., Stress Concentration Design Factors, John Wiley and Sons, N. Y., N. Y., 1953

25. WADC TR 59-676, "A New Look at Structural Peak Distributions Under Random Vibration," H. C. Schjelderup, pp 413 - 426

Lebensdauer von
26. Palmgren, A., Die ~~Liebensdaver~~ Van Kugellagern Ver. Deut. Ingenieure, Vol 68, No. 14, pp 339 - 341, 1924

27. Miner, M. A., "Cumulative Damage in Fatigue," Journal of Applied Mechanics, Vol 12, pp A - 159, September 1945

28. NASA TN D-663, "Experimental Investigation of Effects of Random Loading on the Fatigue Life of Notched Cantilever-beam Specimens of SAE 4130 Normalized Steel," Fralich, R. W.

29. Freudenthal, A. M., "Fatigue of Structural Metals Under Random Loading," ASTM Preprint, 1960-67b

30. Smith, C. R., "A System for Estimating Cumulative Fatigue Damage by Using Miner's Rule Corrected for Residual Stress," SAE Preprint 61-353B

31. Shanley, F. R., "Discussion of Methods of Fatigue Analysis," The Rand Corp Paper, p-1749, July 1959

32. Henry, D. L., "A Theory of Fatigue Damage Accumulation in Steel," Transactions ASME, Vol 77, pp 913 - 918, August 1955

33. WADD TN R 60-410, Part I, "Investigation of Thermal Effects on Structural Fatigue", Douglas Aircraft Company Inc.

34. Eshleman, Van Dyke, and Belcher, "A Procedure for Designing and Testing Aircraft Structure Loaded by Jet Engine Noise," Paper 59-AV-48, American Society of Mechanical Engineers, March 1959

35. Belcher, P.M., Eshleman, A.L., and Van Dyke, J.D., "A Comparison of Stress Response and Fatigue Test Results under Random and Sinusoidal Acoustic Loading," The Journal of the Acoustical Society of America, Vol 31, No. 1, p 125 (A), January 1959

36. Report No. NA-60-1480, "Turbulence - Pressure Measurements and Acoustical Fatigue Evaluation - XB-70 Primary Inlet Duct," Belcher, P.M. and Ancell, J.E., North American Aviation, Inc, Los Angeles 45, California, 1960 (Confidential)

37. "Space Time Correlation and Spectra of Wall Pressure in a Turbulent Boundary Layer," Willmarth, W.W., Memorandum No. 3-17-59W, National Aeronautics and Space Administration, 1959

38. "Pressure Fluctuations on the Wall Adjacent to a Turbulent Boundary Layer," Harrison, M., Report No. 1260, David Taylor Model Basin, December 1958

39. WADC TR 58-343, "Methods of Flight Vehicle Noise Prediction," Franken, P.A., et al, p 27

40. Bishop and Johnson, "The Mechanics of Vibration," Cambridge University Press, Cambridge, pp 282 - 486, 1960

41. Lin, Y.K., "Free Vibrations of Continuous Skin-Stringer Panels," Journal of Applied Mechanics, December 1960

42. G. B. Warburton, "The Vibration of Rectangular Plates," Proceedings of the Institute of Mechanical Engineers, Vol 168, pp 371 - 384, 1954

43. Wojtaszak, I. A., "Design Data," Journal of Applied Mechanics, pp 4-71-A-73, (Date unknown)

44. WADC TR 58-343, "Methods of Flight Vehicle Noise Prediction" Appendix A, Vibration Frequency Charts, pp 175 - 181, February 1957

45. Hess, Herr, and Mayes, "A Study of the Acoustic Fatigue Characteristics of Some Flat and Curved Aluminum Panels Exposed to Random and Discrete Noise," NASA Report TND-1, 1959

46. S. Timoshenko, "Vibration Problem in Engineering," D. Van Nostrand Co, N.Y., N.Y., (3rd Edition) pp 443 - 444, 1955

APPENDIX A

PREDICTION OF RESONANT FREQUENCY

Although prediction of resonant frequency is not an essential of the sine-random equivalence approach, since it must ultimately be determined by test, this section is included for its informative value.

If it is assumed that structural components onto which skin plates or other forms of plain surfaces are attached, possess far more rigidity and relative stiffness, it is then possible to consider skin-plate deflections relative to these supports as absolute values in order to carry out theoretical analysis of the vibration mode pertaining to the skin plate. Test results have tended to substantiate the validity in this approach. In some cases, according to Lin (Reference 41), it may be necessary to allow a certain degree of twisting motion for the conditions of constraints, at intermediate rib stations for example, when such conditions become structurally more appropriate in vibratory motions. In all cases, however, the vibratory mode of a skin plate would be frequency-sensitive since the elastic action due to inertia is a force that may be represented by the equation:

$$F = \frac{w}{g} y\omega^2$$

where F is the inertial force at a unit area (sq in) of density w in lbs/in^2; y is the resultant deflection, and ω is the angular frequency.

According to Bishop and Johnson (Reference 40), the angular frequency can assume only those values that satisfy the following equation,

$$\frac{d^4y}{dx^4} - \frac{w\omega^2}{D} y = 0 \qquad (23)$$

D, the flexural rigidity of the plate, $= \frac{E h^3}{12(1-\mu^2)}$

where E = modulus of elasticity in psi

h = plate thickness, in inches

μ = Poisson's ratio

These frequencies are termed the mode frequencies. The solutions will depend on the boundary conditions of the plate or its subdivided areas in a particular mode shape. For example, a rectangular plate a x b x h, with

all edges completely clamped, will have as mathematical constraining conditions $y = 0$ as $\frac{dy}{dx} = 0$ applicable to all edges for the fundamental mode.

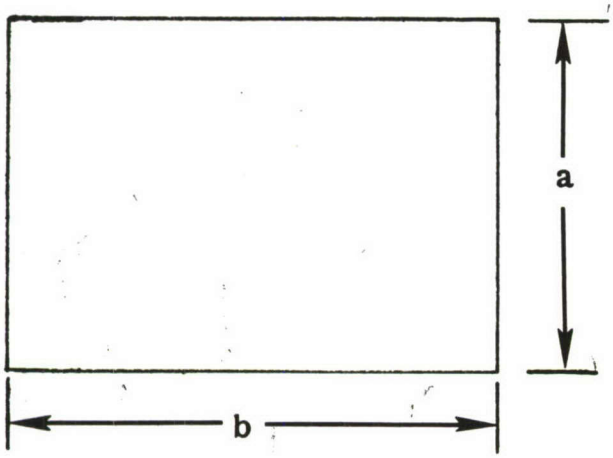

Figure 49. Fundamental Mode

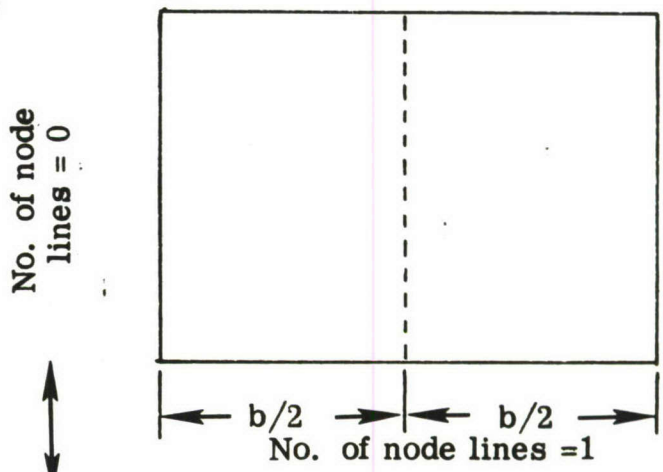

Figure 50. Second Mode

For secondary modes, additional node lines are created which may then be considered as boundaries of separate areas or elements. In the last example shown, element a x $\frac{b}{2}$ x h will have the same constraints on three clamped sides as in the original area; but the new boundary would be simple supported with $y = 0$ and bending moment = 0 as necessary conditions towards a solution in mode frequency determination. An example will be given at the end of this appendix, using solutions from basic boundary conditions.

While detailed solution of Equation (23) may be found in Reference 40, it is convenient to express the general solution in the following form.

$$f_s = \frac{Ch}{a^2} \quad ,$$

where f_s = mode frequency for steel plate f or $E = 30\ (10)^6$ psi

C = a constant per specified edge conditions.

Values of C were given in many references (References 43 and 44) and were covered extensively by Warburton (Reference 42). Figure 51 shows these constants for some selected conditions of edge constraints calculated by Warburton's method. Figure 52 shows an alignment chart for reducing to mode frequencies of steel plates, with corrections for other materials shown in the following chart.

	Correction Factor = $\frac{E\rho_S}{E_S\rho}$					
	Temperature (°F)					
Material	80	200	400	600	800	1000
Steel	1.000					
Aluminum alloys	0.985					
Titanium Ti-50A	0.985	0.966	0.932	0.896	0.866	0.828
Ti-75A	0.975	0.945	0.910	0.873	0.835	0.784

EXAMPLE CALCULATION

An example in mode frequency calculation is shown, using a simple aluminum plate configuration given by Hess, Herr, and Mayes (Reference 45), with four mode shapes shown in figure 53. Over-all dimensions were 9.5- x 11.6- x 0.032-inches.

OVER-ALL MODE, FULLY CLAMPED EDGES - FIGURE 53-a.

$$\frac{b}{a} = \frac{11.6}{9.5} = 1.21$$

$$\frac{c}{10^4} = 29.8$$

$$f_s = 106 \text{ cps}$$

From the table above, material correction factor = 0.985

f_a = 104 cps compared to test result of 105 cps

$$\frac{C}{10^4} = \frac{f_s \quad a^2/h}{10^4}$$

where $C/10^4$ = FREQ CONSTANT
f_s = FREQ CPS
h = PLATE THICKNESS IN.

a = SHORT SIDE IN.
b = LONG SIDE IN.
a & d APPLICABLE TO OVERALL AS WELL AS ELEMENT DIMENSIONS

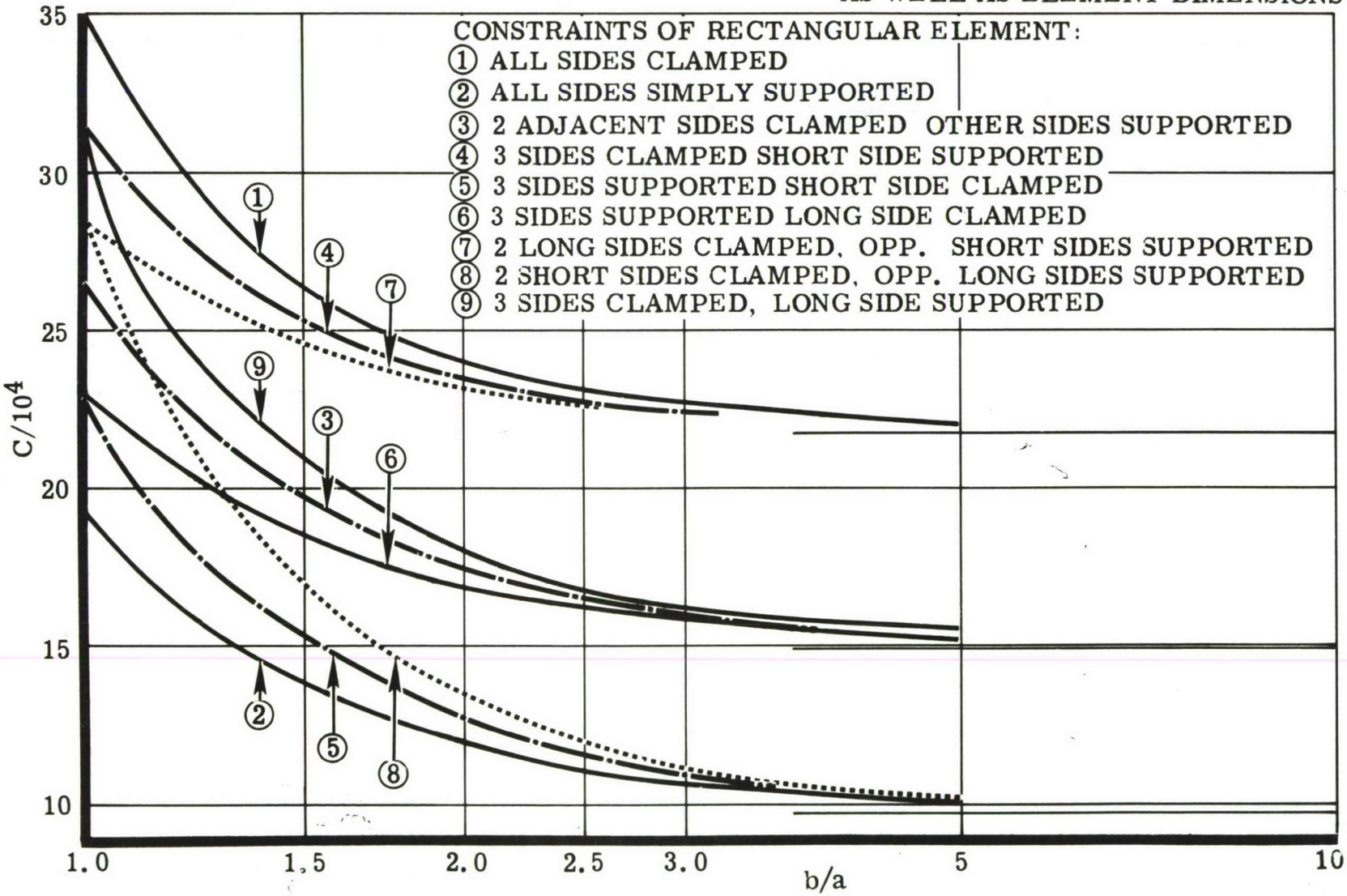

Figure 51. Vibration Frequency Constant of Steel Plates.

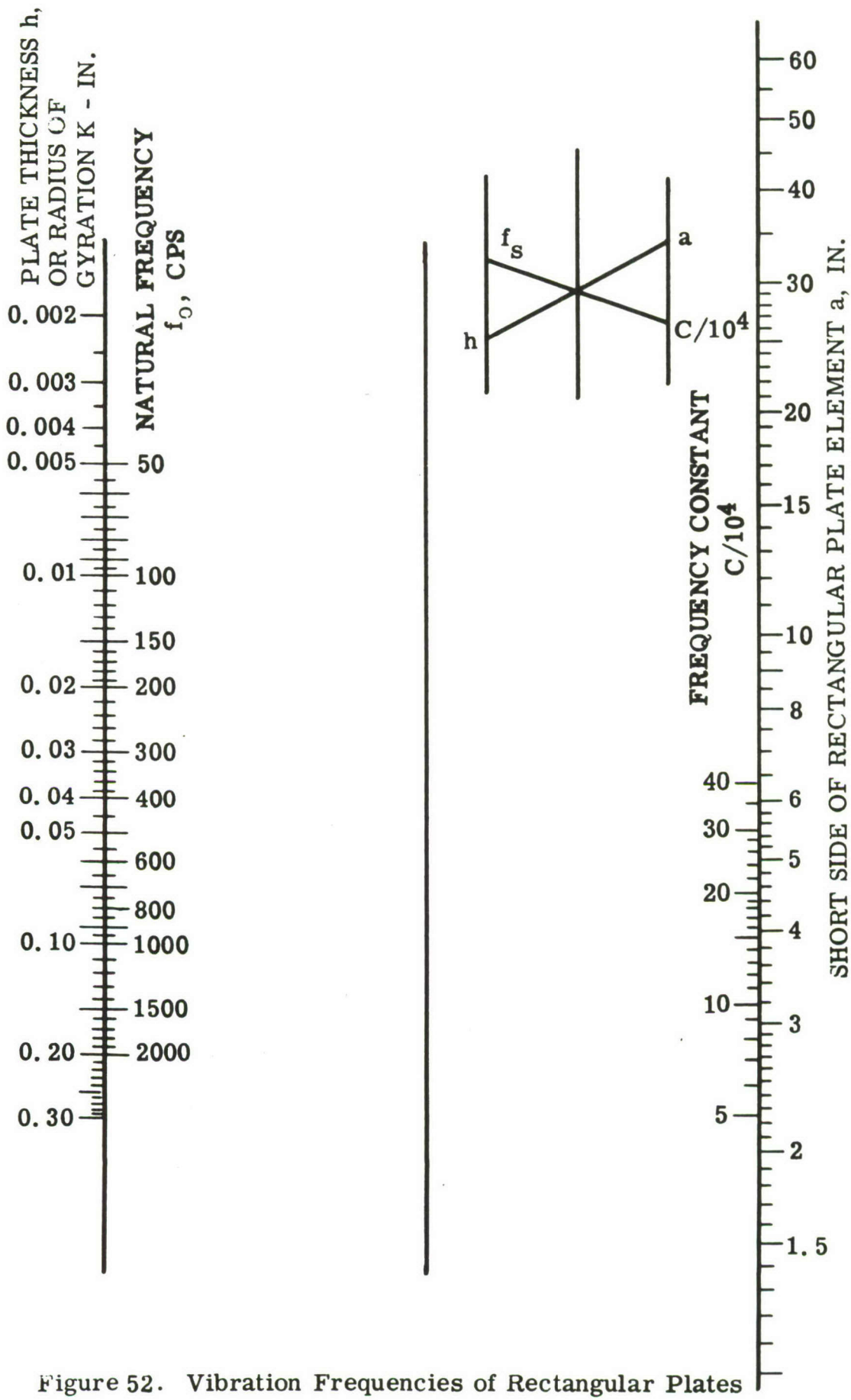

Figure 52. Vibration Frequencies of Rectangular Plates

a

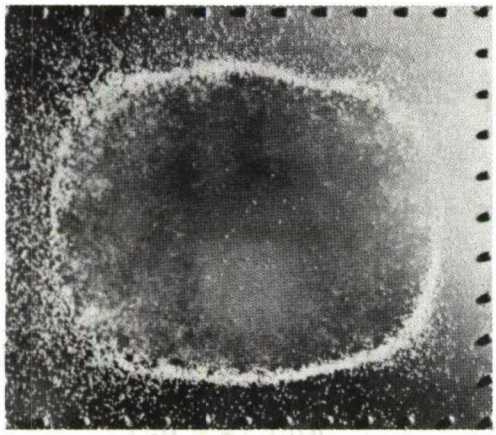

f = 105 CPS

b

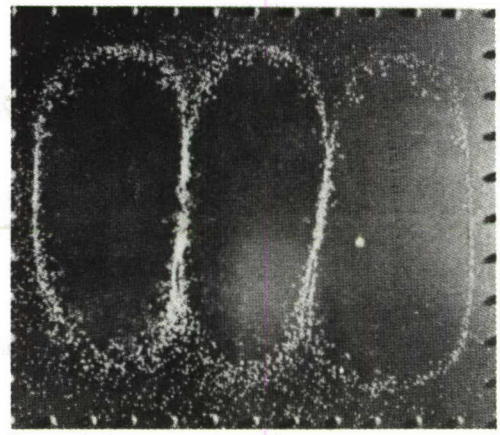

f = 300 CPS

c

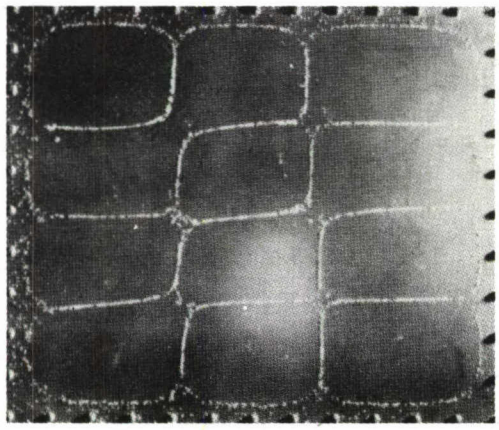

f = 890 CPS

d

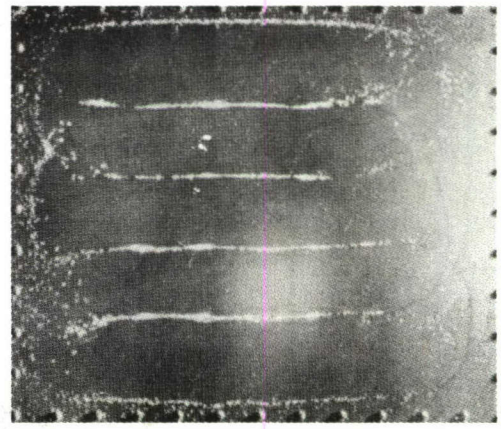

f = 1025 CPS

Figure 53. Mode Shape Examples

CALCULATIONS FOR THE MODE OF FIGURE 53-b.

Using Warburton's convention:

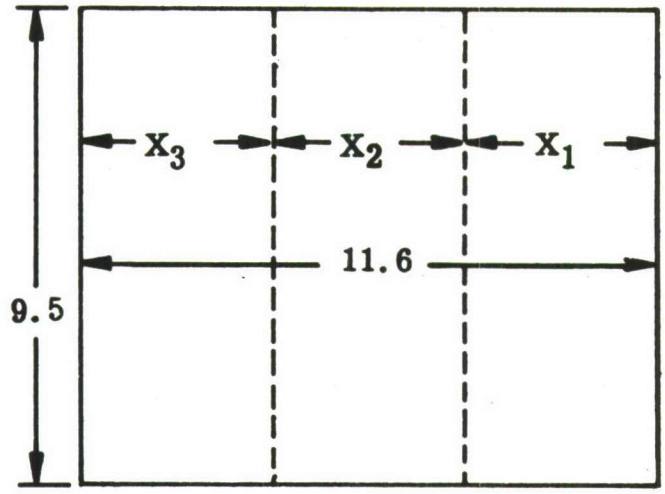

Figure 54. Schematic of Mode b

m = number of node lines along X direction

n = number of node lines along Y direction

m = 4
n = 2
} mode

By trial and error methods:

$x_1 = 3.95$ and $x_2 = 3.7$

So that for end elements,

$$\frac{b}{a} = \frac{9.5}{3.95} = 2.4$$

$\frac{c}{10^4}$ = 16.8 per condition 9, shown in figure 51

f_a = 316 cps

And for center element:

$$\frac{b}{a} = \frac{9.5}{3.7} = 2.55$$

$\frac{c}{10^4}$ = 11.8 per condition 8, shown in figure 49

f_a = 316 cps

Note that for every element, the same mode frequency must prevail. It is suspected that had the frequency used in Reference45 been more accurately set, rather than at 300 cps, the mode lines would probably come out more squarely than the slanted lines observed.

CALCULATION OF THE MODE OF FIGURE 53-c.

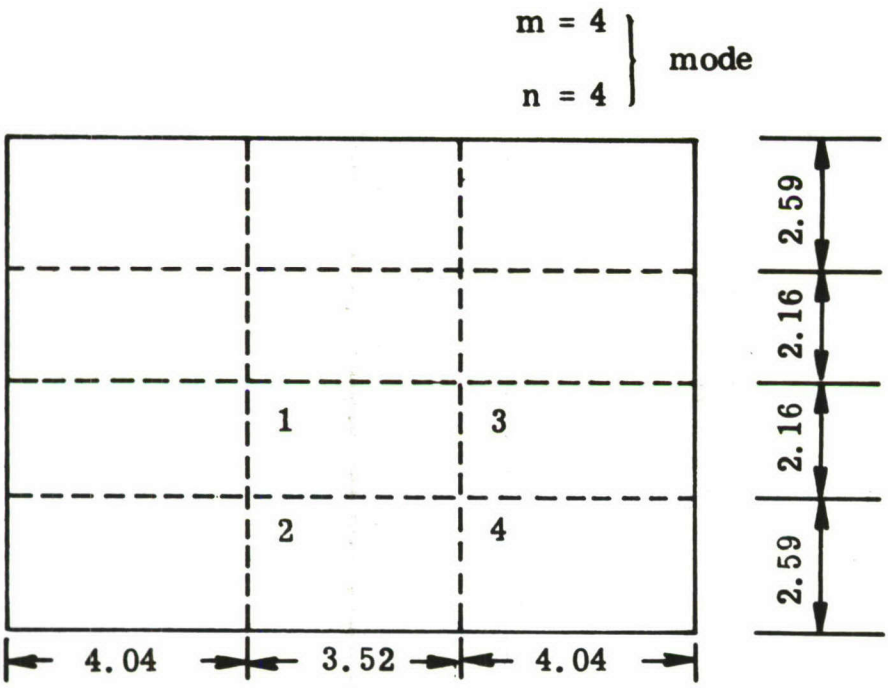

Figure 55. Schematic of Mode c

After repeated trials, establish dimensions for elements 1, 2, 3, and 4 as indicated.

For element 1,

$$\frac{b}{a} = \frac{3.52}{2.16} = 1.63$$

$$\frac{c}{10^4} = 13.1, \text{ figure 51,}$$

$$f_s = 900 \text{ cps}$$

For element 2,

$$\frac{b}{a} = \frac{3.52}{2.59} = 1.36$$

$$\frac{c}{10^4} = 19.1, \text{ figure 51,}$$

$$f_s = 900 \text{ cps}$$

For element 3,

$$\frac{b}{a} = \frac{4.04}{2.16} = 1.87$$

$$\frac{c}{10^4} = 13.0, \text{ figure 51,}$$

$$f_s = 900 \text{ cps}$$

For element 4,

$$\frac{b}{a} = \frac{4.04}{2.59} = 1.56$$

$$\frac{c}{10^4} = 19.1, \text{ figures 51, 52}$$

$$f_s = 900 \text{ cps}$$

Corrected f_a = 888 cps compared to test result of 890 cps

CALCULATION OF THE MODE OF FIGURE 53-d.

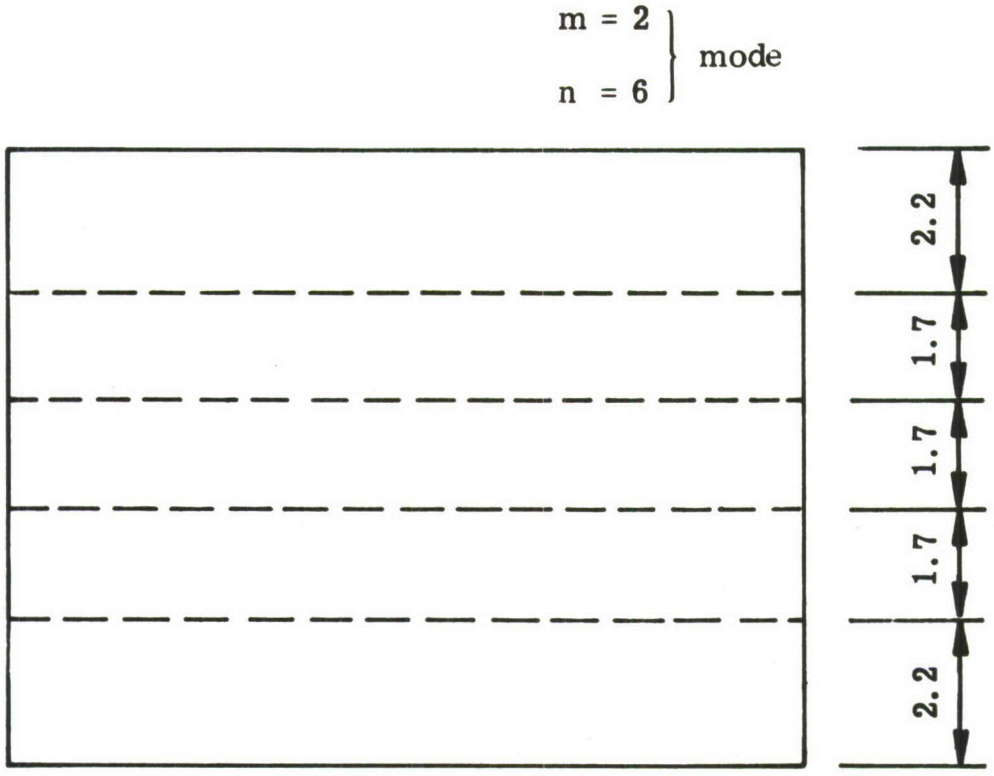

Figure 56. Schematic of Mode d

It is difficult to rely on calculations in this case, because of the high-aspect ratios in each element. However, measured spacings may be used to verify observations.

Mode frequency of 1025 cps. Thus, for end elements:

$$\frac{b}{a} = \frac{11.6}{2.2} = 5.3$$

$$\frac{c}{10^4} = 15.5$$

$$f_s = 1050 \text{ cps}$$

for intermediate elements:

$$\frac{b}{a} = \frac{11.6}{1.7} = 6.8$$

$$\frac{c}{10^4} = 9.6$$

$$f_s = 1050 \text{ cps}$$

Corrected f_a = 1035 cps against 1025 observed. These results tend to support the belief that structural element mode frequencies may be so calculated in the design stage.

DETERMINATION OF THE PRIMARY RESONANT FREQUENCY OF SANDWICH PANELS

The following curves, figures 57 through 65, present a graphical means of determining the primary resonant frequency for honeycomb sandwich panels having various edge conditions. The curves were developed from Reference 46, by modifying the equation for the natural frequency of a solid plate. This approach does not account for the effect on natural frequency of core shear modulus. The parameters required for the use of the curves are defined on each graph.

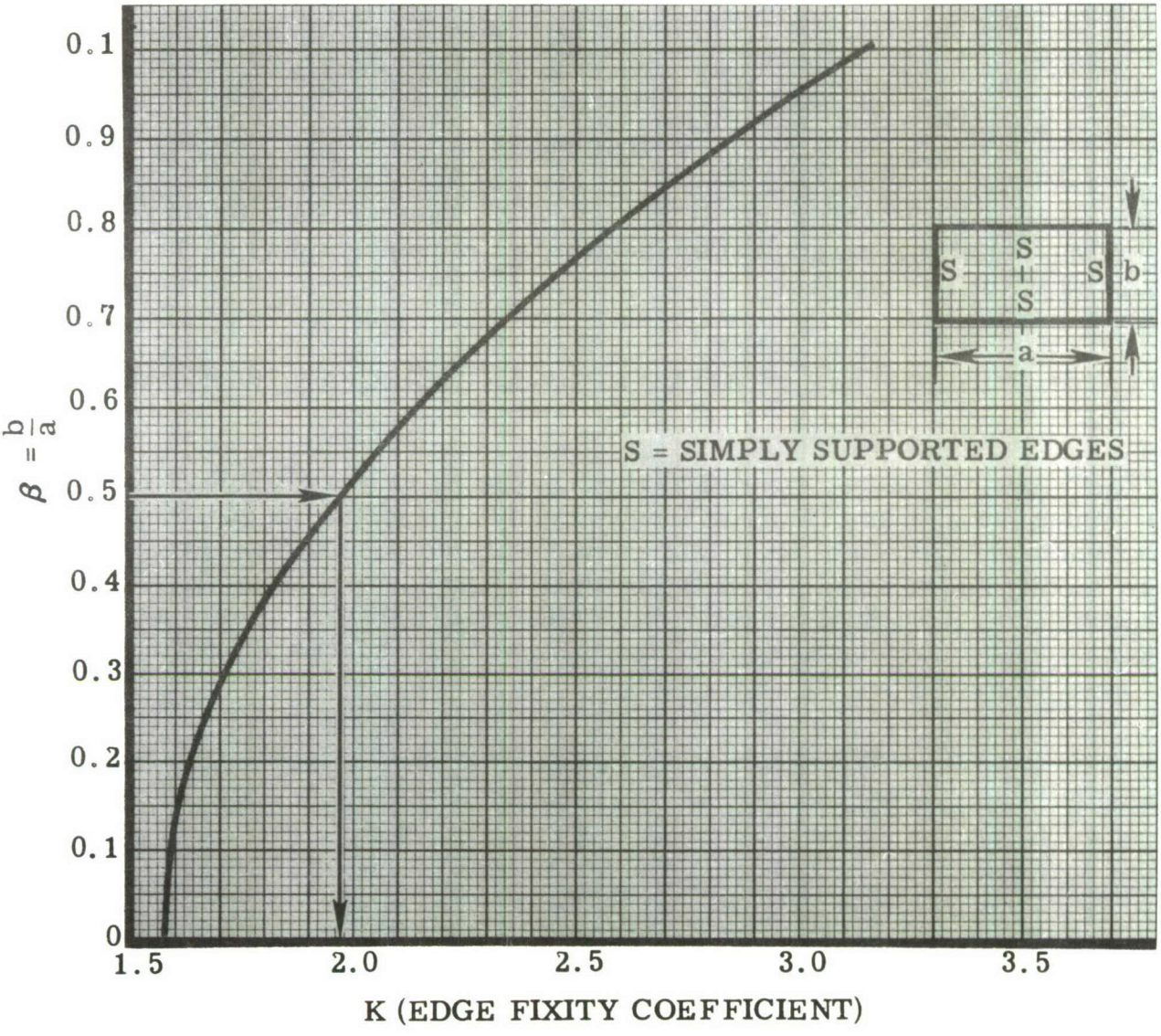

Figure 57. K Versus Aspect Ratio (Four Sides Simply Supported)

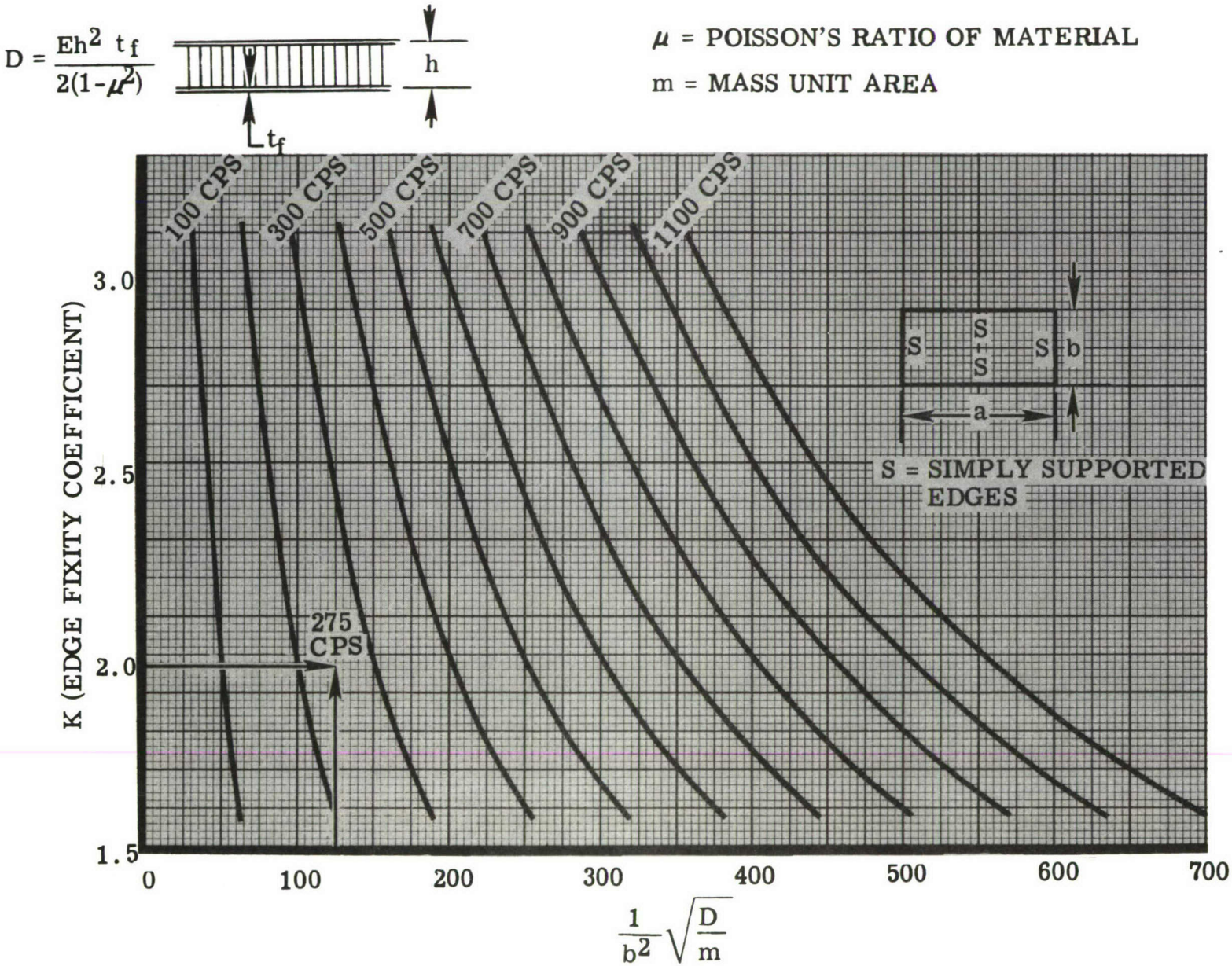

Figure 58. Primary Resonant Frequency (Four Sides Simply Supported)

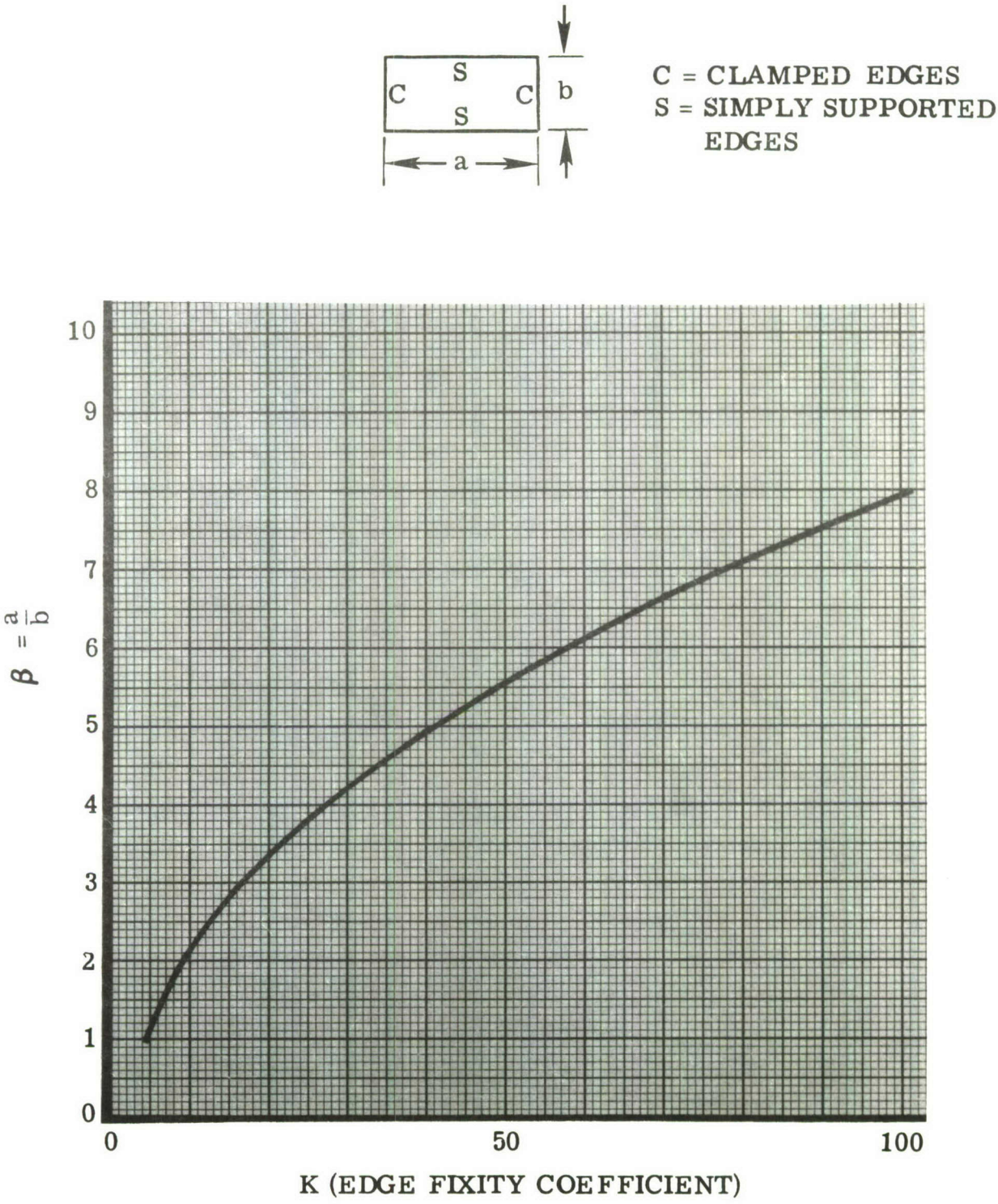

Figure 59. K Versus Aspect Ratio (Two Sides Simply Supported, Two Sides Clamped)

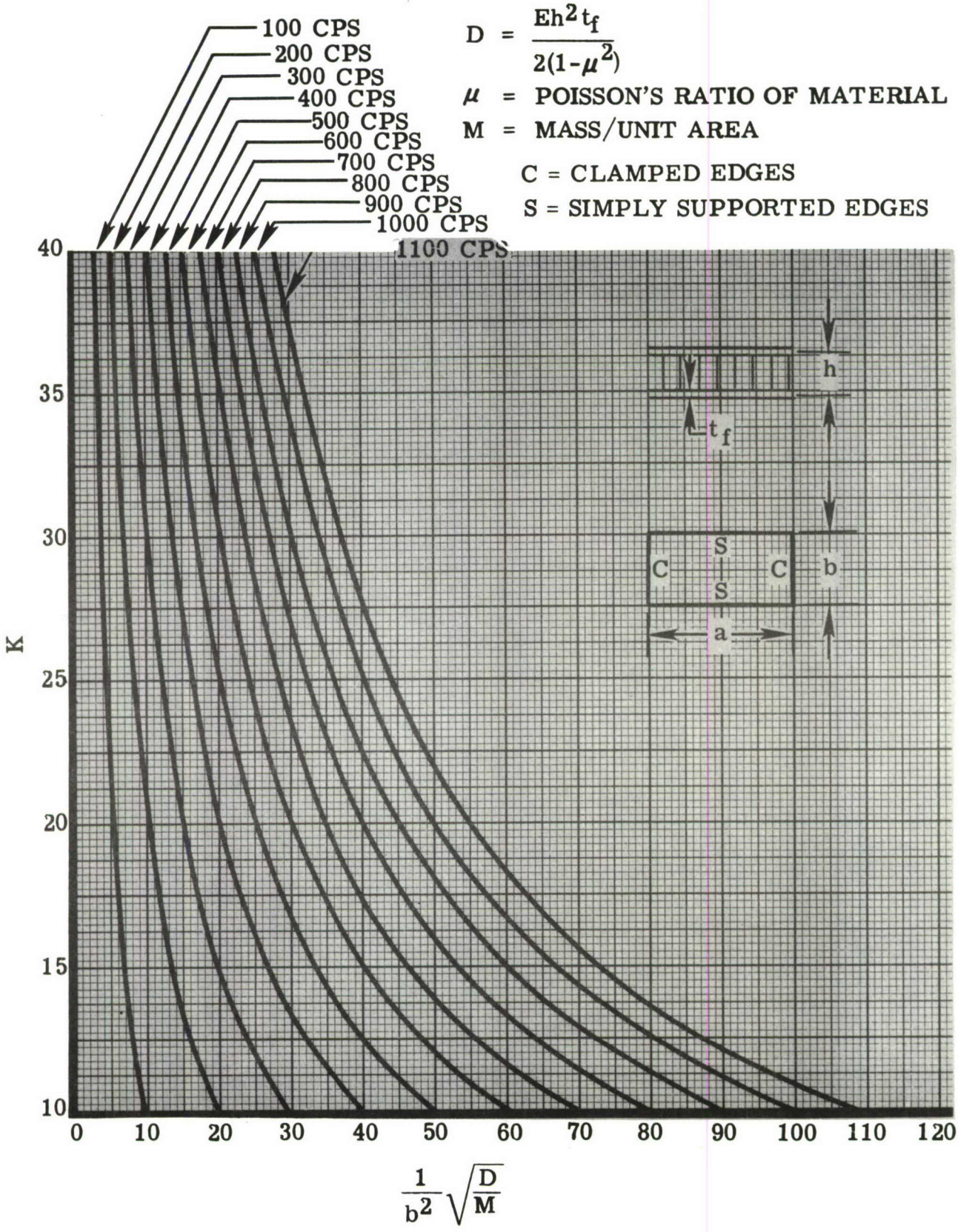

Figure 60. Primary Resonant Frequency

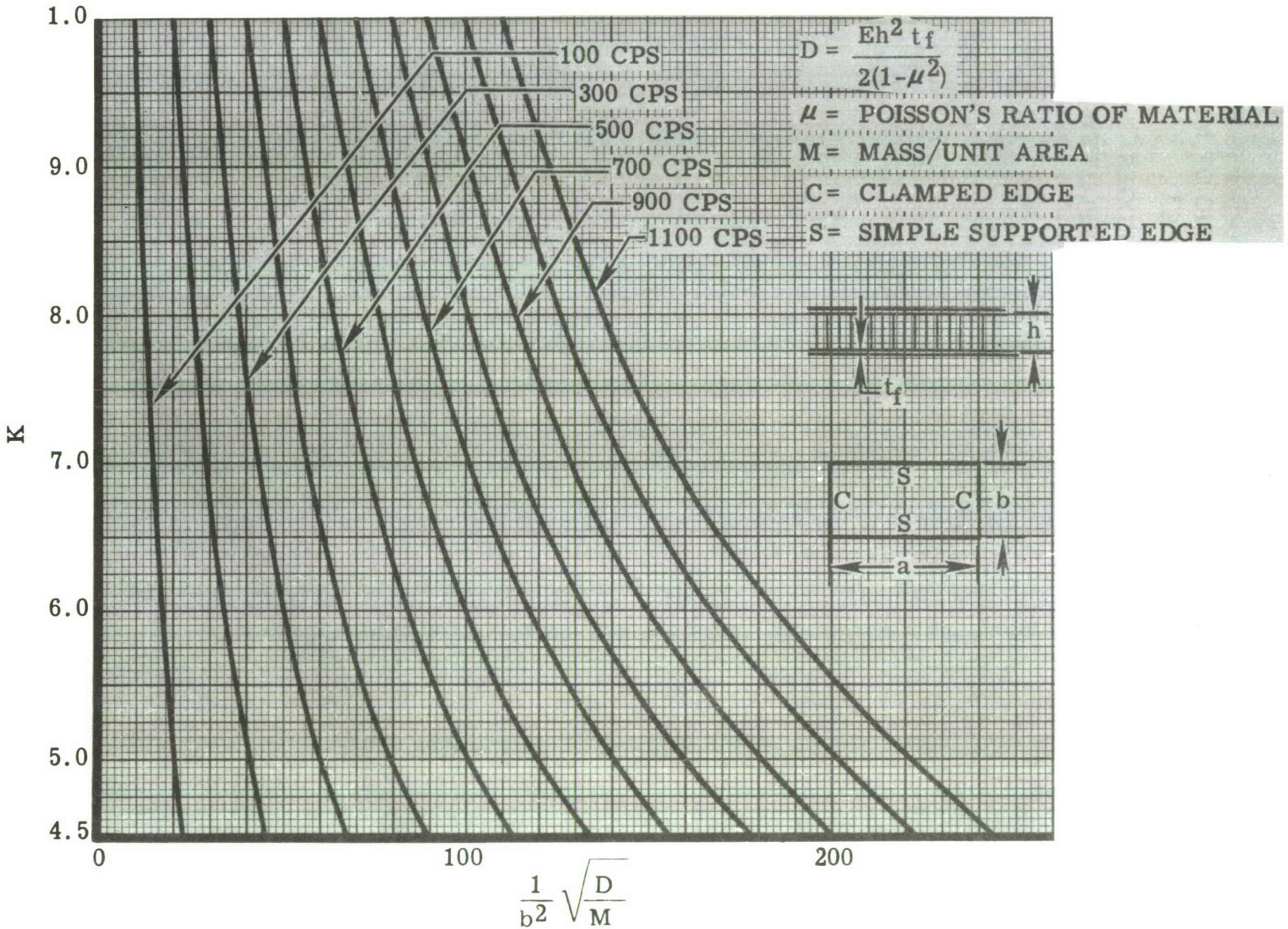

Figure 61. Primary Resonant Frequency (Two Sides - Simple Support, Two Sides - Clamped)

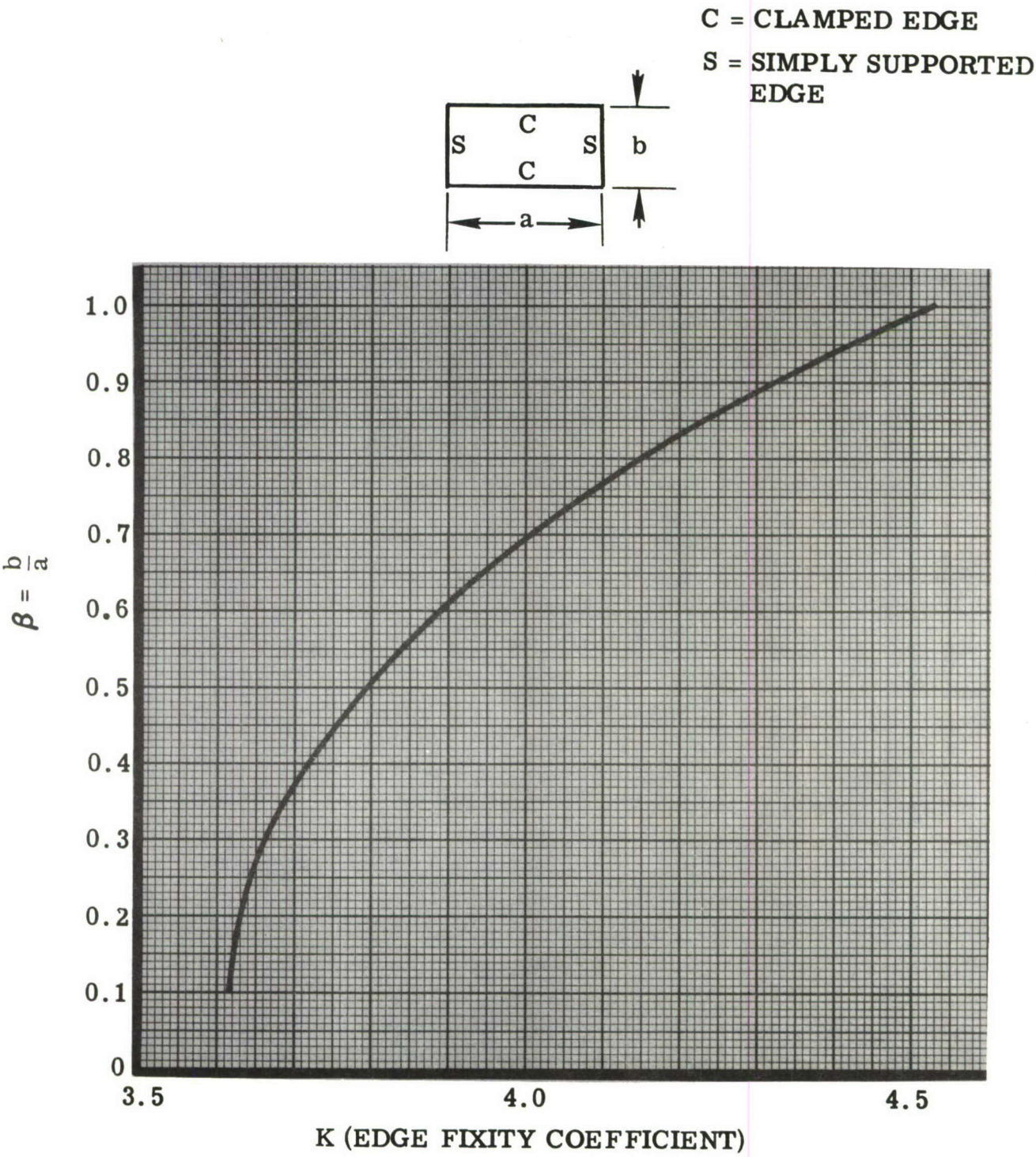

Figure 62. K Versus Aspect Ratio
(Two Sides Clamped, Two Sides Simply Supported)

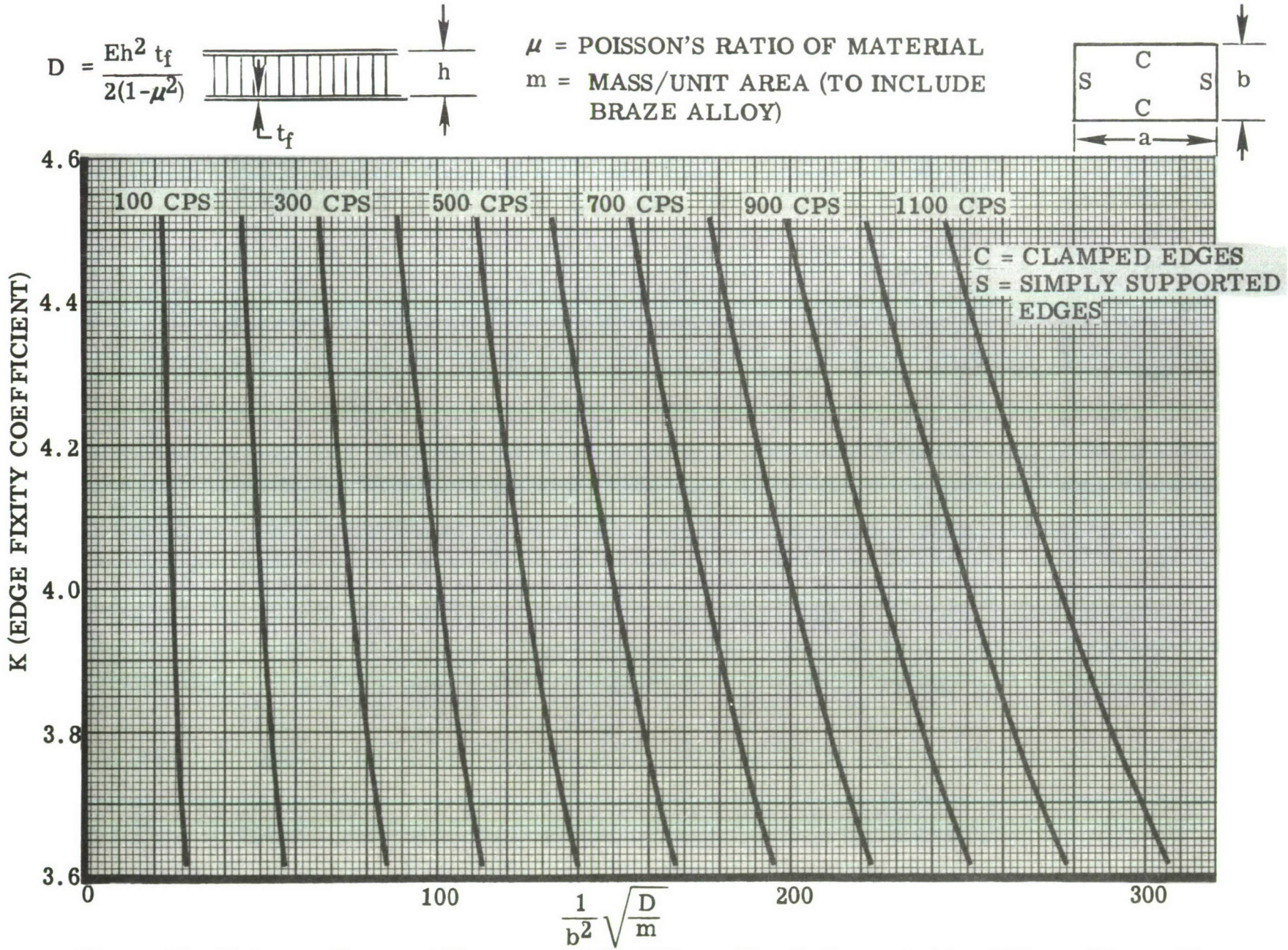

Figure 63. Primary Resonant Frequency (Two Sides - Simple Support, Two Sides - Clamped)

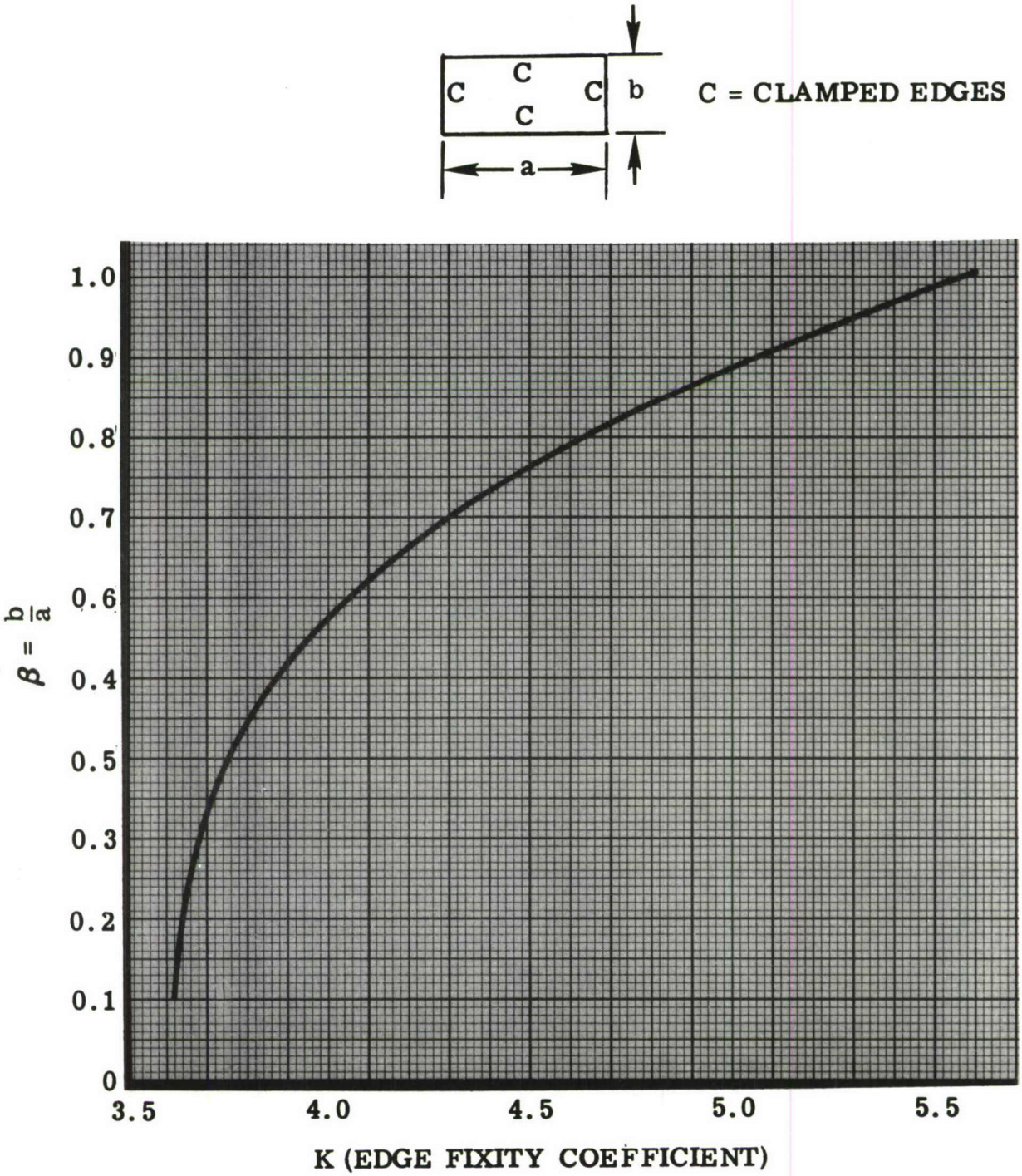

Figure 64. K Versus Aspect Ratio (Four Sides Clamped)

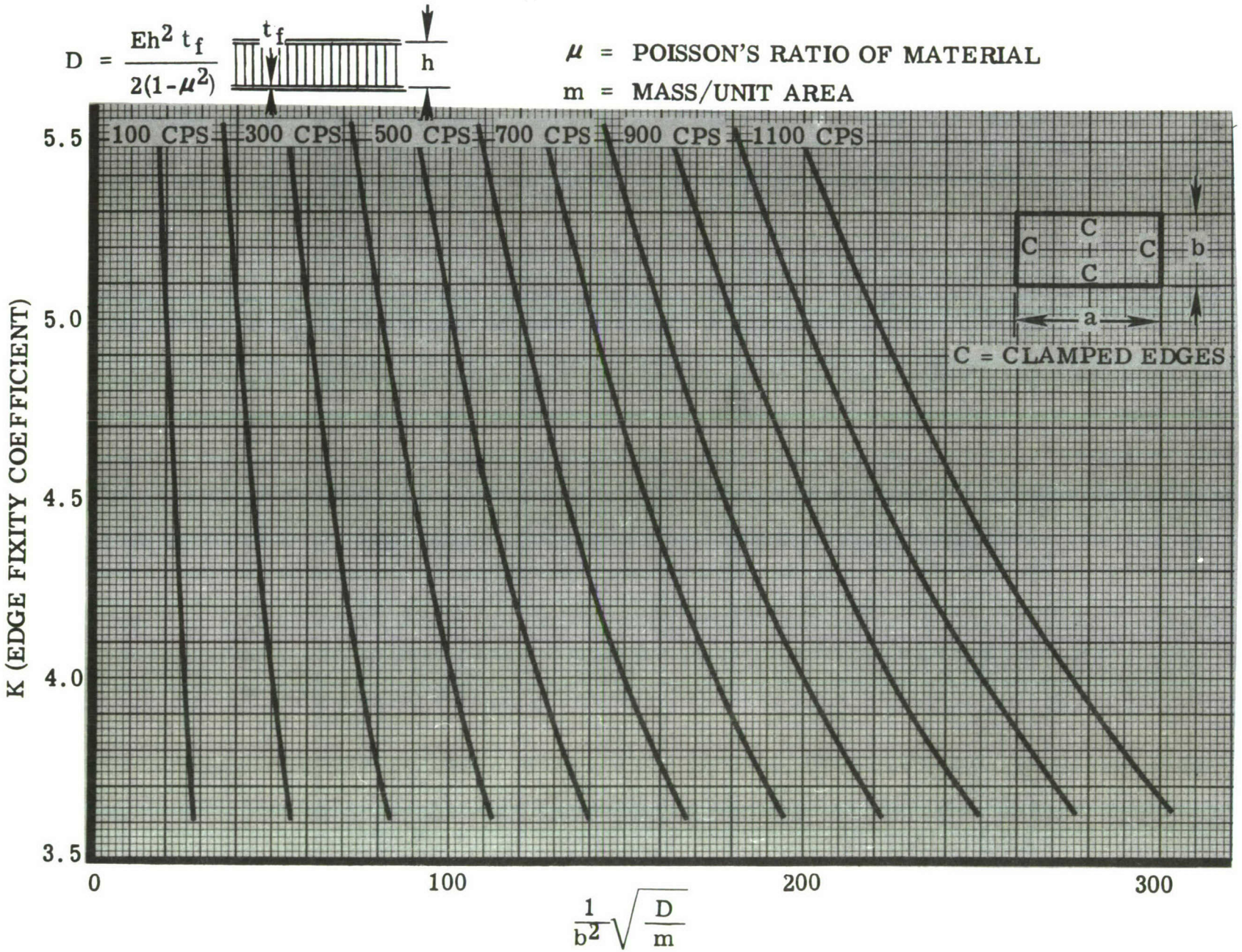

Figure 65. Primary Resonant Frequency (Four Sides Clamped)